DOE/ET/15421-1

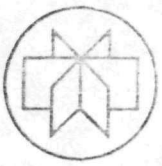

MASTER

STATE UNIVERSITY OF NEW YORK AT BUFFALO

NEW APPROACHES FOR THE REDUCTION OF PLASMA ARC DROP IN SECOND-GENERATION THERMIONIC CONVERTERS

FINAL REPORT

by

M.E.Hatziprokopiou and D.T.Shaw

Laboratory for Power and Environmental Studies

Faculty of
Engineering and
Applied Sciences

DISCLAIMER

NEW APPROACHES FOR THE REDUCTION OF PLASMA ARC DROP IN SECOND GENERATION THERMIONIC CONVERTERS

FINAL REPORT

by

M.E.Hatziprokopiou and D.T.Shaw

Prepared for

Owen Merrill

Department of Energy
Office of Coal Utilization
Washington, D.C.

Southeastern Center for Electrical Engineering Education
11th & Massachusetts Ave.
St. Cloud, Florida

Contract No. DE-AC02-79ET15421

March 31, 1981

TABLES OF CONTENTS

NOTICE

ACKNOWLEDGEMENT

We would like to thank Dr. Owen Merrill, Fossil Energy, Office of Coal Utilization, Department of Energy and Dr. James F. Morris, Space Power and Advanced Energetics, NASA, for their support and initiative which helped to insure the successful completion of this project.

LIST OF FIGURES

LIST OF TABLES

ABSTRACT

This work investigates ion generation and recombination mechanisms in the cesium plasma as they pertain to the advanced mode thermionic energy converter. The changes in plasma density and temperature whithin the converter have been studied under the influence of several promising auxiliary ionization candidate sources..

Three novel approaches of external cesium ion generation have been investigated in some detail, namely vibrationally excited N_2 as an energy source of ionization of Cs ions in a DC discharge, microwave power as a means of resonant sustenance of the cesium plasma, and ion generation in a pulse N_2-Cs mixture.

The experimental data obtained and discussed in this work show that all three techniques -i.e. the non-LTE high-voltage pulsing, the energy transfer from vibrationally excited diatomic gases, and the external pumping with a microwave power - have considerable promise as schemes in auxiliary ion generation applicable to the advanced thermionic energy converter.

I. INTRODUCTION

Thermionic energy conversion is a method for converting heat directly into electicity utilizing the phenomenon of thermionic emission of electrons. The thermionic converter, in it's most elementary form, consists of one electrode connected to a heat source, a second electrode connected to a heat sink and separated from the first by an intervening space, leads connecting the electrodes to the electrical load, and an enclosure, as shown in Fig. 1. The space in the enclosure is either highly evacuated or filled with suitable rarefied vapor. It may thus be considered to be, in thermodynamic terminology, a heat engine whose working fluid is the electron gas. The basic phenomena characteristic of thermionic conversion can be conveniently divided into two classes, emission and transport phenomena.

The most significant transport phenomenon is the negative electrical charge of the electrons in transit in the interelectrode space (see Fig. 1). These electrons constitute a negative space charge. Unless precautions are taken to suppress the electrostatic effects of this negative space charge, the current flow through a thermionic converter is greatly reduced. The suppression of space-charge effects is the contemporary development that permitted efficient energy conversion to be obtained. The suppression can be achieved by a variety of methods, in our case by adding cesium into the converter. Thermionic converters are of great practical interest since they are characterized by a wealth of attractive features:

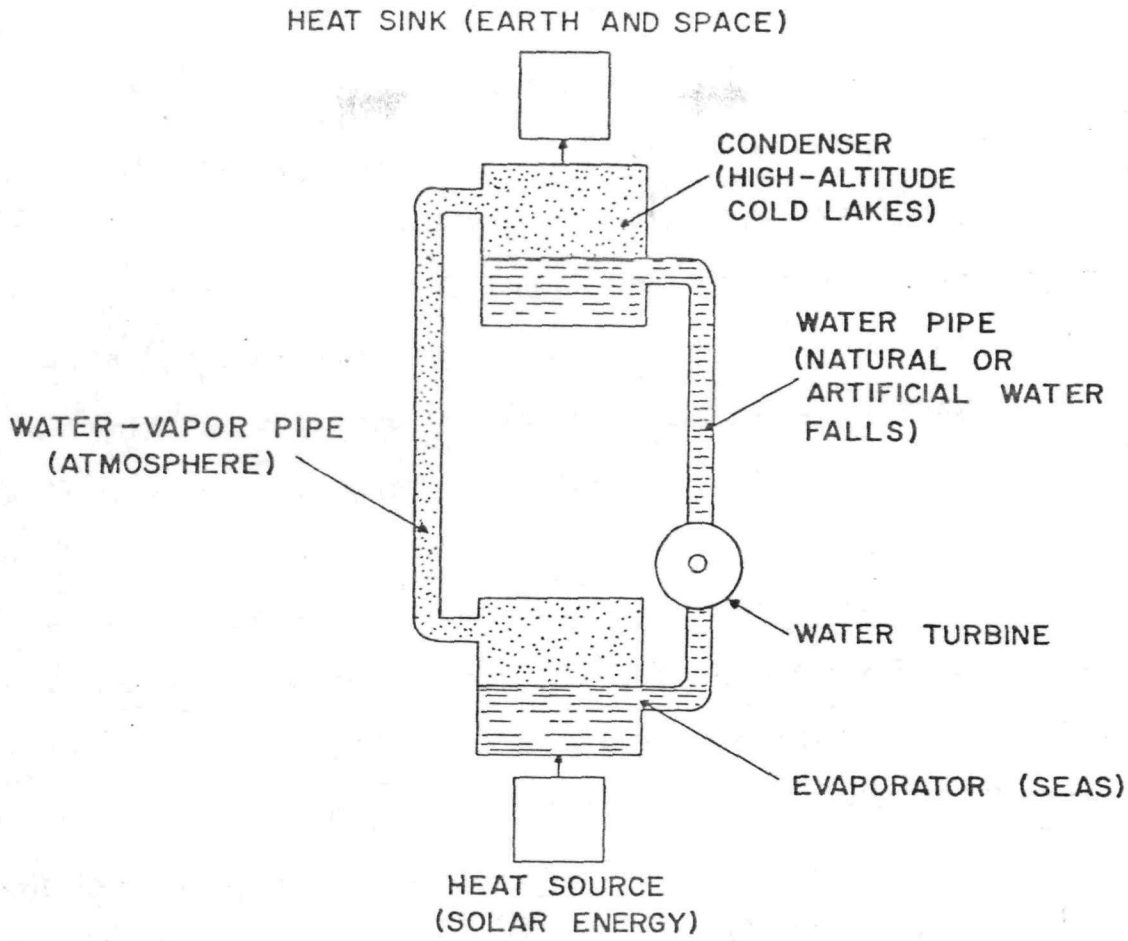

(b) Vapor cycle analogy to a thermionic converter.

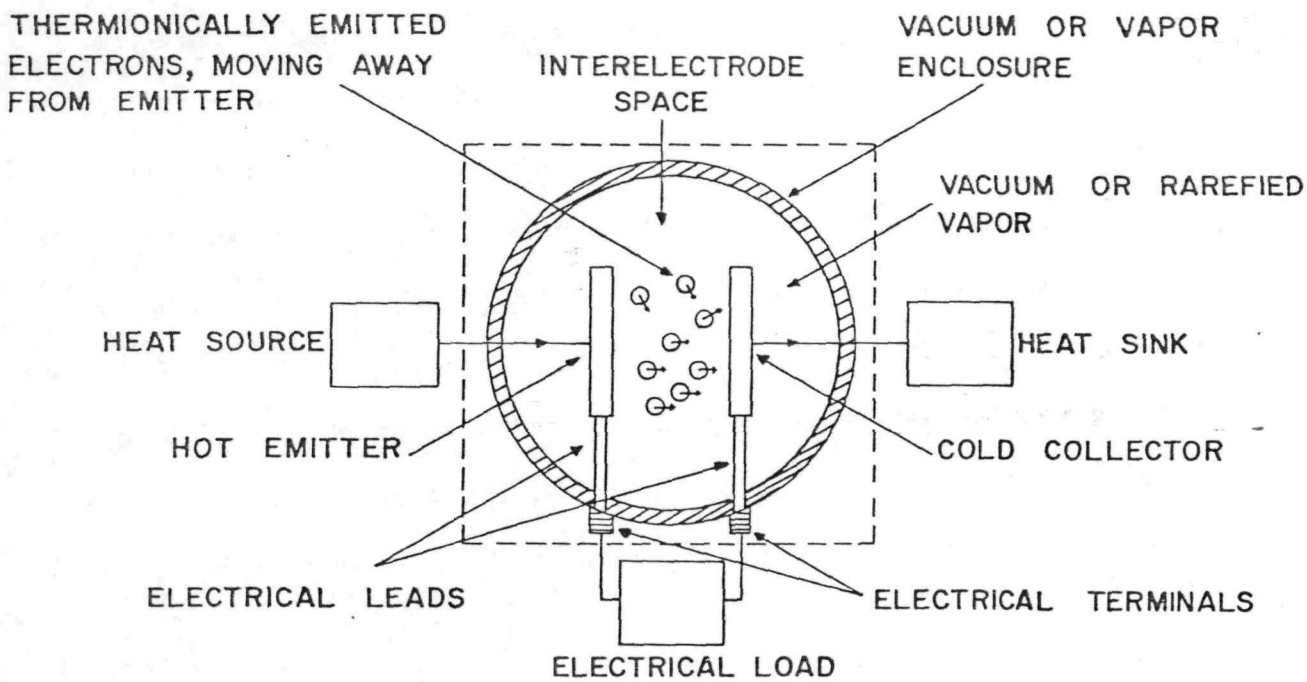

(a) Essential components (inside dashed box) and processes of a thermionic converter.

Fig. 1.

1) No moving parts,

2) Heat rejection at relatively high temperatures,

3) Heat input at very high temperatures,

4) Lends itself to modular construction,

and 5) Potential for efficiencies up to 40%.

Thermionic converters are originally developed primarily for use in the space program. Their high efficiency at high heat rejection temperatures and the high reliability that results from their static modular structure make them particularly well suited for this application.

This is the first generation of thermionic converters where the emitter material is of refractory metals (mostly tungsten and molybdenum) because they can tolerate high temperature.

However, thermionics has yet to achieve practical application because the emitter temperatures currently required for competitive power densities and efficiencies limit the operating life of the "hot shell" (i.e. the protective structure which isolates the converter, per se, from the combustion atmosphere) to several hundred hours only. In order to reduce the operating temperatures of converters to levels so that the hot shell will have greatly extended life while maintaining converter efficiency, it is necessary to develop improved emitter and collector surfaces as well as decrease the plasma losses occuring as the electrons flow across the interelectrode space.

In the advanced thermionic converter (also called second generation) intended for use in terrestrial applications, the emphasis is now in the improvement of efficiency and in reduction of costs. To reduce cost, the

emitter must operate at a temperature where the more popular stainless steel can be utilized to replace expensive and difficult to machine refractory metals. In the development of the second generation thermionic converters, there are some drastic changes in the uprating parameters which can be listed as follows:

1. The emitter temperature drops from 2,000°K to 1,400°K.
2. The interelectrode space is relatively wide, probably 0.5mm or larger.
3. The output current is decreased some what, but still is relatively high of the order of 0.5amp/cm^2.

It is immediately noticeable that we are demanding a surprisingly large reduction of the emitter temperature, and at the same time producing a relatively high diode current output. The consequence of the temperature reduction, is to reduce the capability of the emitter as a positive ion generator. Consequently, the converter must operate with external positive ion sources. Different theories and schemes have been proposed for the improvement of the converters. It is S. Lam[1] who approached the problem from a new point of view.

In his theoretical investigation of the performance of the advanced thermionic converters, Lam has reached the following conclusions about plasma arc drops:

1. The normalized plasma resistance is relatively constant and has a theoretical minimum value under the practical constraints and the assumption that a motive peak exists in the emitter sheath.
2. The plasma density required to significantly affect the existence of the motive peak is of the order of $10^{13} - 10^{14} cm^{-3}$.
3. After the motive peak is suppressed further increase of plasma

density will lead to the significant reduction of the plasma arc drop.

In his analysis, Lam assumes that the positive ions are provided at no energy cost to the converter. Thus all the three constraints concluded from his analysis had nothing to do with the ion generation efficiency in the space. This come as quite a surprise since there is a general feeling that the reduction of plasma arc-drop might depend on the improvement of ionization efficiency which is considered to be very low. The so-called spontaneous ionization mechanism which is responsible for the ion generation in the first-generation converter relies on the electron in the Maxwellian tail to provide the energetic electron impact process. Lam assertes that since the number of ions needed for space charge neutralization is so small that the efficiency of the spontaneous ionization processes is of secondary importance in comparison with the inefficiency of electron transport across the interelectrode spacing.

The principal inefficiency in electron transport comes from the fact that the current output from the converter is essentially maintained the same when one changes from the first generation to the second generation, despite the fact that emitter temperature has significantly dropped from the original 2000^{o}K to 1400^{o}K for the second generation converters. For a given value of the current output, if the plasma density is significantly reduced, as in the case for the second generation converter, the required electron flow velocity must be increased. This large drift velocity leads to large momentum losses between collisions, which is causing a very large resistivity loss in the interelectrode spacing. The only way to reduce such a large resistivity loss is to increase the ion concentration by some external

means so that the corresponding electron drift velocity can be reduced.

For the verification of this theory, two steps can be envisioned:

1) The motive peak is eliminated by some external energy pumping,

and 2) after the motive peak is eliminated, another ionization scheme by external source is used to increase the ionization level in the interelectrode spacing for the observation of possible plasma arc drop as predicted by the theory.

In the present work three novel approaches have been investigated as possible schemes in auxilliary cesium ion generation for the thermionic plasma discharge. These are a direct current discharge of a Cs - N_2 mixture, a pulse discharge of the same, and microwave pumping of the cesium plasma.

The use of molecular nitrogen in thermionic converters is attractive since it may be a way to reduce the large arc-drop in converters of appropriate geometry. The nitrogen molecules, when vibrationally excited, can be used as an energy storage medium, which in turn ionize Cs atoms. In this project a stationary system with a hot cathode has been utilized to study the interaction of N_2^* with Cs. Measurements have been carried out for a variety of mixing ratios, molecular nitrogen pressure in the range of 1 to 50 torr and cesium pressures between 0.01 and 0.2 torr have been employed. Spectroscopic measurements of the line emissions have been carried out as a function of discharge current as well as a function of position in the interelectrode gap. Studies of the discharge current-voltage characteristics and the corresponding line of the excited species allow for the evaluation of plasma density.

The behavior of a pulse mixture of molecular nitrogen and atomic cesium has been studied for a variety of mixing ratios in the plasma afterglow. The nitrogen pressure is in the range of 1 to 100 torr while the cesium

pressure is between 0.05 to 0.5 torr. A hot tungsten cathode is employed with an interelectrode separation of several millimeters. The characteristic emission lines of the excited species in the decaying plasma are studied as a function of position in the interelectrode gap for each mixing ratio. Enhanced emission line strength and unexpectedly long decay times are observed for mixing ratios of nitrogen to cesium of about 20.

Another interesting possibility is the application of microwave power into the interelectrode space in order to reduce the plasma resistivity. Measurements of the current-voltage (I-V) curves of the thermionic diode are made as a function of cesium pressure and applied microwave power[2],[3]. The double sheath ordinary erected in front of the emitter is found to disappear at higher power levels. It is also possible to deduce a qualitative description of the variation of plasma resistivity with the discharge parameters.

2. THE EXPERIMENTAL SET - UP

The set-up for each of the series of the experiments is generally very similar, yet slight differences exist, the changes tailored to the specific experiment. However there are many common elements, which will be described in this section.

All the designs and the experimental sequense used are done with the following considerations in mind:

a. Use of the minimum number of vacuum components possible. This sometimes means some loss of flexibility, e.g. the nitrogen gas line is shared with the vacuum line.

b. A strict cleaning procedure is utilized on each particular material in the vacuum chamber.

c. The only materials inside the vacuum system are 304 stainless steel, oxygen free copper, pyrex, and tungsten.

d. Outgassing for extended period at high temperature, i.e. $\geq 300^{\circ}C$.

Fig. 2 shows an overall picture of the standard experimental set-up. Particular variations will be shown in the individual chapters. Fig. 3 shows the individual components used.

The demountable cesium thermionic diode and vacuum components consist of an 1½ inch O.D. Varian stainless steel disk, the collector, separated by one half inch from a swirl tungsten emitter filament inside a pyrex glass envelope. Another arrangement includes an electron bombardment emitter in a stainless steel metal cross. The glass tube is connected to a double side conflat flange where two conections are made; one for the Cs reservoir and one for the N_2 gas inlet line (which also serves a second pumping port). Two bakeable valves are used to isolate the system just before

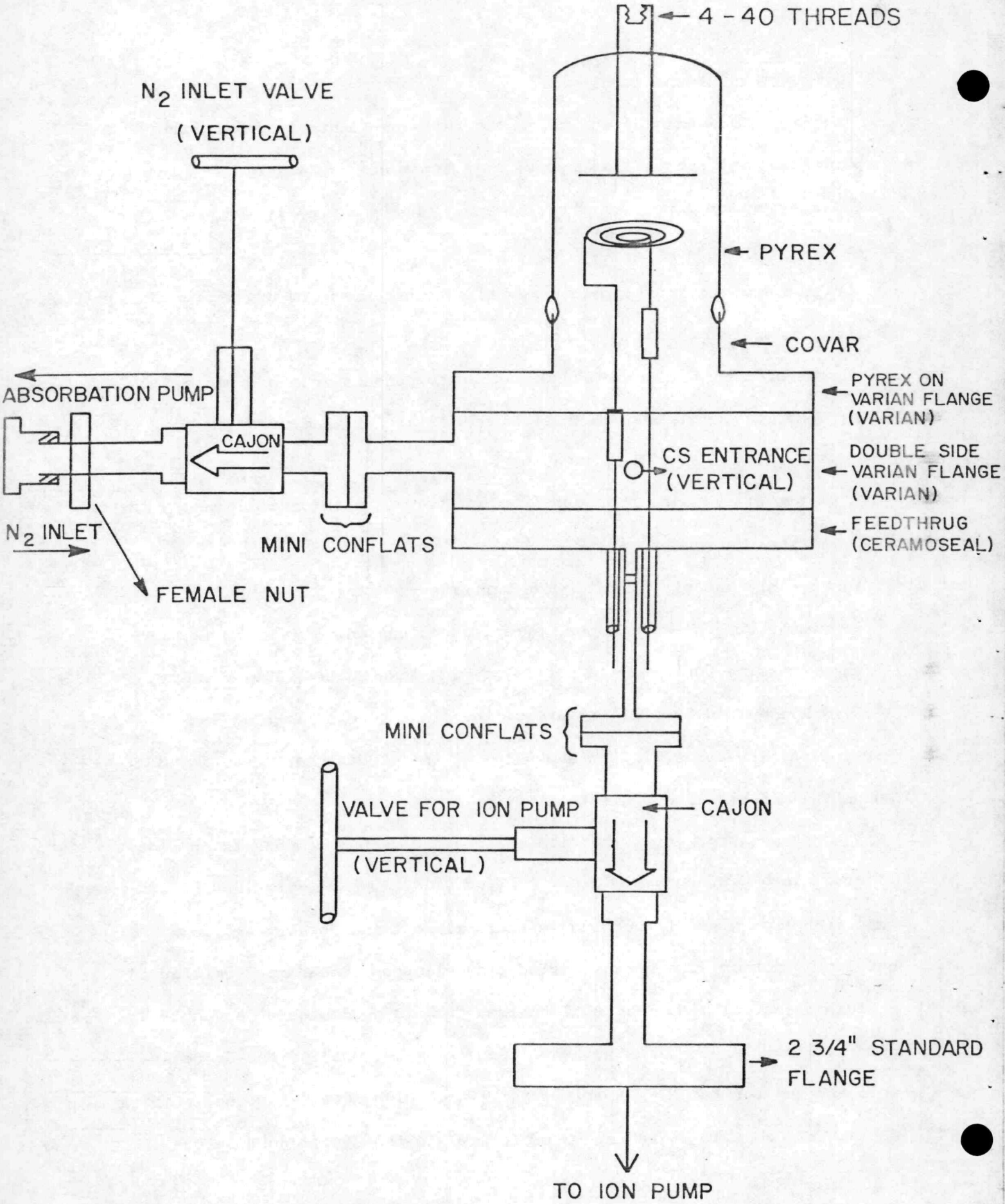

Fig. 2. Standard experimental vacuum set-up.

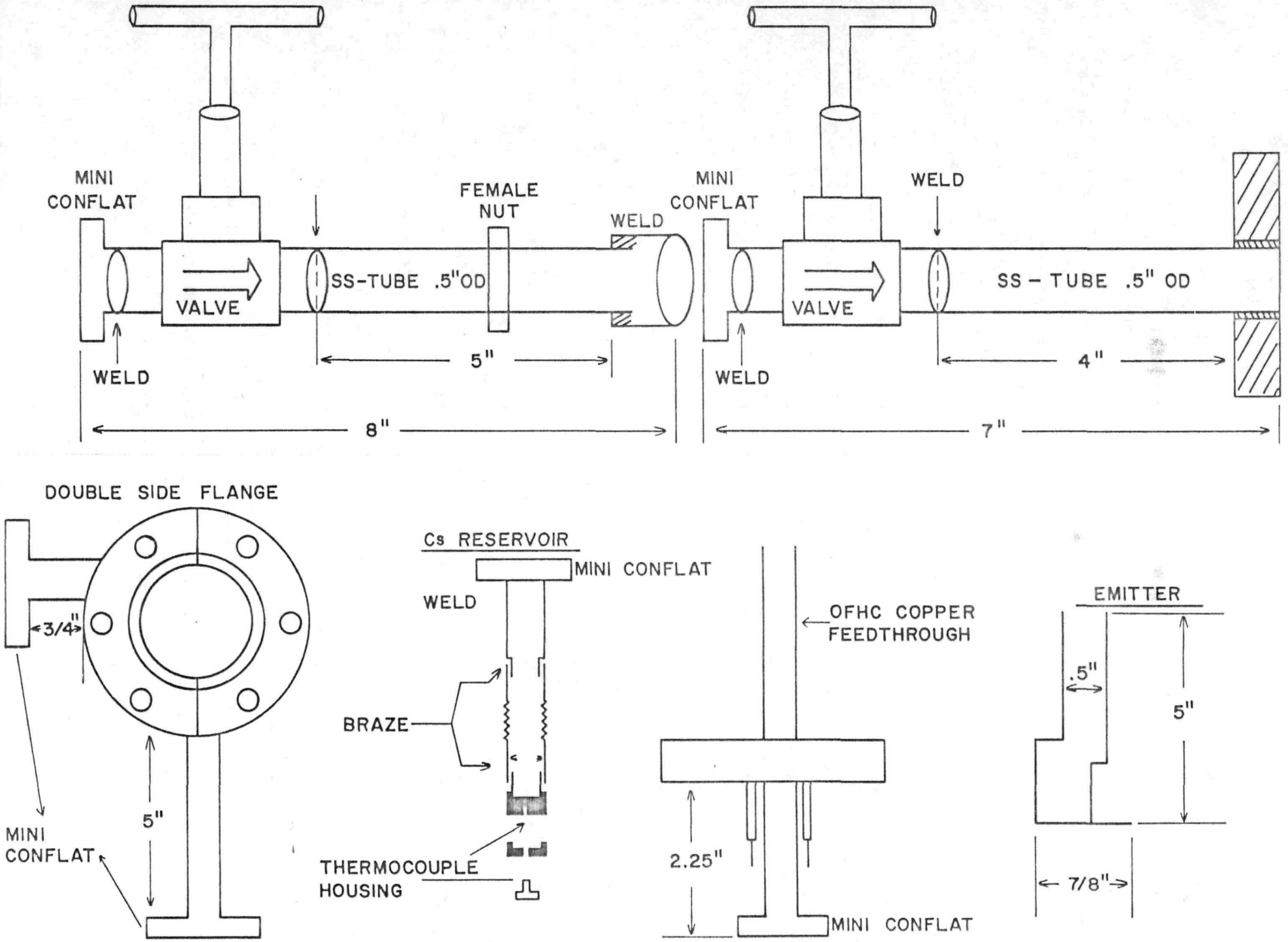

Fig. 3. View of individual components.

the Cs vapor is introduced.

The system is pumped down to a pressure of approximately 10^{-1} torr by an EDWARDS model EDM-12 mechanical pump, then down to $10^{-3} \sim 10^{-4}$ by a Varian absorption pump, and then differentially pumped from the two ports by two 20 l/s Varian ion pumps, while the oven is heated-up to 350°C for a week, until a residual gas pressure of less than 10^{-8} torr is reached. Then the temperature is reduced to the operating point and the emitter outgassed at 1500°C for 48 hours.

Next the bakeable valve is closed and the Cs vapor introduced to the system by braking the cesium ampule in the reservoir. The reservoir is heated in an oven located just below the oven of the converter diode. Temperature controllers are used to keep the oven at the desired temperature. Iron constantan thermocouples are placed at various positions for temperature measurements.

The cesium pressure in the experimental chamber is determined by the reservoir temperature which is established in the independent oven and controlled to ± 0.1°C. One of the thermocouples is mounted just below the cesium physical position. All other parts of the vacuum system in the cesium atmosphere are kept at a temperature at least 50°C higher than the reservoir temperature by another oven in order to avoid cesium cold spots. Temperature measurements are made at several judicious locations by iron constantan thermocouples.

Two double walled 2-inch thick asbestos ovens are constructed around the diode and cesium reservoir. In order to avoid noise from switching transients only variable autotransformers (VARIACS) are used instead of temperature controllers. Regular heating elements are used to heat-

up the two ovens. Two windows mounted on the walls of the oven facilitated the alignement of the optical system and permitted the collection of the light from the plasma discharge for the measurements.

The cesium vapor pressure in the diode is determined by assuming the vapor phase is in equilibrium with the liquid phase cesium in the reservoir at the reservoir temperature. To assure that the reservoir is the controlling element, the temperature at the diode is kept at least 50°C higher than the temperature at cesium reservoir. The relationship between the reservoir temperature and cesium vapor pressure is determined experimentally by Taylor and Langmuir in 1937[4]. Their results are summarized as follows

$$\log_{10} P_{Cs} = 10.5460 - 100 \log_{10} T_R - \frac{4150}{T_R} \quad T_R < 302^{\circ}K \qquad (1)$$

$$\log_{10} P_{Cs} = 11.0531 - 1.35 \log_{10} T_R - \frac{4041}{T_R} \quad T_R \geq 302^{\circ}K \qquad (2)$$

where P_{Cs} is the cesium vapor pressure in torr and T_R is the cesium reservoir temperature in degrees Kelvin. More recently, Shelton Wuerker and Sellen[5] and Marino, Smith and Caplinger[6] have repeated the measurements of Taylor and Langmuir and have confirmed them. In our case Eq. 2 is to determine the cesium vapor pressure, and the relationship between P_{Cs} and T_R is shown in Fig. 4.

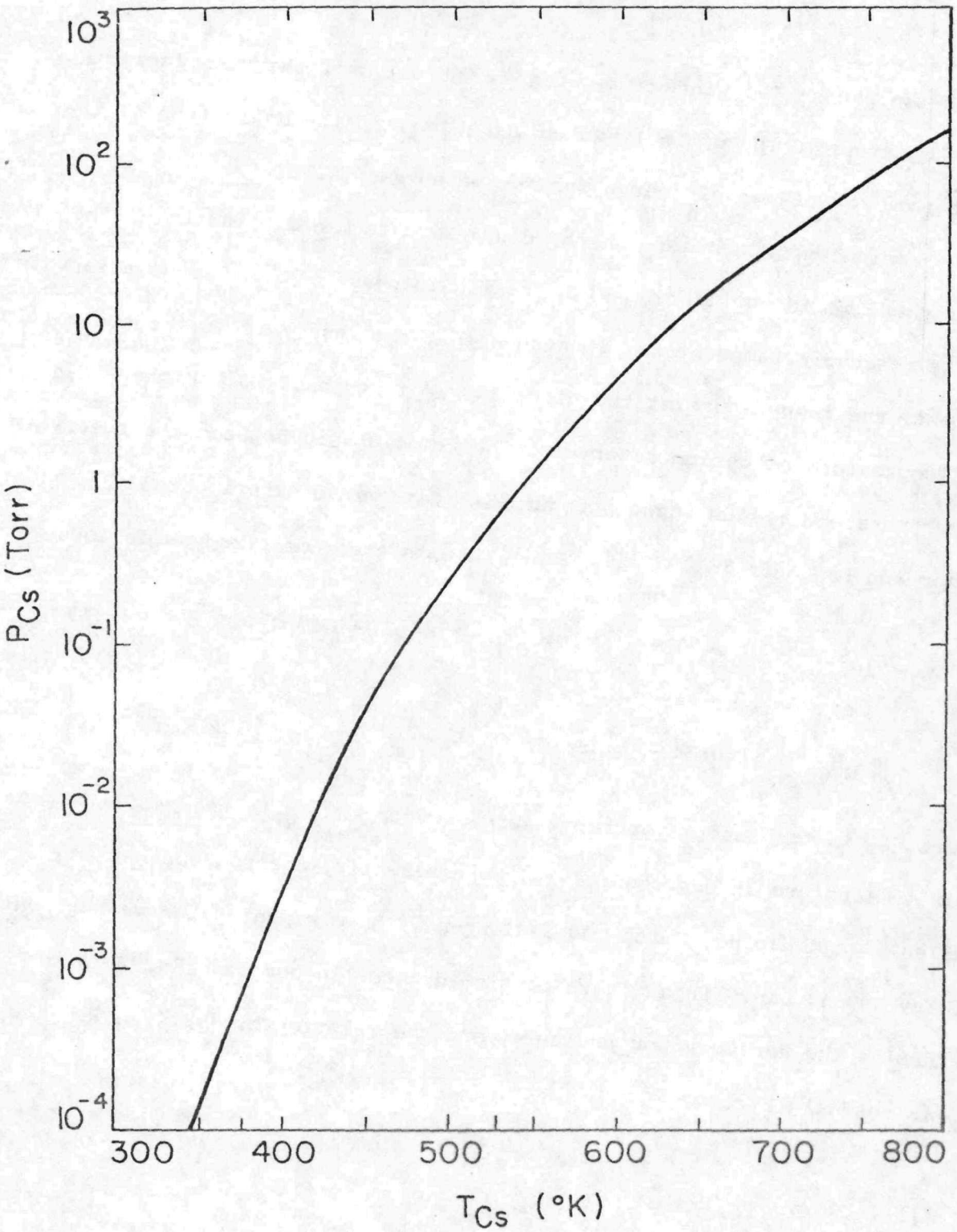

Fig. 4. Variation of cesium vapor pressure with cesium reservoir temperature.

3. THE ELECTRICAL, ELECTRONIC, AND OPTICAL MEASUREMENT TECHNIQUES

First, the emitter is heated with an NJE model TC-80-20 high current low voltage power supply (PS) and its temperature is measured with a MICRO OPTICAL PYROMETER mounted permanently on the optical table and focused at the emitter. The range of the pyrometer is 700-3200^{o}C. Then the discharge is created. Since each experiment has its own different way of producing the plasma, appropriate details shall be given at the corresponding sections.

Second, because of the low intensity light output and the limitations of the spectroscopic measurement method used, one has to use the best possible optical arrangement. To facilitate the optical alignement, the oven has been built with two windows along the axis of the interelectrode space. During the focusing procedure a high power light output beam (200,000 candles) is placed at one window to illuminate the emitter-collector space. At the second window the light is collected with the optical system which is shown in Fig. 5, and the image of the discharge section is projected on the entrance slit. In this way, the specific point to be studied can be precisely selected and focused. Next (as shown in Fig. 6) the light travels through an Ebert-Turner (Jarrel-Ash. model 82-020) monochromator which can be moved precisely perpendicular to the optical axis of the plasma column. The exit slit of the monochromator is fixed at 15μ while the entrance slit is varied between 15μ to 250μ depending on the kind of measurements. At the exit slit an EMI photomultiplier tube (PMT) model 9658A is mounted inside an EMI FACT-50-MK II thermoelectric cooler. A high voltage power supply, Pacific model 7102, is used to supply the photomultiplier tube, which is operating at -1300 Volts

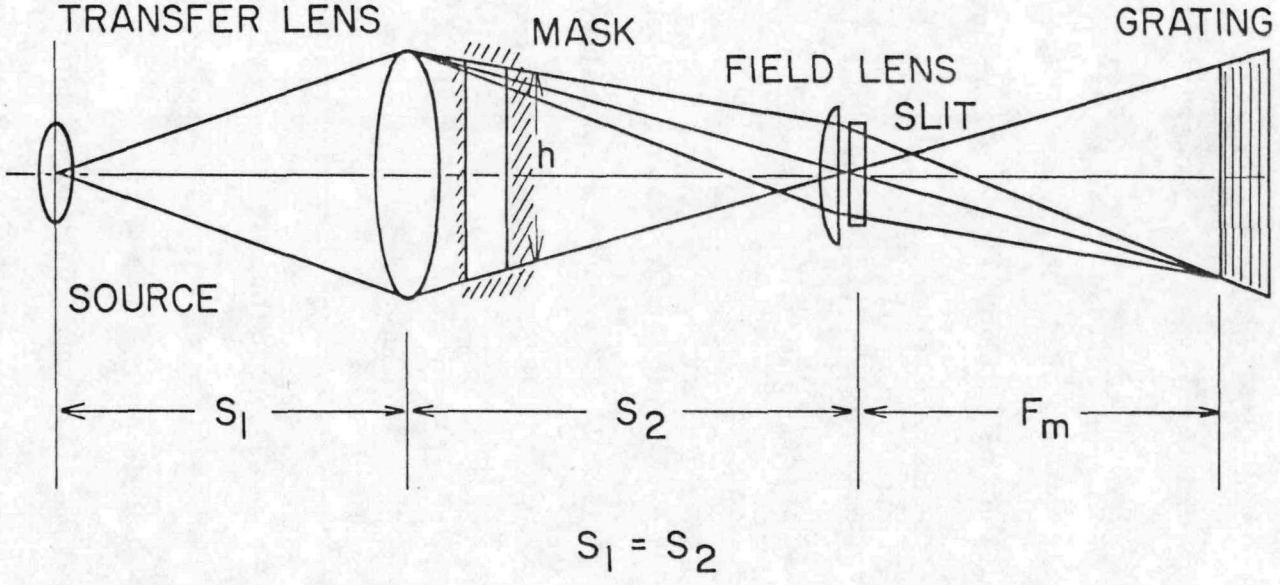

Fig. 5. Optical system.

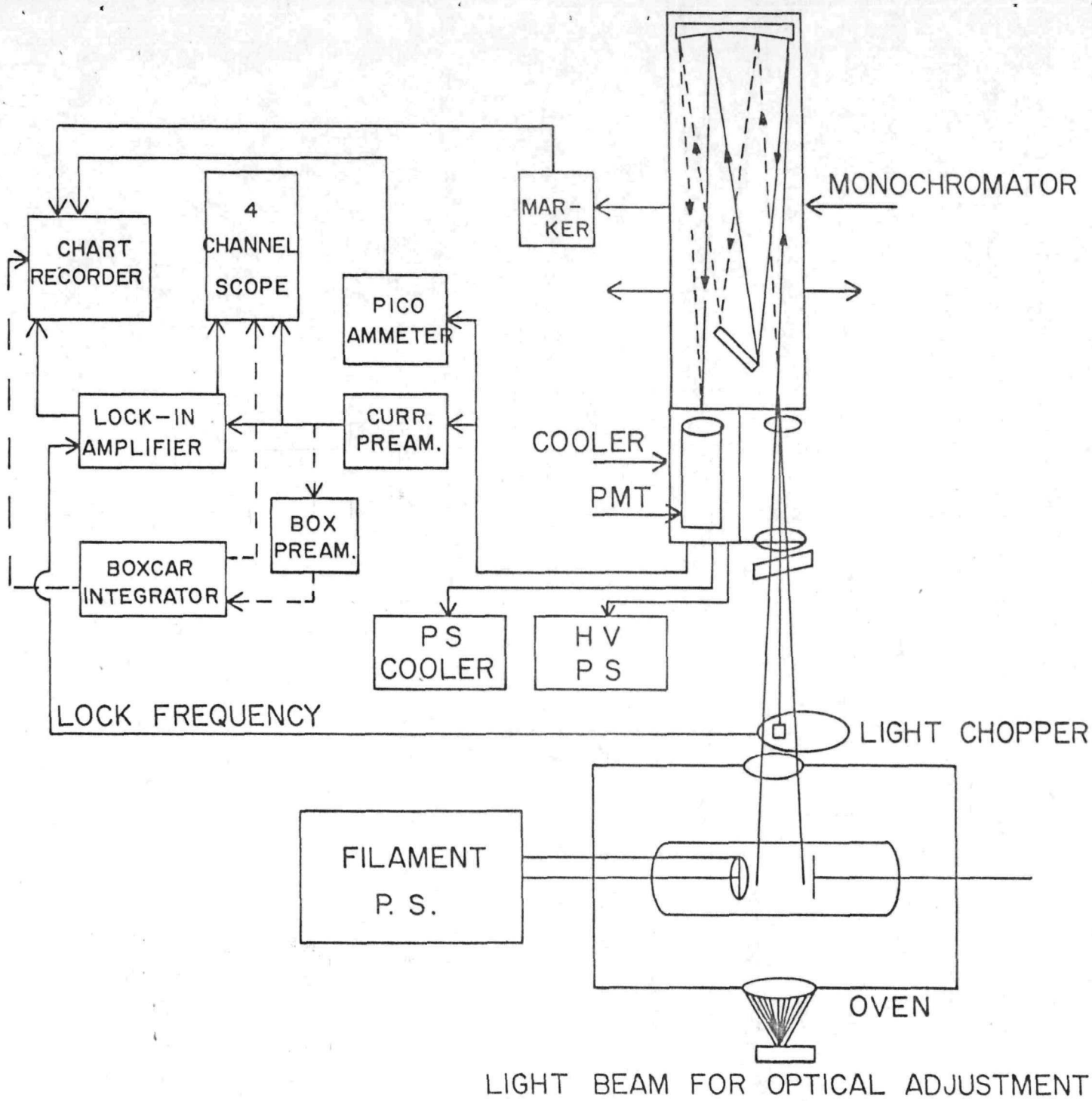

Fig. 6. Schematic drawing of the spectroscopic apparatus and associated electronics.

bias and -26°C (the dark current is reduced by two orders of magnitude because of the low temperature as it is shown in Fig. 7). Because the PMT is under high voltage, i.e. high gain and very low residual dark current condition, as would be encountered in a cooled environment, the outside glass side walls of the tube is coated with a black conductive material (Hydrograf, Grafo Celloids Corp.) electrically connected to the high voltage of the tube. This has eliminated scintillations in the glass walls due to internal potential charging. Then the output is amplified by a Princeton Applied Research (PAR) model 181 current sensitive preamplifier, or by a Keithley model 410A picoameter. The output is then routed to a PAR boxcar signal averager model 160 for the pulse discharge case or to a PAR lock-in amplifier model 126 for the DC case. The latter is locked to a chopping frequency of 833 Hz from a mechanical light chopper.

The outputs are monitored with a two beam four channel model 551 Tectronix oscilloscope and recorded with a Heath-Schlumberger model SR-205 chart recorder. Both the chart recorder and the monochromator are synchronized by an event marker which is triggered by the monochromator and produces outputs selectively every 10, 100, 200, 500, or 1000 Å. Details are shown in Fig. 8.

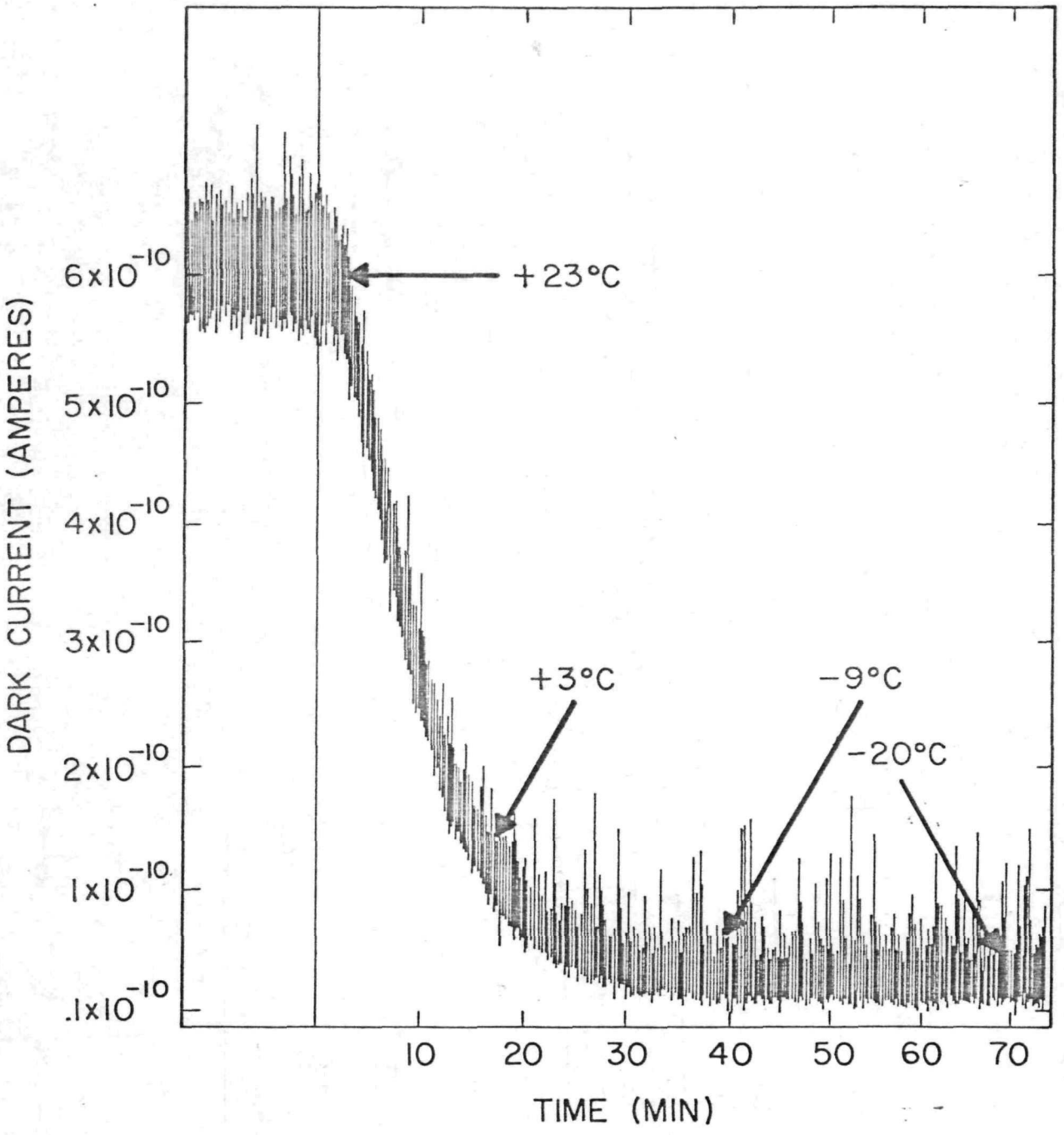

Fig. 7. Dark current reduction as a function of time and temperature.

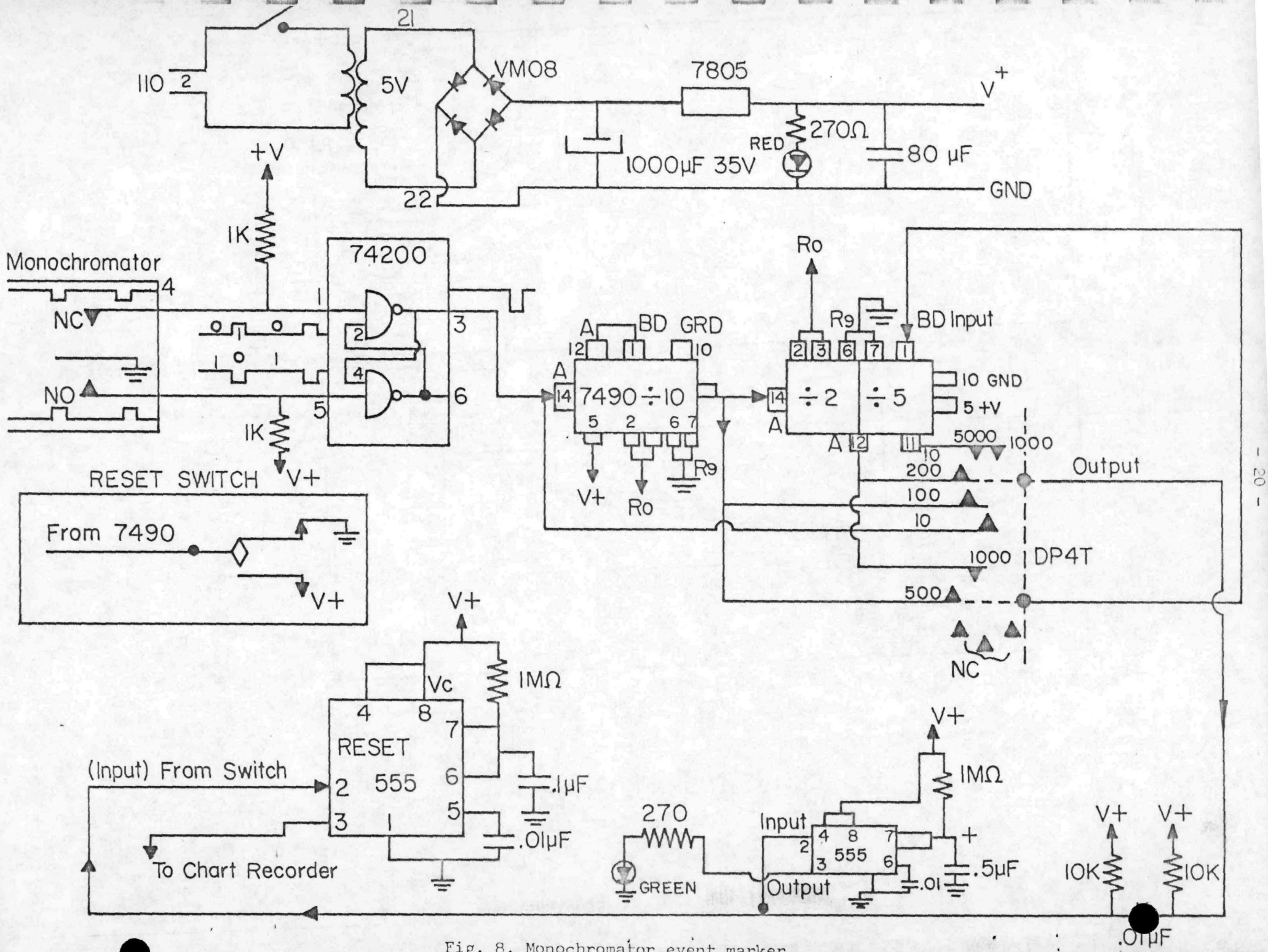

Fig. 8. Monochromator event marker.

4. MICROWAVE PUMPING

a. Theory

This section deals with the investigation of the potential of applying microwave power in the interelectrode spacing of the converter as an external ion generation source. It has long been known, from fusion plasma research, that by applying microwave power to a plasma discharge it is possible to raise the plasma density, as well as the plasma temperature.

Such a plasma generation scheme is very attractive because of the simplicity of application (electrodeless), high flexibility in adjustment of the operation parameters (frequence and power) and high efficiency in the generation of microwave power from line power (better than 50%).

Moreover, it allows for continuous as well as pulsed operation and the possibility of utilizing resonant cavity configurations to introduce the microwave power which may lead into lower losses. Also clearly minimal disturbance would result to the emitter and collector surfaces. This is very important in view of the fact that to date these surfaces have been optimized in performance more or less independently of the thermionic plasma.

Furthermore, utilization of microwave energy for plasma support offers the possibility of utilizing resonant configurations with well established plasma configurations and low losses.

An RF discharge in a plasma depending on the background pressure and driving frequency can be classified in three kinds:

a. multipacting plasma

b. resonantly sustained plasma

c. diffusion controlled plasma

At pressure of approximately 0.1 torr, collisions are dominant in the plasma. This type of plasma is called a diffusion controlled discharge. At lower pressure of about 10^{-3} torr, the RF plasma has the characteristic of a plasmoid which is characterized by its sharp luminous boundaries and the fact that it can be maintained by a relatively low power driving source, and is called a resonantly sustained discharge. For very low pressure, approximately 10^{-5} torr, the plasma is a multipacting discharge.

Taillet[7] observes that in resonantly sustained plasmas, the electric field in the plasma is much larger than the field without the plasma. The reaction of an ionized gas to very high frequency electric waves has been the subject of many investigations. Oscillations in the neighborhood of 10^9 hertz have originally been found by Penning and further investigated by Tonks and Langmuir using the low pressure mercury arc. They find that the observed high frequency oscillations corresponds to the plasma electron oscillations as shown in Fig. 9 and to the equation shown below:

$$f_p = (N_{res} e^2 / \pi m_e)^{1/2} = 8980 \, N_{res}^{1/2}, \qquad (3)$$

where f_p is the oscillation frequency, m_e is the electron mass, N_{res} is cut-off or critical density, and n_p is the plasma density. Clearly, if the applied frequency is the same as the plasma electron oscillation frequency, the plasma will absorb most of the applied power and will resonate.

An important property of plasma oscillation is that half period represents a response time in which the plasma reacts to an externally applied electric field. Hence if a microwave radiation f_m is applied to a plasma where the plasma electron oscillation frequency f_p is larger than f_m, electrons will move so as to oppose the applied field by setting up a

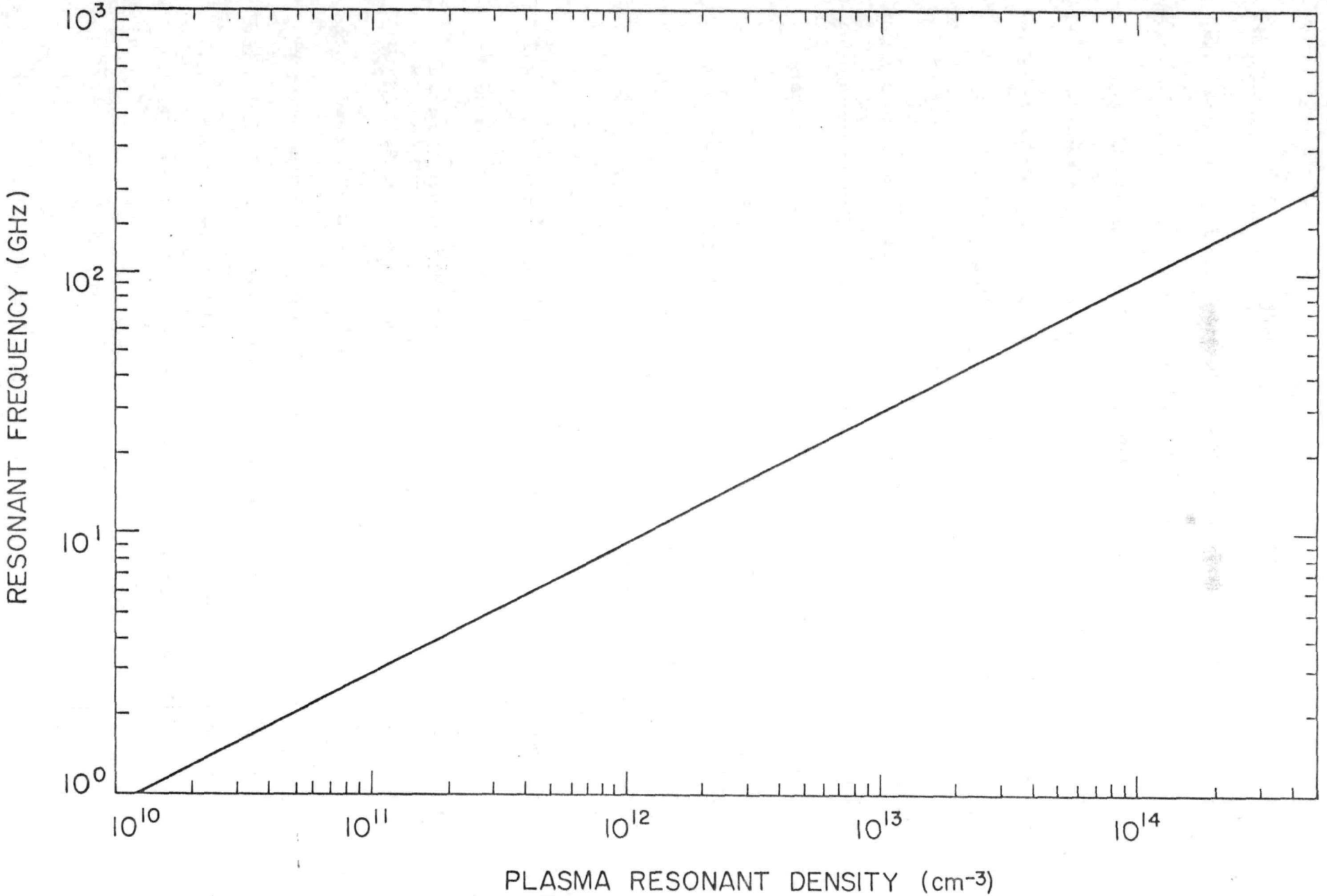

Fig. 9. Plasma resonant frequency versus resonant density.

field between them and the stationary ions. The shielding movement tends to reduce the net field in the interior of the plasma to zero. However, if $f_m > f_p$, the electrons cannot respond rapidly enough to cancel the externally applied field, and consequently the field penetrates the plasma. Thus for $f_p / f_m < 1$, the field penetrates the plasma or the plasma is transparent, where as for $f_p / f_m > 1$, the electron motion shields the interior and the plasma is opaque to the externally applied fields.

A bounded plasma in a hollow enclosure exhibits resonance responce to an applied electromagnetic field. The state which corresponds to a plasma density of N_{res} (cut-off or critical density) is dynamically unstable and the plasma cannot be sustained at this value at the steady state.

If the tuning of the waveguide is proper and the power enough, then the plasma density can be significantly increased. Fig. 10 gives a satisfactory explanation for the fact that it is able to sustain the plasma above critical density. In this figure a family of curves is presented corresponding to different values of incident power. Also shown in Fig. 10 is a power loss line which represents the power lost in the plasma due to inelastic ionization, excitation, and diffusion losses to the walls. For an incident power of magnitude of P_2, there are two points where the power absorbed by the plasma is equal to the power lost by the plasma. In resonantly sustained plasma, the power absorbed is indeed equal to the power loss in the plasma. Thus with steady operation of incident power P_2, there are two equilibrium states A and B as shown in Fig. 10. State B is in a stable equilibrium because at point B, any reduction in the plasma density has the tendency to increase the power absorbed by the plasma, which in turn causes an increase in ionization, hence increases the plasma

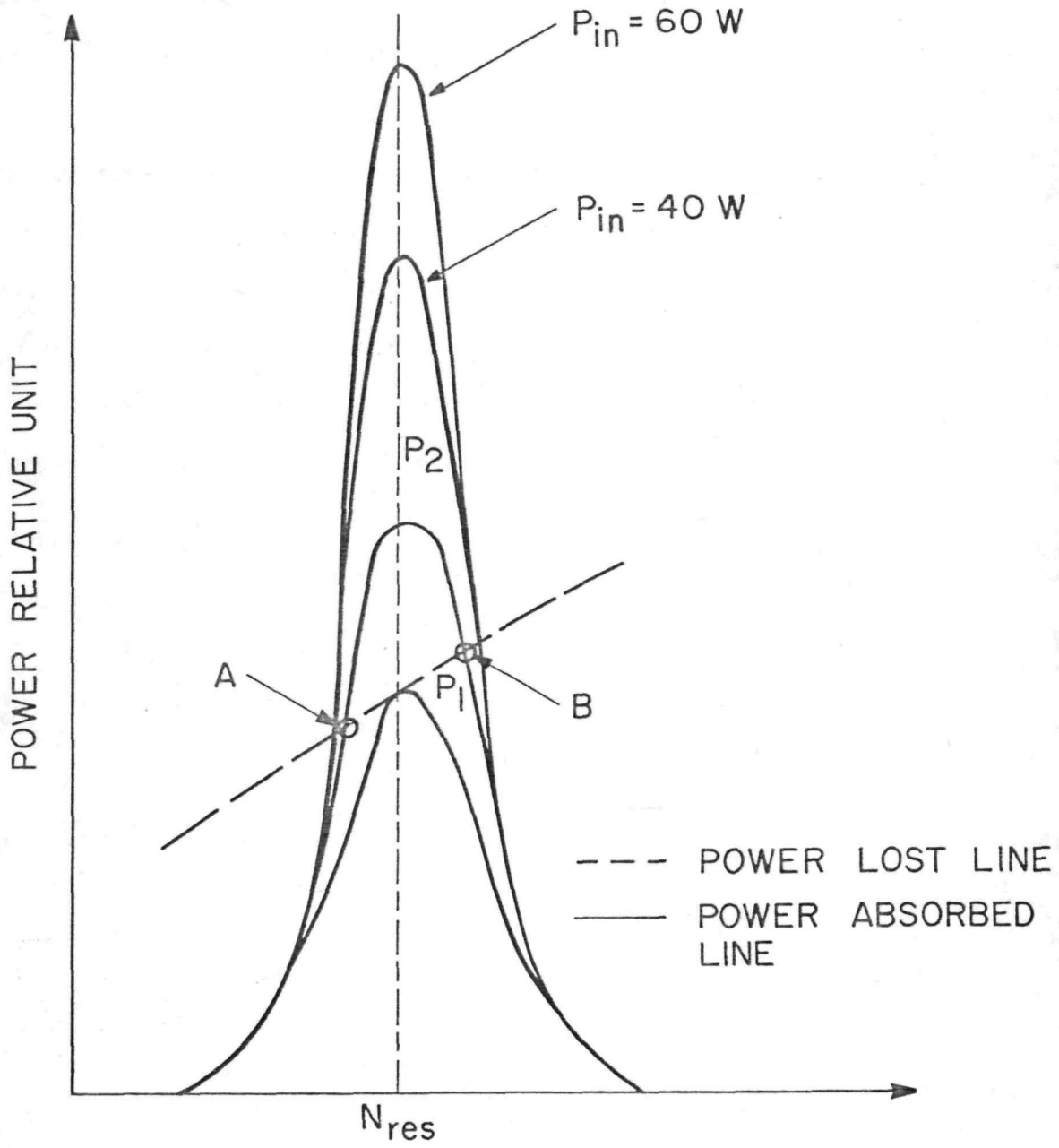

Fig. 10. Power absorbed and lost versus plasma density.

density. On the other hand an increase in plasma density at point B has the tendency to reduce the power absorbed by the plasma, which in turn causes a reduction in the plasma density. Hence state B is in stable equilibrium.

Similar reasoning shows that point A is unstable because an increase of plasma density will increase the absorbed power, which will eventually bring the plasma to point B. But a decrease of the plasma density at point A will extinguish the plasma. So point A is unstable. The resonantly sustained plasma density must be above N_{res} where the plasma begins to be opaque to the applied field. That is why it is very difficult to resonantly sustain a dense plasma.

b. Experimental Apparatus and Results

A sketch of the microwave transmission and measurement system is shown in Fig. 11 . The microwave signal is generated by a microwave power generetor, equiped with a power meter, and an output of 100 watts which supplies the tunner and wavequide.

A circulator is installed between the travelling wave tube (TWT) and the rest of the system to protect the TWT's output helix from damage by the reflected microwave power. The third port of the circulator is connected to a matched load which can absorb up to 150 W of reflected power.

A pair of directional couplers are used to measure the incident and reflected power. The reflected signal power level is measured by a power meter and is displayed on an oscilloscope. It serves to indicate the resonance condition. A section of coaxial slotted line is used to measure the input impedance of the cavity. A reference plane is established on the slotted line for a short circuit load. The phase of the cavity impedance is measured by the difference of the null and the reference plane in the SWR pattern which also serves as an indication for a resonant condition of the plasma-cavity system.

The basic task of the experimental structure is to provide for the application of microwave power into the interelectrode spacing of a thermionic converter. Several techniques have been used in the past to couple microwave power into a plasma load. The two most common and successful have been to either locate the plasma column along the axis of a resonant cylindrical cavity or to introduce it into a waveguide in a direction perpendicular to the broadside of the rectangular guide. It is important that proper coupling provisions be made in order to match the microwave transmission

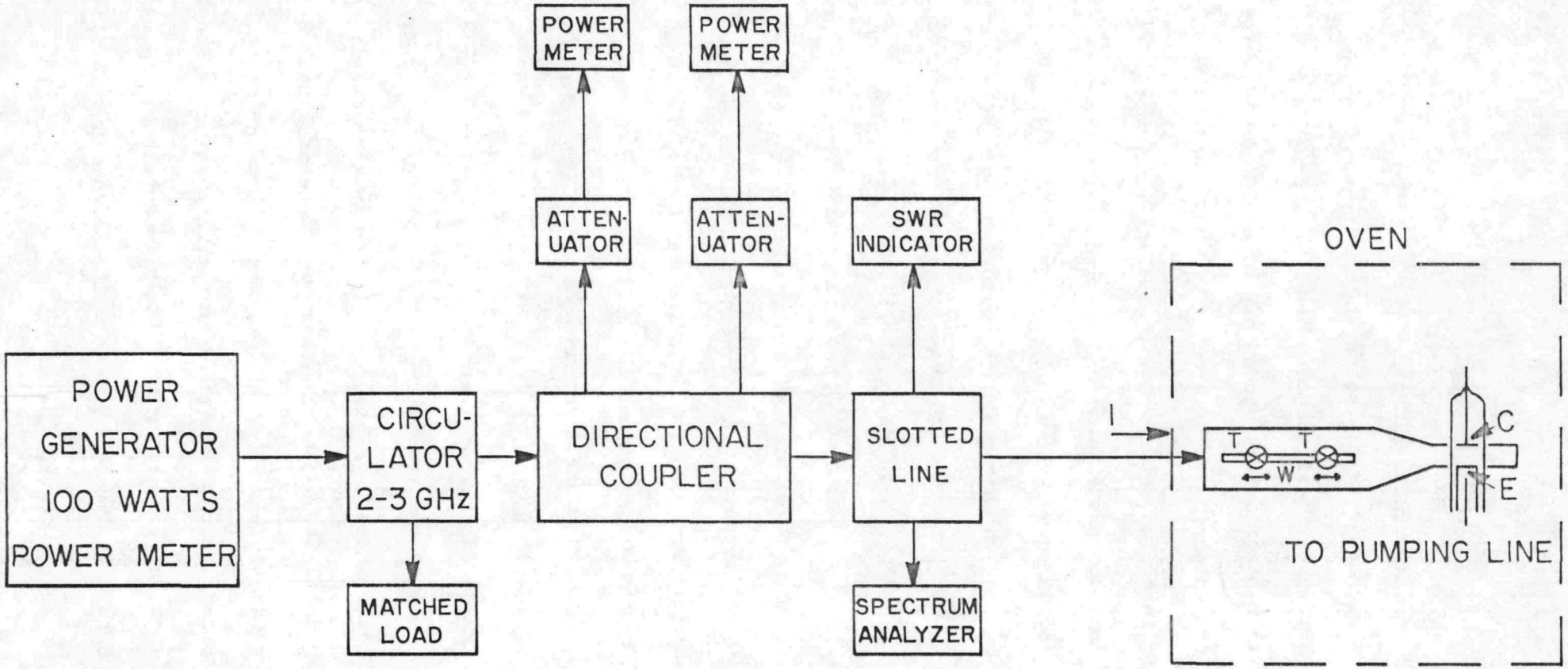

Fig. 11. Microwave set - up.

line to the plasma load so as to make accurate microwave power consumption measurements at the load possible.

The axis of the converter diode is aligned to be perpendicular to the broad side of this waveguide and thus parallel to the local microwave electric field lines in the guide in the TE_{10} mode. This scheme has been very successful in terms of operational ease and measurement accuracy of the consumed microwave power.

When a resonant cavity is used the resonant frequency and the Q of the empty cavity change substantially when the cavity is loaded by the plasma. It is difficult under these circumstances to initiate and sustain a microwave discharge without tedious adjustments. Thus it is necessary to start the discharge by DC applied voltage, raise the current to the desired operating level, and then turn on the microwave power, tune the cavity and adjust the coupling in the microwave line for the best impedance match and finally slowly turn off the applied DC power while keeping the microwave power to the plasma load constant.

The electrical circuit configurations used to discharge the plasma are shown in Fig. 11. Rectified alternating current (AC) signals are used to ignite or discharge the cesium plasma. A variable non-inductive resistor is connected in series with the power supply as a ballast resistor to limit the diode current. A 220 V AC power supply is stepped down to 120 V AC through an isolation transformer to discharge the plasma. With AC discharge, the I-V characteristics can be displayed on an oscilloscope. In the AC discharge circuit, a rectifying diode is used in series with the AC power supply so that most of the negative voltage cycle is rectified.

The performance of a thermionic converter or diode can be improved

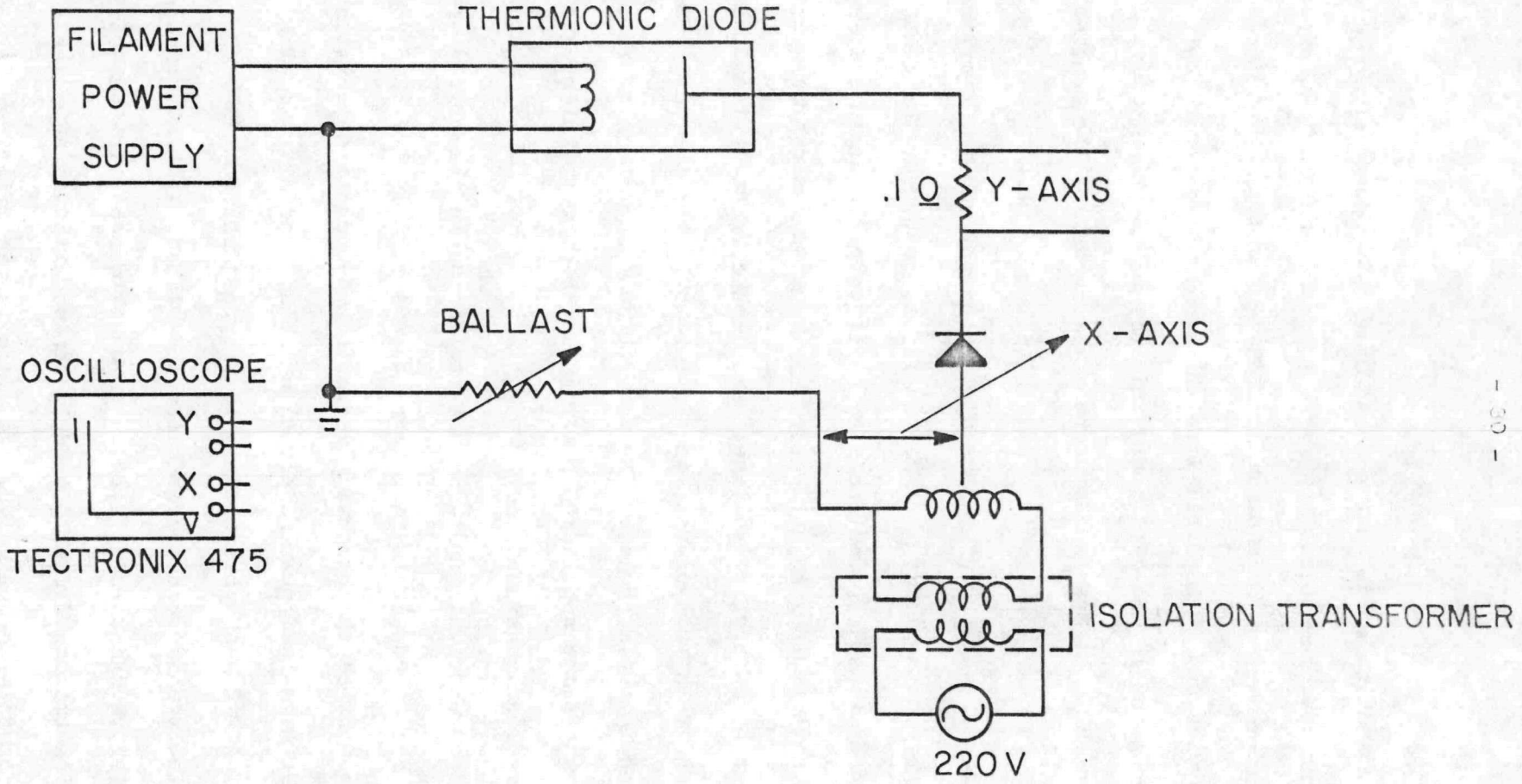

Fig. 12. Thermionic diode electrical circuit set - up.

substantially by lowering the plasma arc drop. The quality of the performance of a converter diode can be deduced from its I-V characteristic curve. The transition point (the "knee") of an I-V characteristic curve of a thermionic diode is also the point of maximum performance of the diode at a certain emitter temperature. The arc drop voltage of the diode measured at the transition is the potential drop across the interelectrode space required to produce just enough ions to balance the plasma losses. In order to maintain the plasma density level, the electron temperature of the plasma must be sufficiently high to produce ions as rapidly as they are lost by the diffusion to the electrodes and by volume recombination. So the reduction of the arc drop voltage of the diode when the plasma is sustained by microwave power can be measured from the shift of the output voltage at the transition point when the I-V curves with or without applied microwave power are compared.

The experiments are carried out under the following conditions:

1. The cesium reservoir temperature ranges from 150^{o}C to 200^{o}C which corresponds to a relatively low cesium pressure from 0.01 to 0.1 torr.
2. The emitter temperature is about 1300^{o}K, which implies an emitter current density of the order of or less than 1 amp/cm^{2}.
3. The microwave power level consumed by the thermionic converter plasma varies from 0 to 5 watts.

It is immediately evident that the thermionic diode is not operated at the optimum performance region or the positive power quadrant. This is not important in this work since the interest lies in the understanding of the plasma properties of the thermionic converter distinct from the

emitter and collector surfaces.

The I-V characteristic is measured either on the oscilloscope or a recorder. Quasi-DC rectified 60 cycle AC electrical power is applied both to ignite or discharge the cesium plasma.

It was expected that the application of microwave power would raise the plasma density and temperature and thus significantly alter the characteristic I-V curves. Numerous curves are obtained but it is found that the important features of the results can be demonstrated by a detailed analysis of the I-V traces obtained at microwave power levels of 0, 1 and 2 watts.

The I-V curves shown in Fig. 13a, exhibit a most dramatic effect displayed by the ignition traces (i. e. increasing voltage) of the thermionic converter. When no microwave power is applied one gets, as expected, the usual I-V curves characterized by a breakdown voltage as signified by the knee of the curve. However, upon application of microwave power the knee of the I-V curve disappears completely and no breakdown voltage is indicated any more. Indeed, current conduction is observed at zero voltage and even at negative applied voltage indicating that there is conversion of microwave power in DC electrical output power.

The return traces of the I-V curves (decreasing applied voltage) shown in Fig. 13b also demonstrate important differences revealed in the amount of current that can be carried by the plasma under the same applied voltage; considerably more current can be carried when microwave power is applied and this current enhancement is greatest at the low current levels. The high current ranges are affected very little and in fact the value of the saturation current is not changed at all.

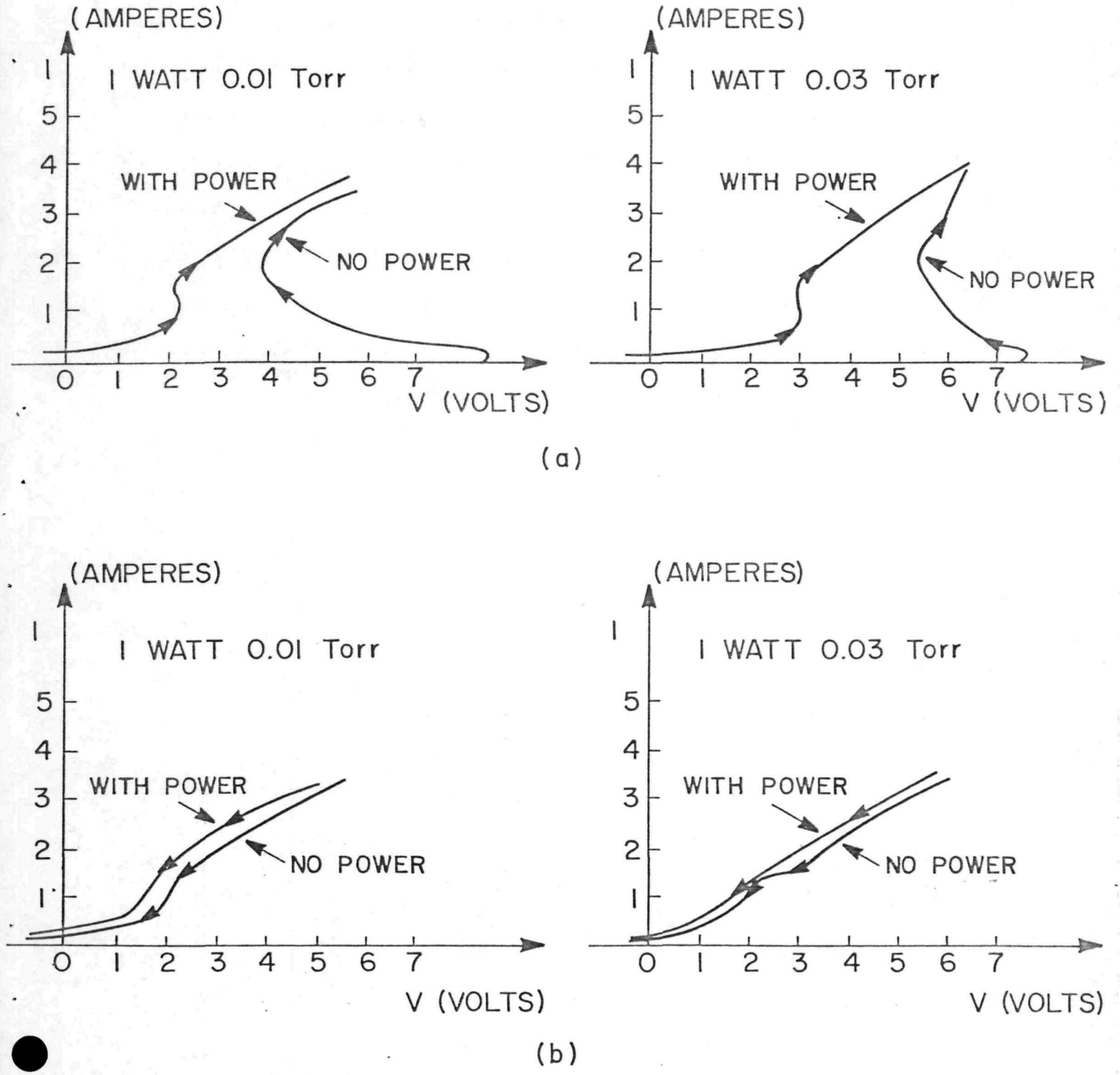

Fig. 13. Split I-V curves with (1 watt) and without microwaves for two Cs pressures.

Moreover, it is also found that the knee of the ignition I-V curves, indicating the presence of a breakdown voltage, is not affected at all at applied microwave power levels below 0.5 watts, then continuously shifted to lower voltages as the power increased from about 0.5 to 1 watt, and completely disappeares when the level of 1 watt is reached. In order to appreciate the effects of varying the applied microwave power level it is shown in Fig. 14 a family of ignition and return curves at cesium pressure P=0.01 torr. At higher microwave power levels only small changes occur mostly in the lower current region. In these lower ranges the current carried at the same voltage rises as a function of the applied microwave power; in particular at zero voltage the transmitted current increases indicating that more microwave power is converted into DC power.

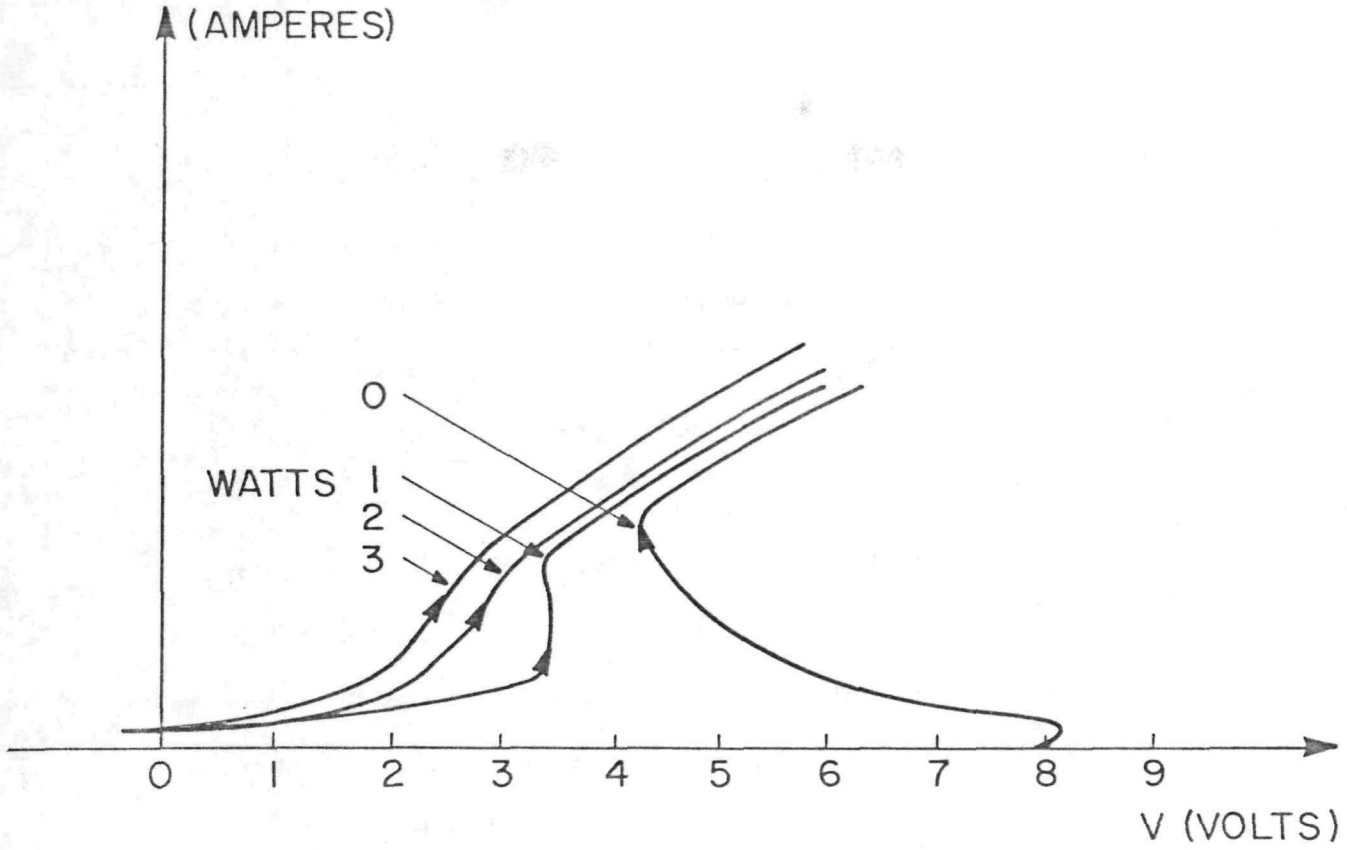

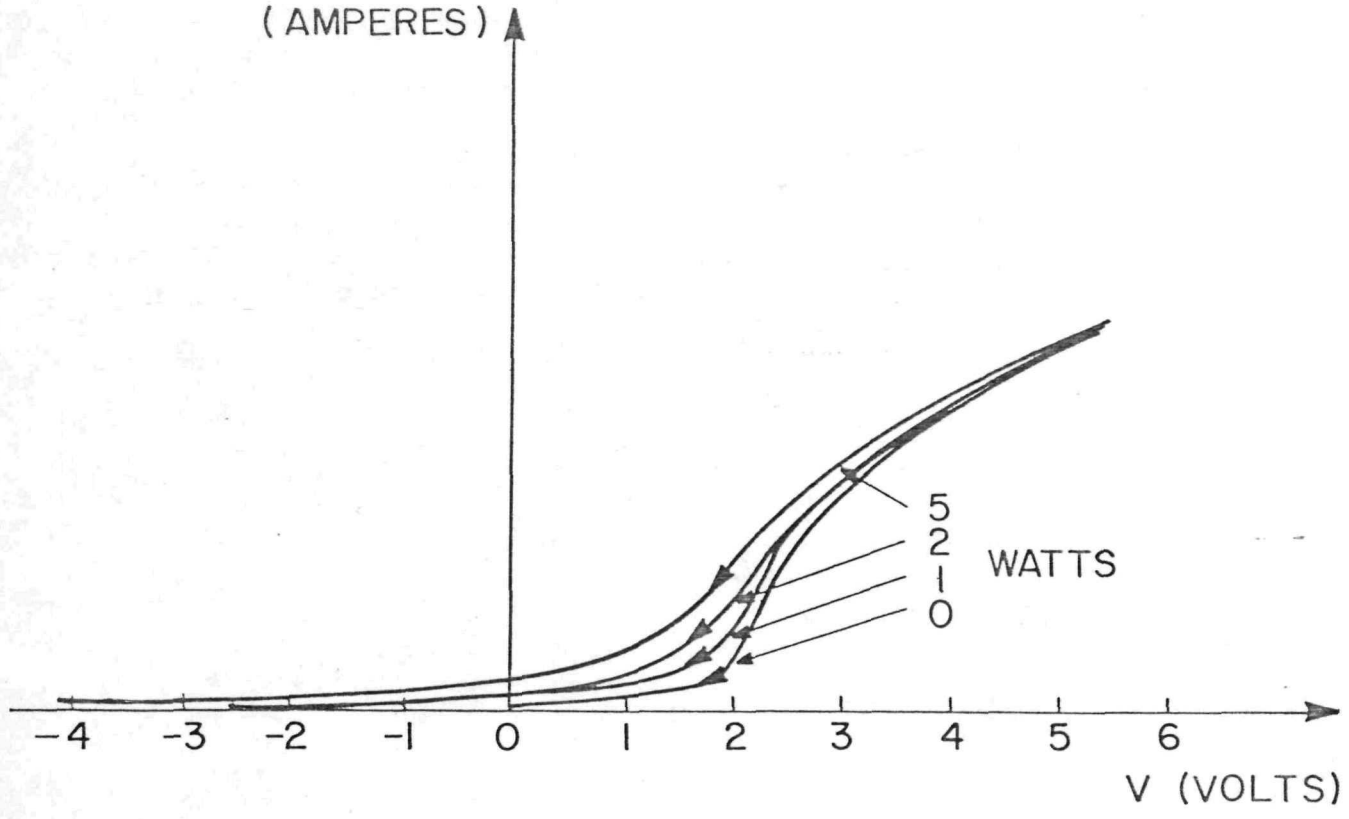

Fig. 14. Split I-V curves for one Cs pressure and three levels of microwave power.

c. Analysis of the Results

A qualitative understanding of the above results can be gained by considering the potential energy diagrams for the converter in the presence or in the absence of applied microwave power. Fig. 15 shows an ignition curve in the absence of microwave power; three main regions can be distinguished characterized by different potential energy diagrams, the unignited mode, the obstructed region, and the saturation region. In the unignited mode no current flows, while in the obstructed region the double sheath erected in front of the emitter dominates the behavior of the converter. The voltage must thus be raised to the breakdown value in order to overcome this motive peak. The double sheath disappears in the saturation region. When microwave power of a sufficiently high level is applied, no such breakdown voltage threshold is observed which immediately indicates that no motive peak exists; the structure of the potential energy diagram under these conditions is very simple, as seen in Fig. 16. An interesting method of evaluating the performance of the thermionic converter is provided by Lam[1] who summarizes the plasma arc drop in terms of a single parameter, the normalized plasma resistance R. According to this theory the converter arc drop V_d is related to the plasma resistance R by the equation

$$j = \frac{1}{1 + \exp \dfrac{jR - V_d}{\tau}} \qquad (4)$$

where j is the converter current and τ the plasma temperature; all V_d, j. R, and τ are in normalized units given by

$$V_d = (\mathbb{D}_E - \mathbb{D}_c + \Delta_X - V_o) / (kT_E / e) \qquad (5a)$$

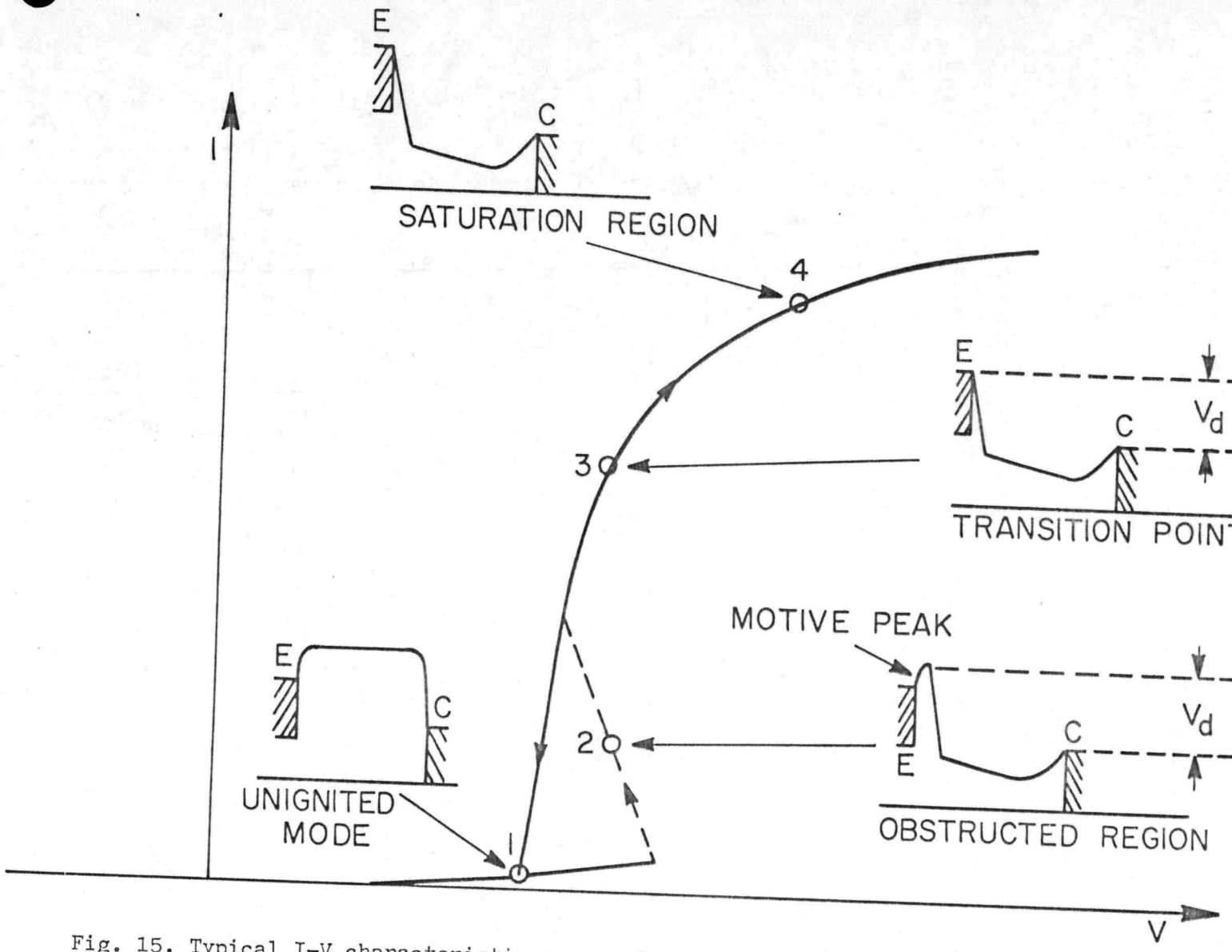

Fig. 15. Typical I-V characteristic curve of cesium thermionic diode in negative power quadrant and the potential distribution diagrams.

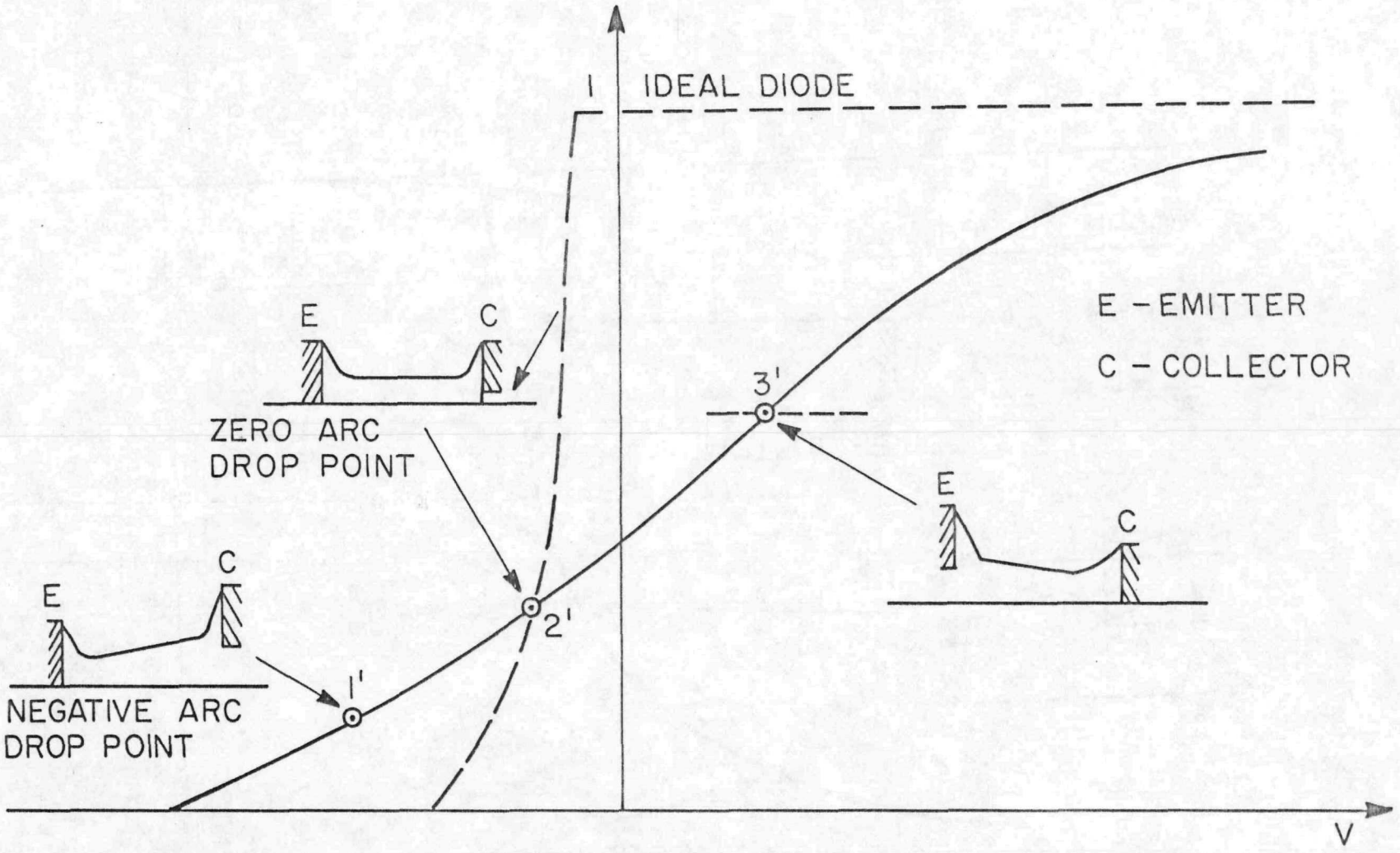

Fig, 16, Typical I-V characteristic curves of microwave thermionic diode and potential distribution diagrams.

where $\mathbb{D}_E$ is the emitter work function, $\mathbb{D}_c$ the collector work function, Δ_X the voltage height of the emitter double sheath measured from the emitter, and V_o is the output voltage. The value for V_d in volts has been normalized to units of $\frac{kT_E}{e}$ where T_E is the emitter temperature, k the Boltzmann constant and e the electronic charge. Furthermore, the normalized current density is defined by

$$j = J / J_E , \qquad (5b)$$

where J is the converter diode current density and J_E is the emitter current density. The normalized plasma resistance R is defined by the expression

$$\Delta_{Xohmic} = jR \qquad (5c)$$

where Δ_{Xohmic} is the normalized (again in units of kT_E / e) ohmic (momentum scattering) contribution to the total plasma arc drop. The plasma electron temperature T_e is also included in dimensionless form τ given by

$$\tau = T_e / T_E \qquad (5d)$$

In the obstructed region we have ,

$$J_E = J_R \exp (-\Delta_{\bar{X}}) , \qquad (6)$$

where $\Delta_{\bar{X}} = \Delta_X / (kT_E / e)$. If the emitter motive peak is suppressed, i.e. if $\Delta_X = 0$, then $J_E = J_R$. Without external heating, R cannot be determined experimentally because J_E and τ both change simultaneously below the transition point of the I-V curve, where the emitter motive peak exists. This can be explained by Fig. 15 which shows the potential diagram between the electrodes at four points on the I-V curve. At point 1, the plasma is unignited and the current density is very low. At point

2, the plasma is in the negative resistance region where the plasma is not completely ignited and the emitter motive peak still exists. At either point 1 or 2, the emitter net current density J_E cannot be determined because J_E is a function of τ and $\Delta_{\bar{X}}$ which are both varying during the transition from point 1 to point 3. It is only when point 3 is reached which is the transition point or the "knee" of the I-V curve, that the plasma is completely ignited, the emitter motive peak disappears, and $J_E = J_R$ becomes a constant. At point 4 the plasma is in the saturation region. Fig. 16 shows the I-V curve and the potential diagrams of the converter diode with microwave heating. The "knee" of the I-V curve disappears and the plasma is sustained at high current density when both AC and microwave power are applied while at low current density the plasma is sustained only by microwave power. Because of the disappearance of the emitter motive peak there is no sudden jump of the diode current and $J_R = J_E$ = constant can be assumed. As a result, Eq. (4) can be used to relate $J = (J/J_R)$ and V_d at a certain value of R and τ. The normalized I-V characteristics of the diode with external heating are plotted as j versus V_d. The best fit of these experimental I-V curves with respect to the parameters R and τ into the curves provided by Lam's theory can be used to give the best values of R and τ. The normalized plasma resistance, R and the normalized electron temperature τ, are tabulated in Table 1 with different emitter temperatures. The cesium pressure is 0.08 torr.

$T_E(^oK)$	935	965	995	1025	1055	1085	1115	1180	1210	1240	1270	1300
R	10	10	15	20	25	25	25	25	30	30	50	50
τ	10	8	7	5	5	5	5	5	5	4	3	3

Table 1

At temperature T_E = 935°K, R is equal to 10 and the best value of τ is also 10. At T_E = 1055°K, R increases to 25 and τ decreases to 5 which is almost constant until T_E = 1180°K. From T_E = 1210°K to 1300°K, R is greater than 30 and τ is less than 4. The table shows that as τ decreases, the plasma resistance increases, which is an indication that in order to reduce plasma resistance or arc drop, higher electron temperature is required.

Finally, an extended plot of the I-V characteristics of the diode with and without microwave heating is shown in Fig. 17 at T_E = 935°K to demonstrate the improved performance of the diode with external microwave heating.

A significant rise in the thermionic converter current level can be seen upon application of microwave power. In the experiments described in this work the improvement is limited to the lower current ranges due to the shielding effects of the plasma at the higher current values. At these high current ranges the plasma density is high and microwave propagation is cutoff if the frequency is not high enough. It is expected though that higher frequency microwave power would suffer no such limitations and would provide current enhancement at high current levels which would be of great interest in practical applications.

It is thus believed that microwave power shows great promise as a source of energy to sustain the cesium plasma in a thermionic converter. At the lower operating temperature of 1600°K the emitter in the advanced converter can no longer supply sufficient ionization levels. An external source of ion generation is needed which does not interfere with the emitter and collector electrodes. Externally supplied microwave power may prove to

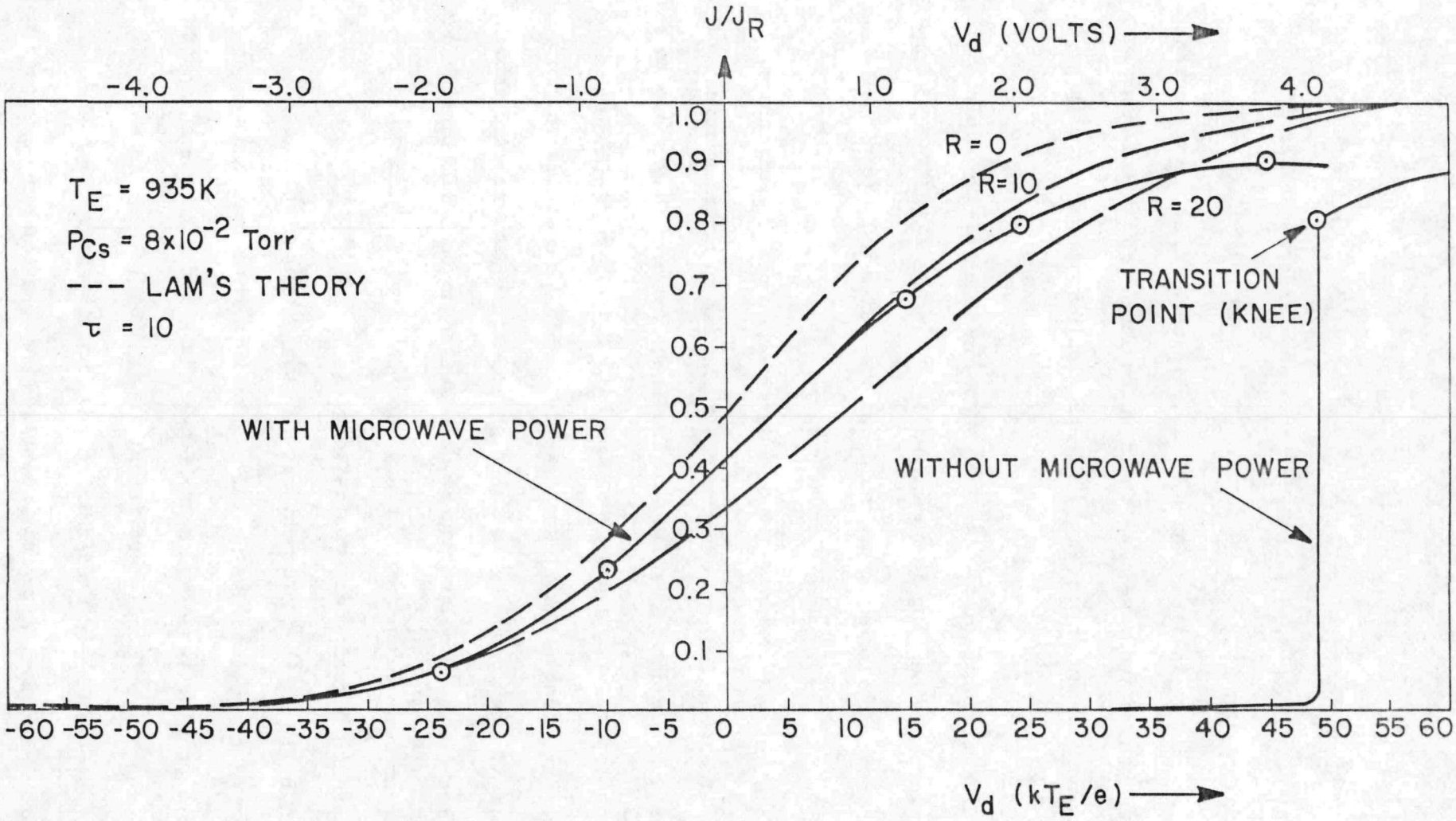

Fig. 17. I-V characteristics with and without microwave power.

be the best agent to perform the task. It is attractive in many ways. There is considerable flexibility to allow adjustment on both the power and the frequency of the applied microwave power to achieve the desired plasma condition. In supplying microwave energy we do not interfere with the inter-electrode spacing by the insertion of extraneous electrodes. Operation may be in the continuous mode in contrast to pulsed systems which would not be available for power generation during the pulse on condition. Furtheremore the geometrical size of the emitter-collector distance envisioned is the correct order of magnitude to allow support of the plasma by microwave fields in a resonant mode. The energy expenditure of microwave power at a resonant plasma system is expected to be smaller in comparison to alternative energy sources. Moreover, the power requirements in the applied microwave field seem rather modest - a few watts - easily available in present day technology even for large thermionic converters. Subsequent experiments should be performed with microwave power of high frequency, i.e. at 10 GHz (X-band) and 20 GHz (K-band). The technology of microwave power generation and transmission is well advanced with many off-the-shelf items available to utilize in our systems.

It is found in the analysis of the experimental data a trend that tends to support Lam's theoretical treatment. More work is needed in this area to provide a comprehensive understanding of the plasma in the thermionic converter. The simplicity of a microwave supported plasma in an optimum diode could allow for easily interpreted data from which conclusions may be drawn about the proper plasma density level for highest overall efficiency. It thus reveals that microwave power sustenance of a thermionic plasma in a resonant configuration is indeed a very attractive choice.

5. Cs - N_2 MIXTURE: THE DC CASE

a. Theory

As previously mentioned, searching is needed for an external ionization source for the thermionic cesium plasma discharge which will not interfere with the two electrodes. One promising possition is molecular N_2 additive gas[8] acting as an energy storage intermediary.

The nitrogen gas discharge has been studied since the 17th century. The reason for nitrogen being so popular is because nitrogen is fairly easy to purify and it is abundant; molecular nitrogen is a simple, symmetric, and very inert gas and easy to deal with, for theoretic analysis. Nitrogen is particularly useful because its excited vibrational energy levels are exceptionally long lived due to the fact that the nitrogen molecule possesses no electric dipole moment. Once the molecular vibrational levels are excited they cannot decay to the ground state ($\nu = 0$) levels through electric dipole radiation[9]. Deactivation can proceed only by collisions with other molecules or atoms or with the walls of the confining vessel. The wall deactivation coefficient of nitrogen is small[10] (about 1×10^{-3} for stainless steel, the same order or less for most other common surfaces) so most of the deactivation proceeds by collisions with neutral cesium atoms which often result in cesium ionization (see Fig. 18)[11].

It has been known for some time that molecular nitrogen in the presence of alkali atoms (Na, K, Cs) will quench the radiation of the alkali metals under a variety of laboratory conditions[12, 13, 14].

The reverse process, also has been reported[15, 16]. These reactions are important in the understanding of certain types of aurora, in which strong alkali metal radiation is observed.

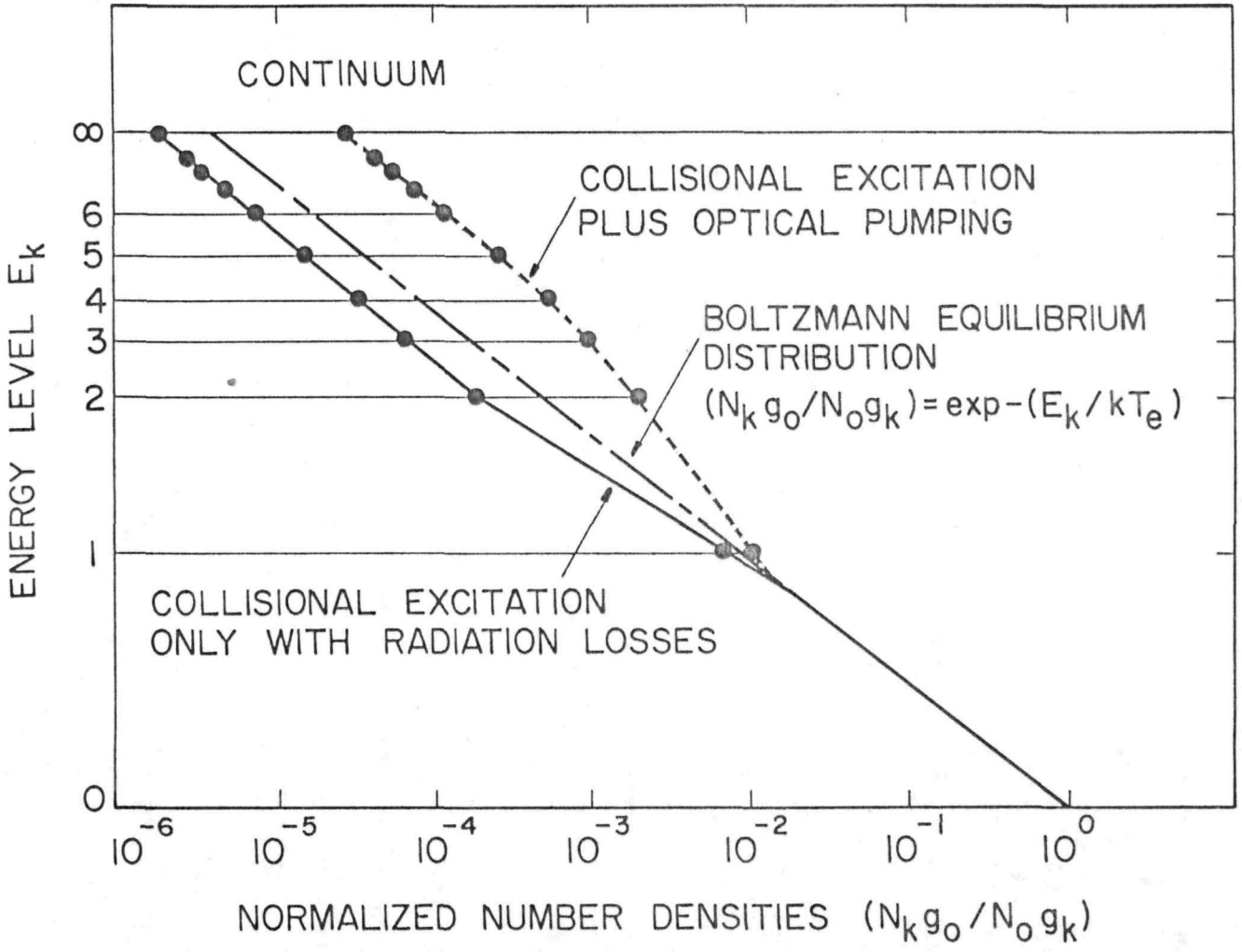

Fig. 18. Schematic of the effect of laser excitation on excited state populations (taken from Oettinger and Dewey 1970).

However, the exact energy transfer mechanism between diatomic molecules and alkali metals have not been satisfactory settled. It is known that vibrationally excited nitrogen can be easily quenched by a small amount of alkali metals, even at mole ratio of 0.002[17, 18]. Such a large collisional cross section is important in the high power laser field, where vibrationally excited species population is a very important parameter for lasing action. The quenching mechanism is mainly vibrational-translational relaxation. The same situation happens to the quenching of electronically excited alkali atoms by diatomic molecules, where electronic-vibrational transitions are responsible.

Much work has been done that treats the ionization or excitation of alkali atoms by excited molecular nitrogen. Most of the work concerned deals with N_2 - Cs interaction either in crossed molecular beam experiments or in glow discharges, the latter produced by either DC or RF power. Overall both vibrational-electronic (V-E) or electronic-electronic (E-E) energy transfer is found to occur. Yet in the majority of cases V-E energy transfer is found to dominate.

On the other hand, Gann and others[19], using a discharge flow system and interferometric technique, have shown that nitrogen in the electronically excited N_2 (A) states are the principal exciting agent for the observed sodium D-lines. Dugen and his colleagues[20] observe the sodium emission and its Doppler temperature from nitrogen and conclude that nitrogen molecules in metastable electronic states are responsible for sodium excitation. Hunten[21] has considered the auroral sodium excitation problem and concluded that direct excitation of sodium by energetic electrons is untenable. The competition for those energetic electrons at the auroral altitudes is

mostly won by the more abundant nitrogen molecules, which become vibrationally excited to the υ=8 states with a large cross section[22]. He proposes that the electronically excited sodium arises through energy transfer of the vibrational states in the nitrogen to the electronic ground state sodium. Krause and others[23] use a beam of excitation and ionization. A close energy match between the vibrational states of molecular nitrogen and electronic levels of the metallic atom is found not necessary; a fact that could be due to the formation of the $(MN_2)^*$ complex when the two species collide.

b. Spectroscopic Measurements for Low Density Plasma

For plasmas with an electron density greater than $10^{16} cm^{-3}$ the intensity of spectral lines is interpreted using the local thermodynamic equilibrium (LTE) hypothesis and the intensity I_{mn} of a spectral line emitted between two levels m and n is written

$$I_{mn} = N_m h\nu_{mn} A_{mn} \tag{7}$$

where m and n are the principal quantum numbers, respectively, of the upper and lower states of transition, N_m represents the population of the state m and $h\nu_{mn}$ the energy of each quantum with frequency ν_{mn} emitted in the transition $m \rightarrow n$. A_{mn} denotes the spontaneous transition probability which is dependent solely on the transition $m \rightarrow n$ and is related to the oscillator strength f_{nm} by[24]

$$f_{nm} = \frac{mc^3}{8\pi^2 e^2 \nu_{mn}^2} \frac{g_m}{g_n} A_{mn}, \tag{8}$$

g_m and g_n are the statistical weights of levels m and n, respectively. The various measurement methods which use the intensity and the profile of spectral lines can then be applied.

If the plasma electron density is situated between 10^{14} and $10^{16} cm^{-3}$, the density may be deduced from the Stark half-width of the lines, provided that the electron temperature is low enough (Doppler broadening is then negligible) and the temperature can be deduced from the relative intensity of lines. For low-density plasmas, it is necessary to test the validity of the LTE hypothesis which can be attained only if collisional processes are of greater incidence than radiative recombination processes. The criteria required to test the validity of complete or partial LTE are given by Griem[24].

There will be total LTE if

$$N_e \geq 9\times10^{17} \left(\frac{kT}{E_H}\right)^{1/2} \left(\frac{E^{Z-1}(2)}{E_H}\right)^3 \quad (cm^{-3}). \qquad (9)$$

The electron density required for partial LTE is

$$N_e \geq 7\times10^{18} \frac{Z^7}{n^{17/2}} \left(\frac{kT}{Z^2 E_H}\right)^{1/2} \quad (cm^{-3}), \qquad (10)$$

n being the main quantum number of the lowest level included in the partial LTE. [E_H is the ionization energy of hydrogen, Z=1 for neutral particles and $E^{Z-1}(8)$ is the energy of the first excited state with respect to the ground state $E^{Z-1}(1)=0$].

In the case of a low-density plasma, not all measurement methods are applicable and, in particular, the Stark half-width is negligible since it is proportional to the density.

Hence, in the case of low densities, $\Delta\lambda_s$ becomes too small to be measured with a low-dispersion apparatus. However, the Stark half-width increases with the quantum number n and measurement becomes possible for high values of n. The most appropriate series are the fundamental ones (5D - nF) but the half-width values where $n>10$ are not given by Ref. (25). On the other hand where $10\leq n\leq 14$ the profiles have been calculated by Sayer et al[26], who in this way measured electron densities for values situated between 8×10^{12} and 3×10^{13} cm^{-3}. Fabry and Cussenot[27] have also worked out the Stark half-widths where $10\leq n\leq 17$ and they compared the results with those previously obtained. Since the agreement between the two sets of results is satisfactory they deduce the electron density N_e for the lines in the series $5D_{3/2} - nF_{5/2}$ and $5D_{5/2} - nF_{5/2,\ 7/2}$ with n varying between 14 and 17. They also used another method of measuring

this density by studying the profiles of two neighboring lines, for example $5D_{3/2} - 13F_{5/2}$ (λ = 6150 Å) and $5D_{5/2} - 14F_{5/2,\ 7/2}$ (λ = 6153 Å). The profile obtained is that shown in Fig. 19a and from the measurements corresponding to I_1, I_2, and I_0, one can determine N_e. The coefficient

$$\beta = I_0 / (I_1 I_2)^{1/2}$$

varies significantly with the electron density[28]. This variation is shown in Fig. 19b, where N_e varies between 0.8 and $3 \times 10^{13} cm^{-3}$. Fabry and Cussenot have continued this curve for lower densities, going as low as $10^{12} cm^{-3}$. In Fig. 20 the theoretical and experimental results of Ref. 28 are shown in addition to the values calculated. Also Fig. 20 gives these values completed for the region situated between 10^{12} and $3 \times 10^{13} cm^{-3}$.

In many of the measurements one must measure the electron density in the low density region. To this purpose the above mentioned method was adopted. In order to get familiarized with this technique and to adopt it to the requirements, a separate experiment has been run with similar conditions, i.e. electron bombardment emitter, comparable cesium pressures, emitter temperatures and current densities. In addition the collector is movable. Fig. 21 shows the appropriate discharge circuitry for this experiment.

The filament is heated with a special purpose power supply capable of delivering 35A at as much as 15KV above ground. The emitted electrons are accelerated by a negative voltage supply, Edwards GD-1, and the main discharge is produced by a Hewlett-Packard power supply model 6268B. Four variables are changed to get the data needed, namely: current densities of 2-9 Amperes, interelectrode space from 3/4 to 1/16 of an inch emitter temperature 1273 - 1573°K and Cs pressure from .01 to 1 torr. The

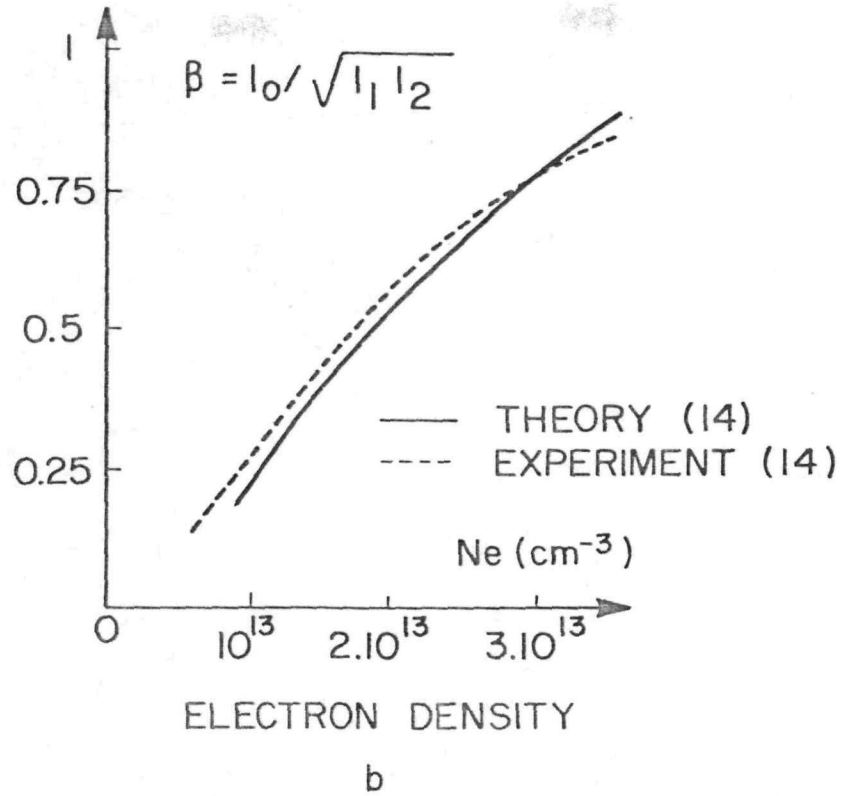

b

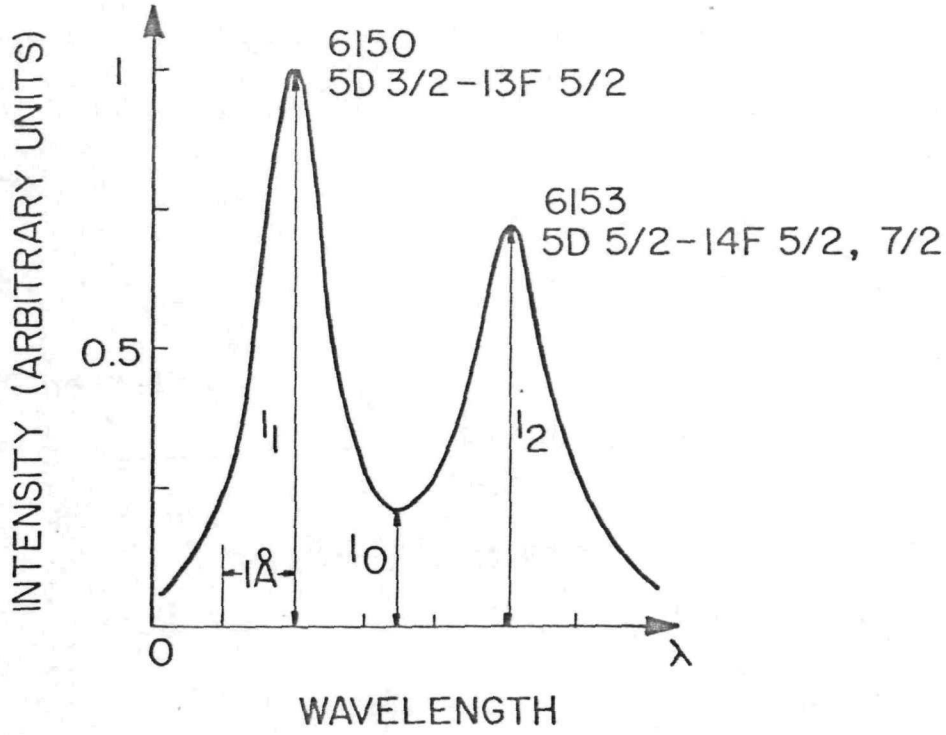

a

Fig. 19. a) Profile of close-lying spectral lines $5D_{3/2}-13F_{5/2}$ and $5D_{5/2}-14F_{5/2}, 7/2$.

b) Variation of $\beta = I_0/(I_1 I_2)^{1/2}$ as a function of electronic density

$10^{13} \leq Ne \leq 3 \times 10^{13}\ cm^{-3}$. Ref. 14

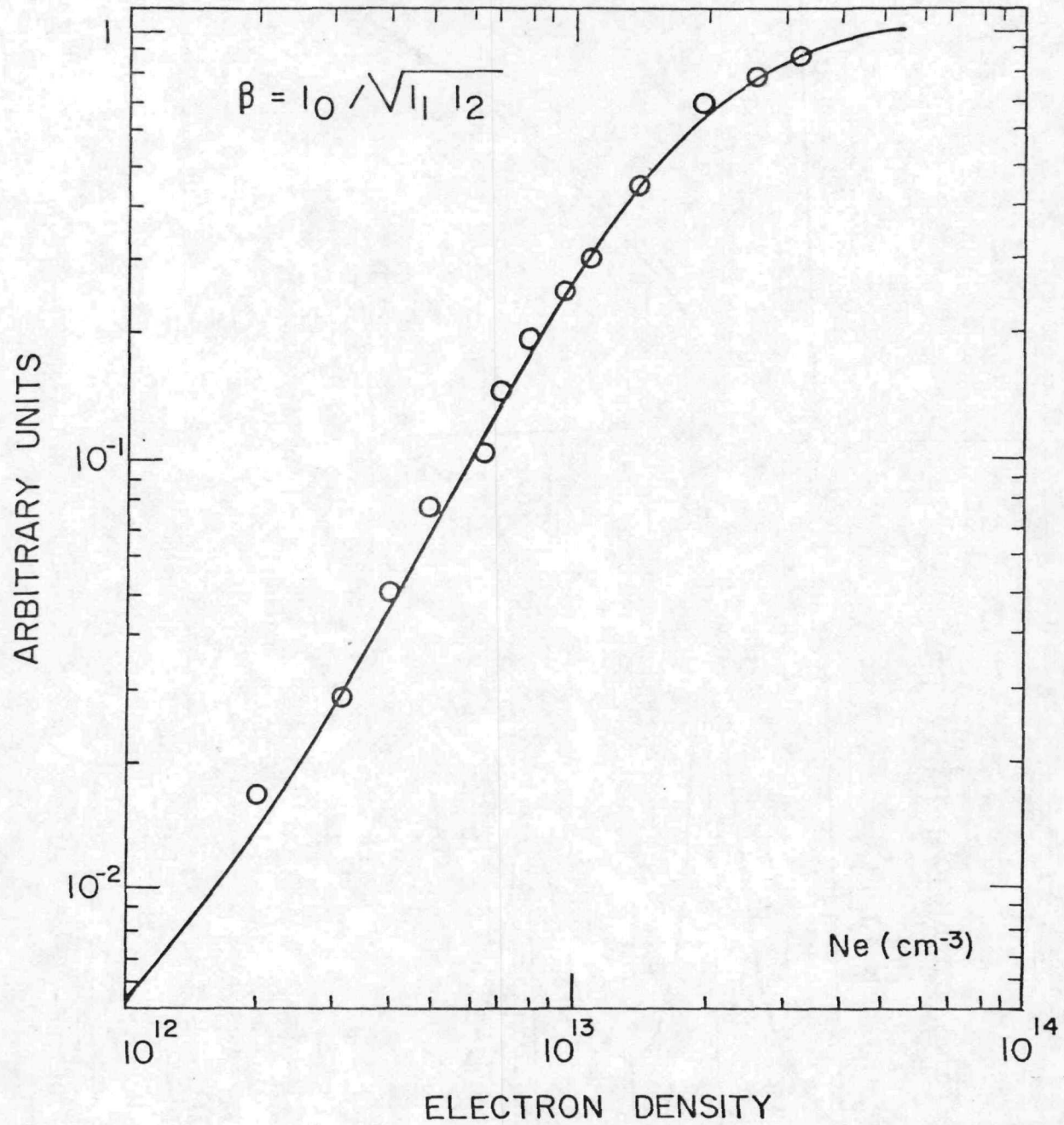

Fig. 20. Variation of $\beta = I_0/(I_1 I_2)^{1/2}$ as a function of electronic density $10^{12} \leq Ne \leq 5 \times 10^{13} cm^{-3}$.

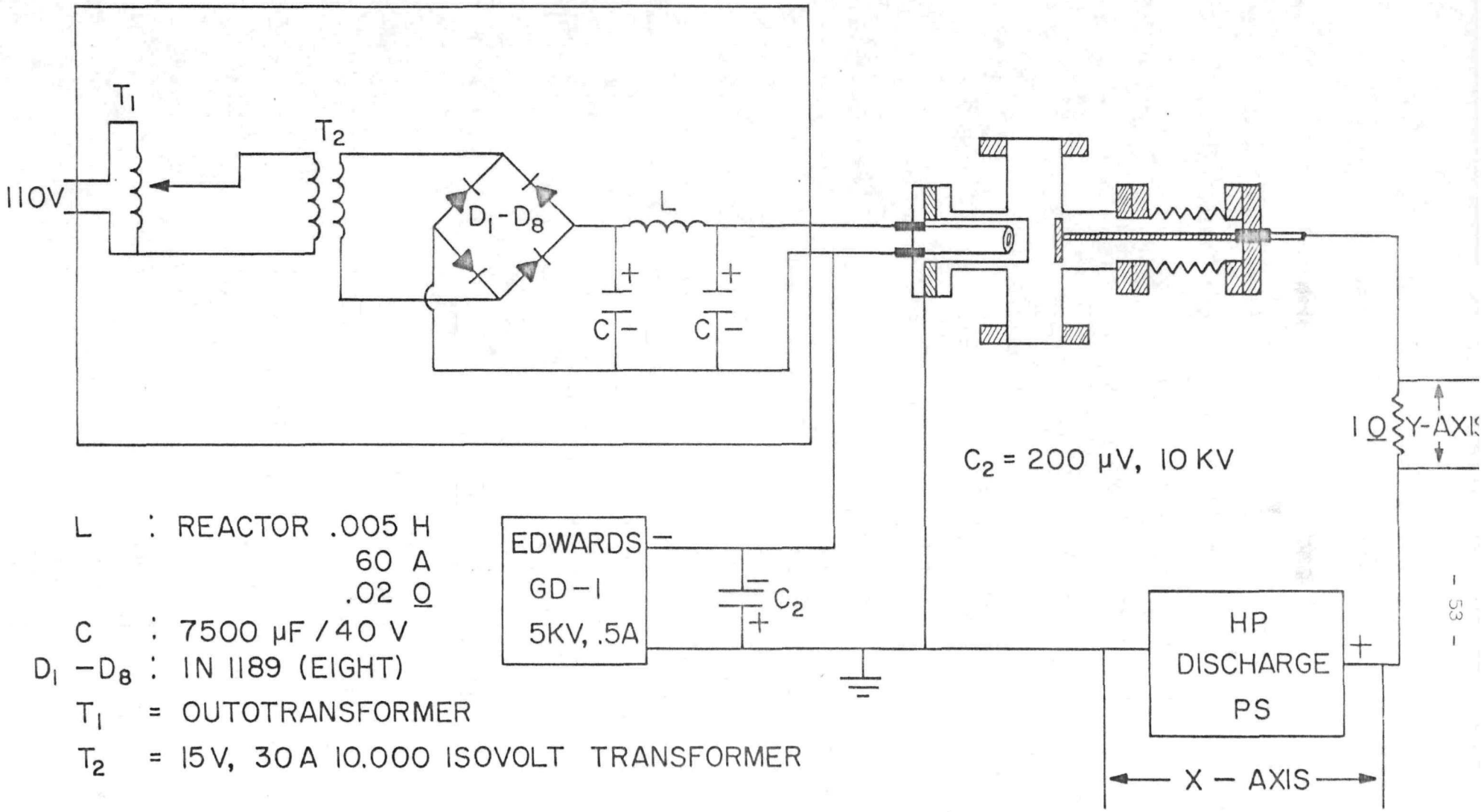

Fig. 21. Electrical circuit set-up for a thermionic diode with electron bombartment emitter.

electron density is calculated from the cesium doublet 6150 Å, 6153 Å. The β coefficient evaluated and the value of N_e deduced from Fig. 20. In addition whenever the electron density is in the vicinity of $5 \times 10^{13} cm^{-3}$ or higher the classical method of measuring the half width of the 6629 Å cesium line is used. Fig. 22 shows some of the results obtained from both of the methods. As it can be seen in Fig. 22c the double line method cannot be applied any more, because of the disappearance of the cesium doublet 6150 - 6153 Å. Instead one has to use the standard Stark broadenning method. The line 6629 Å is shown in Fig. 22d with an electron density of $8 \times 10^{-13} cm^{-3}$ which is well above the limits of the low density method. It should be noted here that the resolution of the monochromatǫr is fixed at 0.3 Å.

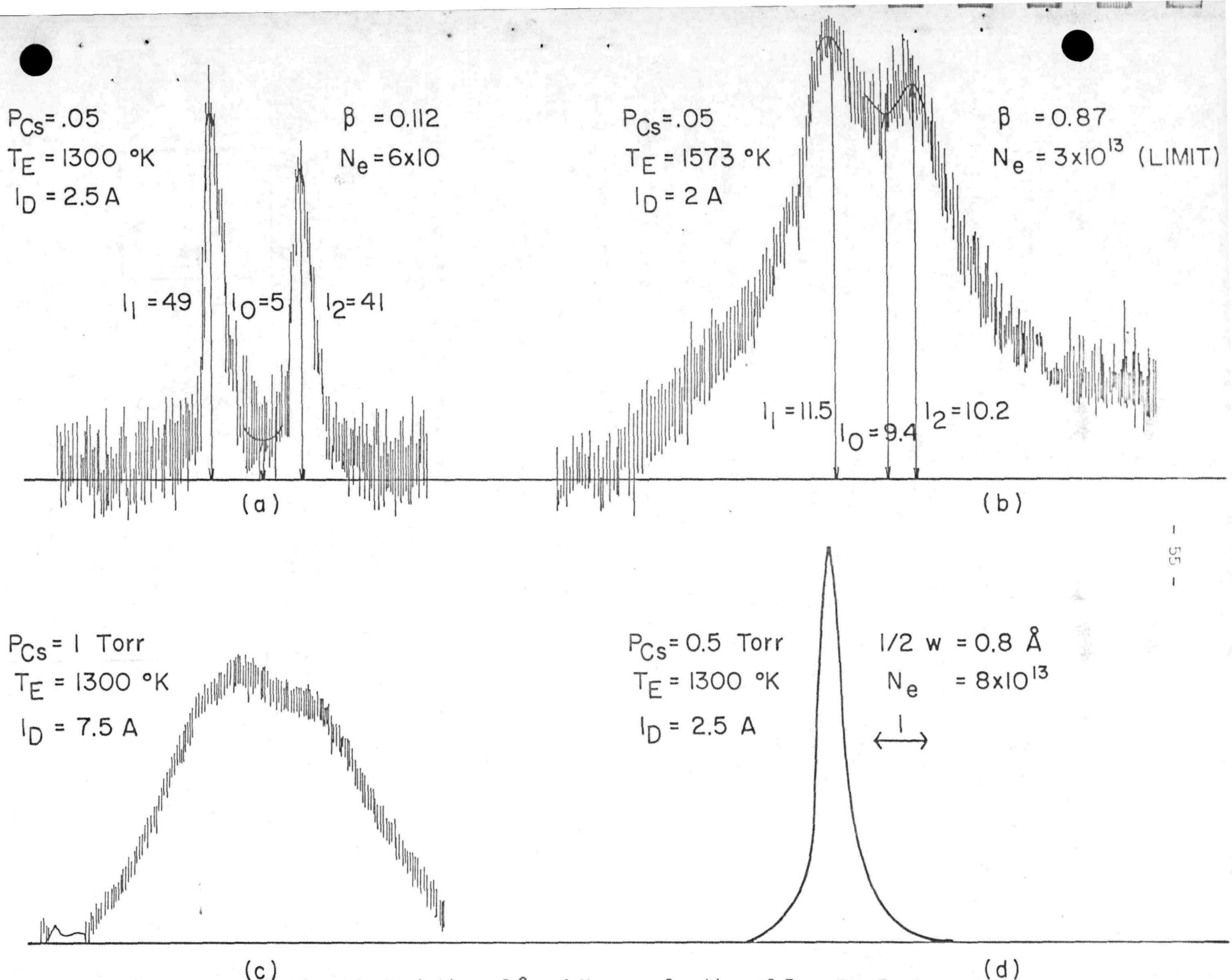

Fig. 22. Variation of β and N_e as a function of P_{Cs}, T_E, I_D.

c. Experimental Apparatus and Results

The spectroscopic method for measuring the plasma density in low density plasmas described in the previous section has been applied to measurements in both pure cesium plasma and N_2 - Cs mixture discharge.

The discharge circuit is shown in Fig. 23. The filament is heated with an NJE power supply, and the main discharge is produced by a Hewlett-Packard model 6268B power supply. A Heath X-Y recorder is used to record the current to voltage characteristics.

As it is expected, a small concentration of nitrogen added to a cesium discharge will quench the radiation of cesium lines, i. e. as the nitrogen pressure goes higher, the ignition voltage increases correspondingly, the voltage needed to sustain a same discharge current level is also higher. Spectroscopic measurements show only cesium line radiation.

When the nitrogen pressure is continuously increased, the I-V discharge characteristics changes to a new shape. The voltage needed to achieve breakdown of the gases is much higher than in the previous case, the current is much lower.

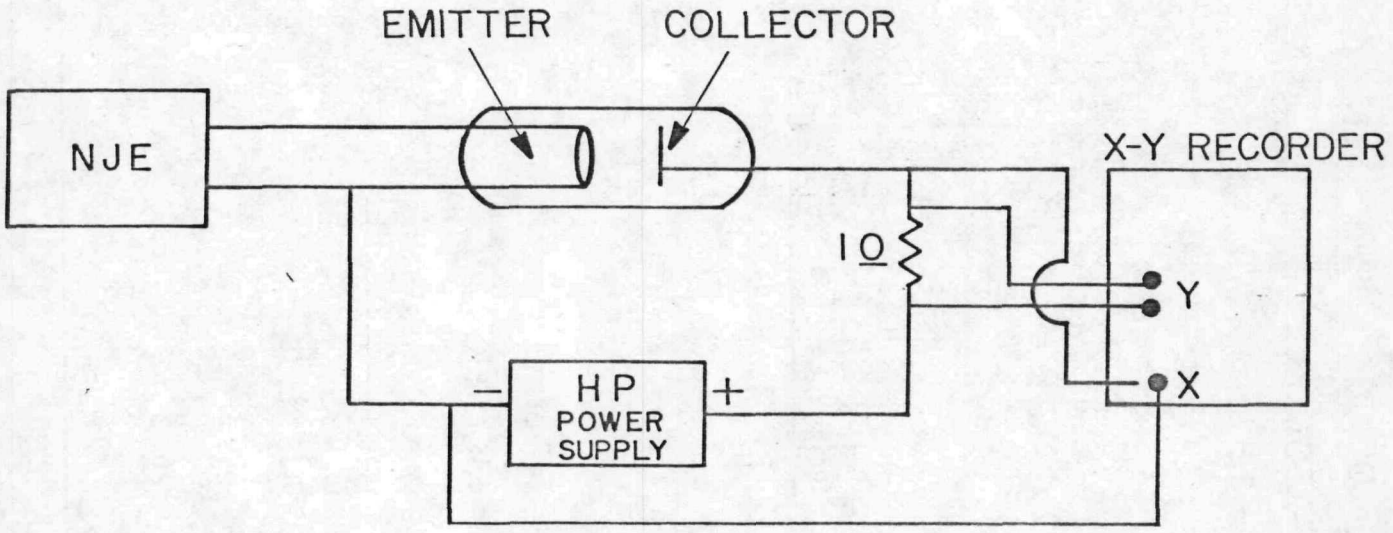

Fig. 23. Electrical discharge circuit for the DC case.

When the voltage decreases from the breakdown voltage, the current reduces a little at first and then increases slowly until at some voltage, the current reaches a maximum, whereupon any further reduction of the voltage causes the current to drop sharply to zero. Fig's 24 through 27 show such typical I-V characteristics for various conditions.

The results for pure cesium vapor discharge are summarized in Table 2. It is important to note the consistency of the method. The deduced plasma density from the measurement of coefficient β does indeed increase as the pressure of cesium vapor is increased and as the applied discharge current is increased. This is shown in the tabulated values as the cesium vapor pressure goes from 0.05 to 0.5 torr and as the current increases at each fixed pressure. There is also a similar relationship of plasma density to emitter temperature; as the emitter temperature increases so does the plasma density. The above relationships are expected from a theoretical point of view and it is gratifying to see that indeed they are followed by the results of the spectroscopic measurements.

The last pressure range for cesium vapor of 0.5 torr provides some more evidence of the validity of this new method and gives more confidence in the experimental measurement procedure. The value of β for this case is close to 1 and the particular spectroscopic method breaks down. In this case, though, the plasma density is high enough that can be measured by more conventional plasma density measurement methods which rely on linewidth measurements. All values of plasma density for 0.5 torr of cesium, are obtained by measuring the half width of the 5D - 8F transition, i. e. $\lambda \approx 6629$ Å, line of Cs. The results are tabulated and they are shown to be in perfect agreement with the established trends in the other cesium pressure regions.

Similar measurements have been made in various combinations in mixtures of cesium vapor with molecular nitrogen. Numerous such cases have been investigated and some representative results are tabulated in Table 3 and presented in Figs 24 through 27. In each case the current-voltage characteristic of the discharge is measured; some of the traces are shown in the upper part of Fig. 24 through 27. Two particularly interesting points on the I-V curves have been further investigated by measuring the plasma density there. These are the points L in the left extreme and R in the right extreme of the trace as shown. These are interesting because previous studies[29] have shown predominance of nitrogen emission spectral lines at R, and of cesium emission lines at L. Measurements of plasma density show consistently a low value at R and a high value at L which agree with low and high current values respectively as well as with low and high cesium emission spectra at those points. So, a consistent picture of N_2 - Cs I-V traces emerges where little excitation or ionization of cesium exists at R but as the voltage reduces, higher and higher excitation and ionization occurs, until at point L almost no nitrogen excitation exists with a maximum in excitation and ionization of the cesium vapor. It is as though all the energy is taken out of the nitrogen molecules and delivered to the cesium atoms, i. e. some kind of energy transfer takes place from nitrogen to cesium.

These results are consistently found for all mixtures studied. In particular they have been obtained at cesium pressure 0.05 torr as function of nitrogen partial pressure from 2.5 to 20 torr. Two such cases, for partial pressures of nitrogen of 2.5 and 5 torr are shown in more detail in Fig. 24 and 25. A case for a lower cesium pressure of 0.005 torr and nitrogen pressure of 10 torr is shown in Fig. 26 with similar general results. Similar conditions

TABLE # 2. VARIATION OF β AND Ne, OF A STEADY STATE Cs DISCHARGE, AS A FUNCTION OF PRESSURE, CURRENT, AND EMITTER TEMPERATURE

P_{Cs} = .005	I_D = 2A β = .14 Ne = 7 x 10^{12}	I_D = 4A β = .16 Ne = 7.5.x 10^{12}	T_{E_1}
	I_D = 2A β = .217 Ne = 8.5 x 10^{12}	I_D = 4A β = .27 Ne = 9.5.x 10^{12}	T_{E_2}
P_{Cs} = 0.05	I_D = 3.5 β = .66		T_{E_1}
	I_D = 1A β = .45 Ne = 1.38 x 10^{13}		T_{E_2}
P_{Cs} = 0.5	I_D = 3A β = .9 Ne = 3 x 10^{13}	I_D = 8A ½ w = 1.15 Å OF 6629 Ne = 1.1 x 10^{14}	T_{E_1}
	I_D = 4.5A ½w = 1.15 OF 6629 Ne = 1.1 x 10^{14}	I_D = 8A ½ w = 1.25 OF 6629 Ne = 1.5 x 10^{14}	T_{E_2}

T_{E_1} = 1300°K

T_{E_2} = 1573°K

TABLE # 3. VARIATION OF β AND Ne AT THE EXTREME POINTS (LEFT AND RIGHT) OF CURRENT VOLTAGE CHARACTERISTICS AS A FUNCTION OF NITROGEN PRESSURE AND EMITTER TEMPERATURE.

$T_{E_1} = 1300^{o}K$, $T_{E_2} = 1573^{o}K$

P_{N_2}	.5 Torr		2.5 Torr		5 Torr		10 Torr		20 Torr		
	L	R	L	R	L	R	L	R	L	R	
$P_{Cs} = .005$	$\beta = .45$ $Ne=1.38x10^{13}$	$\beta = .22$ $Ne=9x10^{12}$	$\beta = 1.6$ $Ne=7.5x10^{12}$				$\beta = .127$ $Ne=7x10^{12}$	$\beta = .08$ $Ne=5.2x10^{12}$			T_{E_1}
			$\beta = .181$ $Ne = 8.2 \times 10^{12}$				$\beta = .142$ $Ne=7.2x10^{12}$	$\beta = .067$ $Ne=4.8x10^{12}$			T_{E_2}
$P_{Cs} = .05$			$\beta = .28$ $Ne=9.6x10^{12}$	$\beta = .147$ $Ne=7x10^{12}$	$\beta=.423$ $Ne=1.3x10^{13}$	$\beta = .389$ $Ne=1.2x10^{13}$	$\beta = .18$ $Ne=8.2x10^{12}$	$\beta = .08$ $Ne=5.2x10^{12}$	$\beta = .173$ $Ne=7.9x10^{12}$	$\beta = .03$ $Ne=3.1x10^{12}$	T_{E_1}
	$\beta = .244$ $Ne = 1 \times 10^{13}$		$\beta = .45$ $Ne=1.38x10^{13}$								T_{E_2}
	$\frac{Ne^{L} - Ne^{R}}{Ne^{R}} =$		.371		.083		.576		1.35		

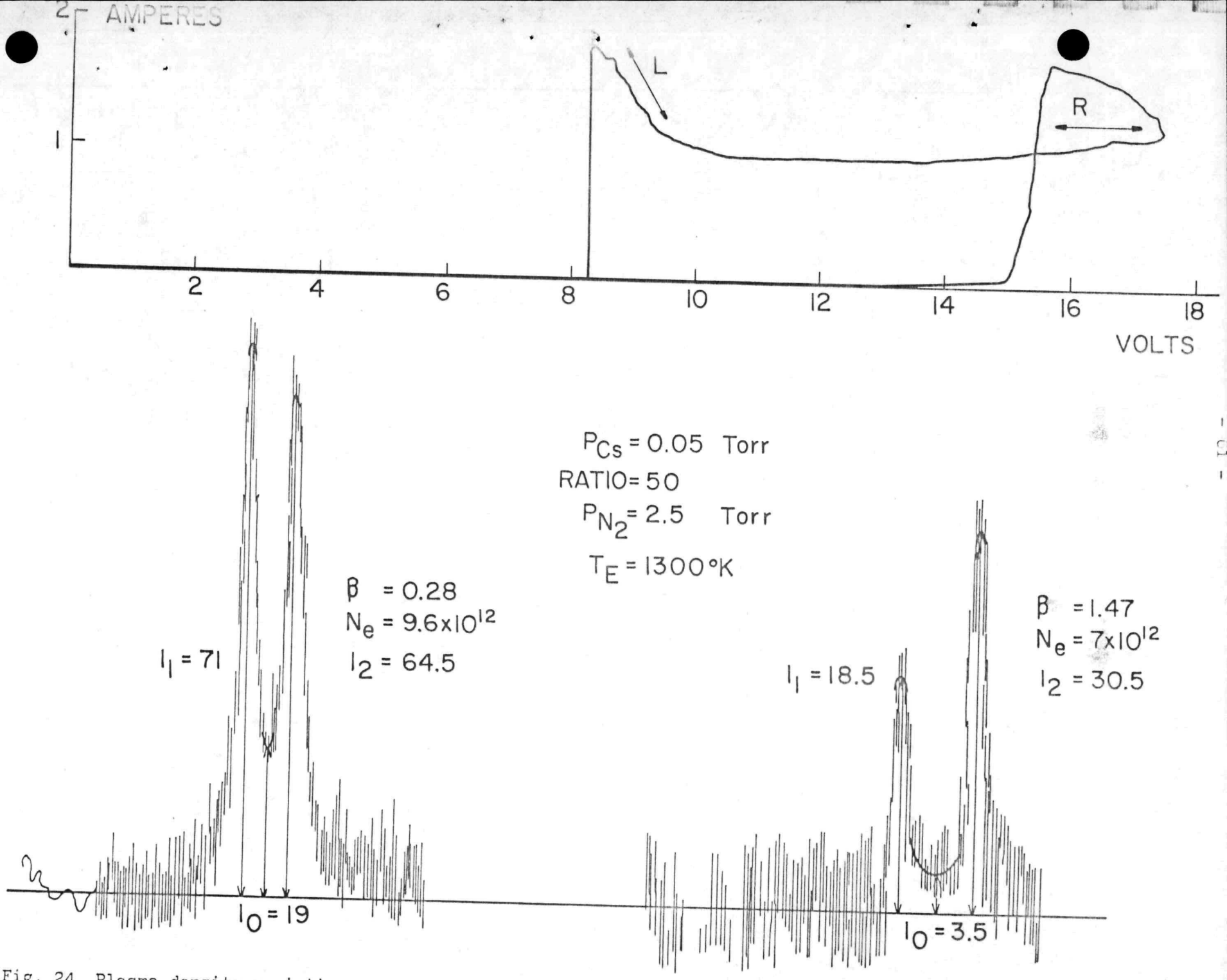

Fig. 24. Plasma density variations at the two extremes (left and right) of the I-V characteristics.

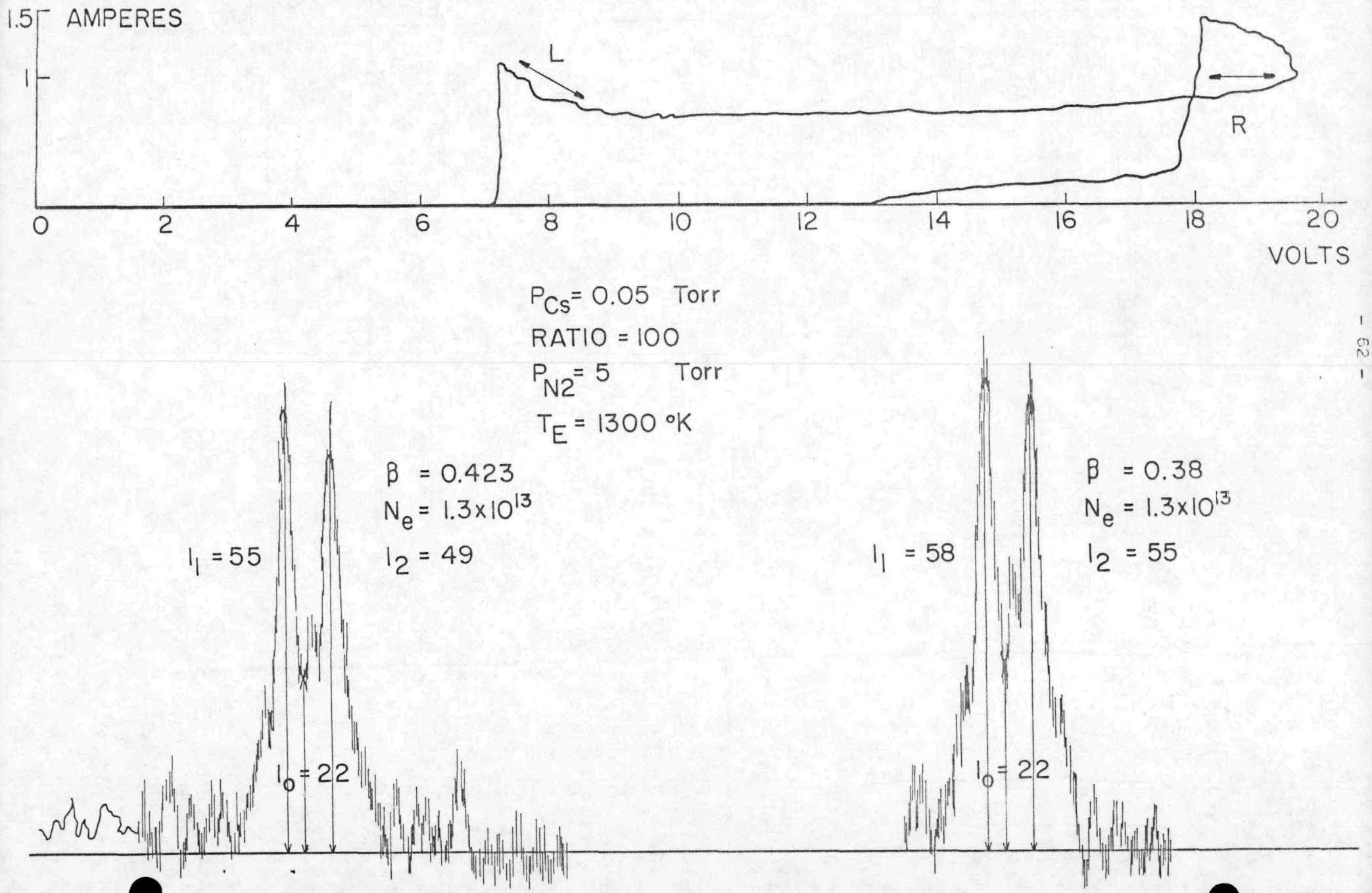

Fig. 25. Plasma density variations at the two extremes (left and right) of the I-V characteristics.

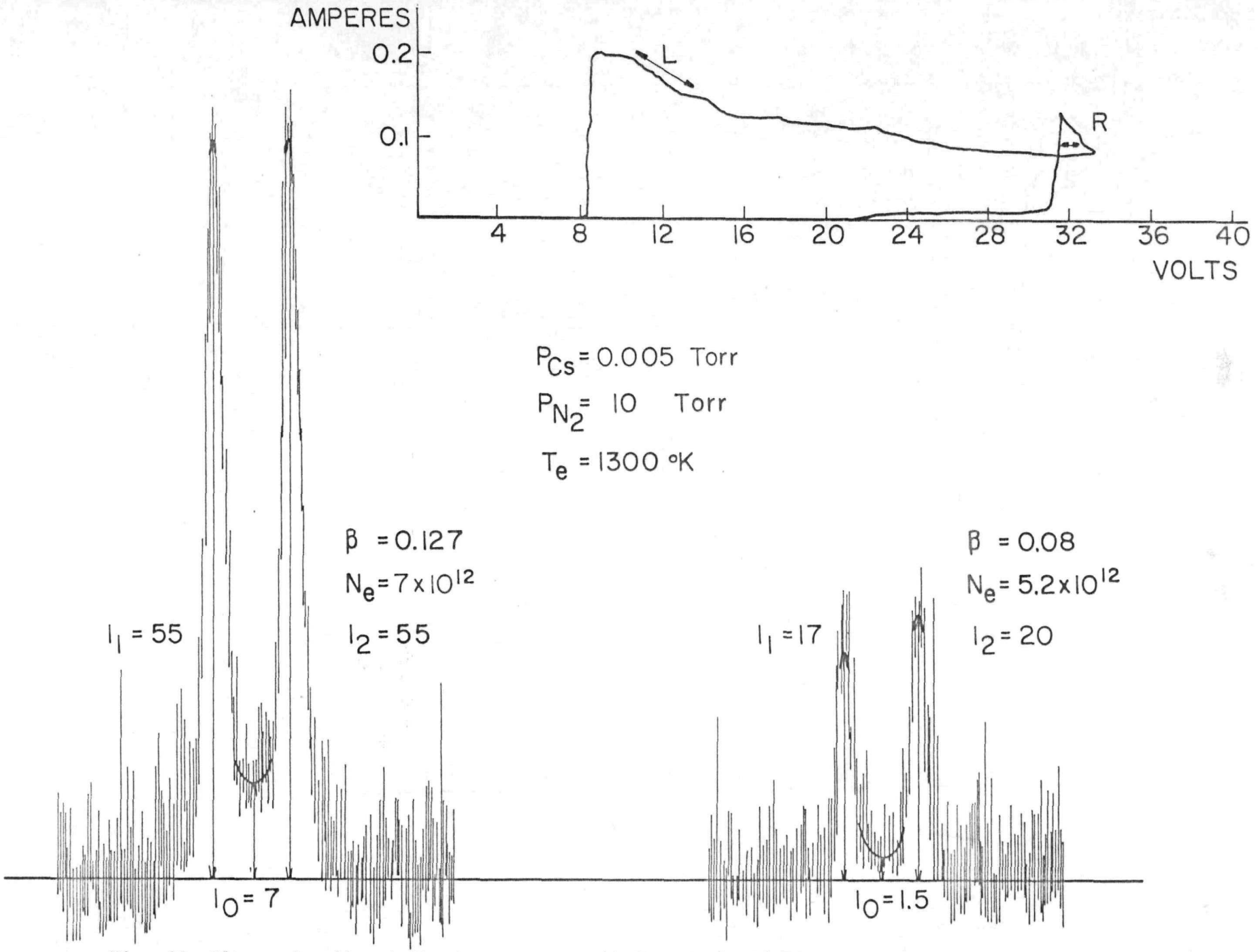

Fig. 26. Plasma density at the two extremes (left and right) of the I-V characteristics.

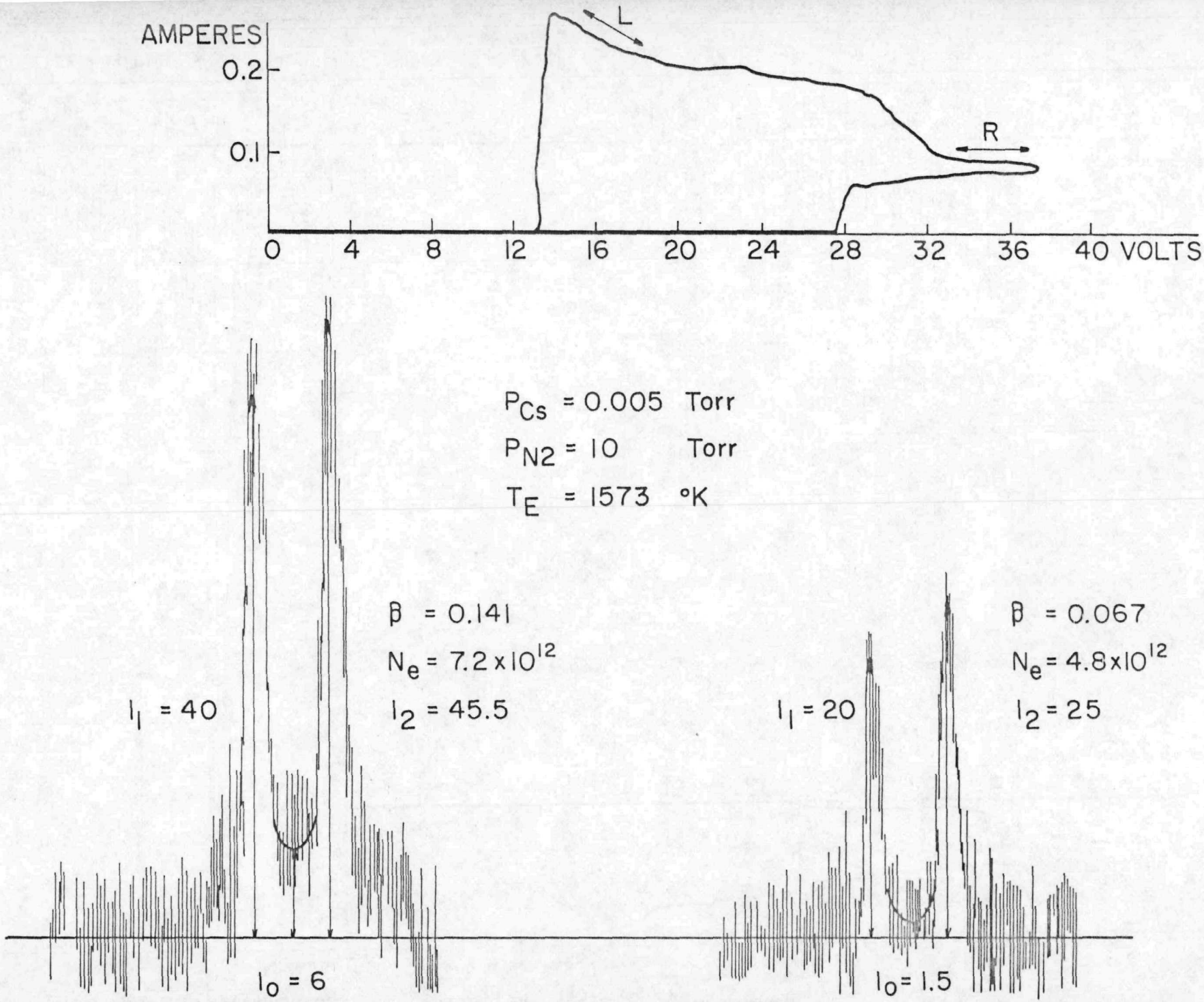

Fig. 27. Plasma density variations at the two extremes (left and right) Of the I-V characteristics.

are true for a higher emitter temperature as shown in Fig. 27.

In Fig. 28 the fractional enhancement ΔNe/Ne is plotted with

$$\frac{\Delta\ Ne}{Ne} = \frac{Ne\ (L) - Ne\ (R)}{Ne\ (R)} \qquad (11)$$

in plasma density in moving from point R to point L as a function of nitrogen partial pressure for cesium pressure of 0.05 torr. The smallest change occurs around 5 torr; the corresponding plasma density values are very high there so that little change is registered. On either side of 5 torr very small initial values for Ne exist at point R so there is much room for improvement which is duly accomplished.

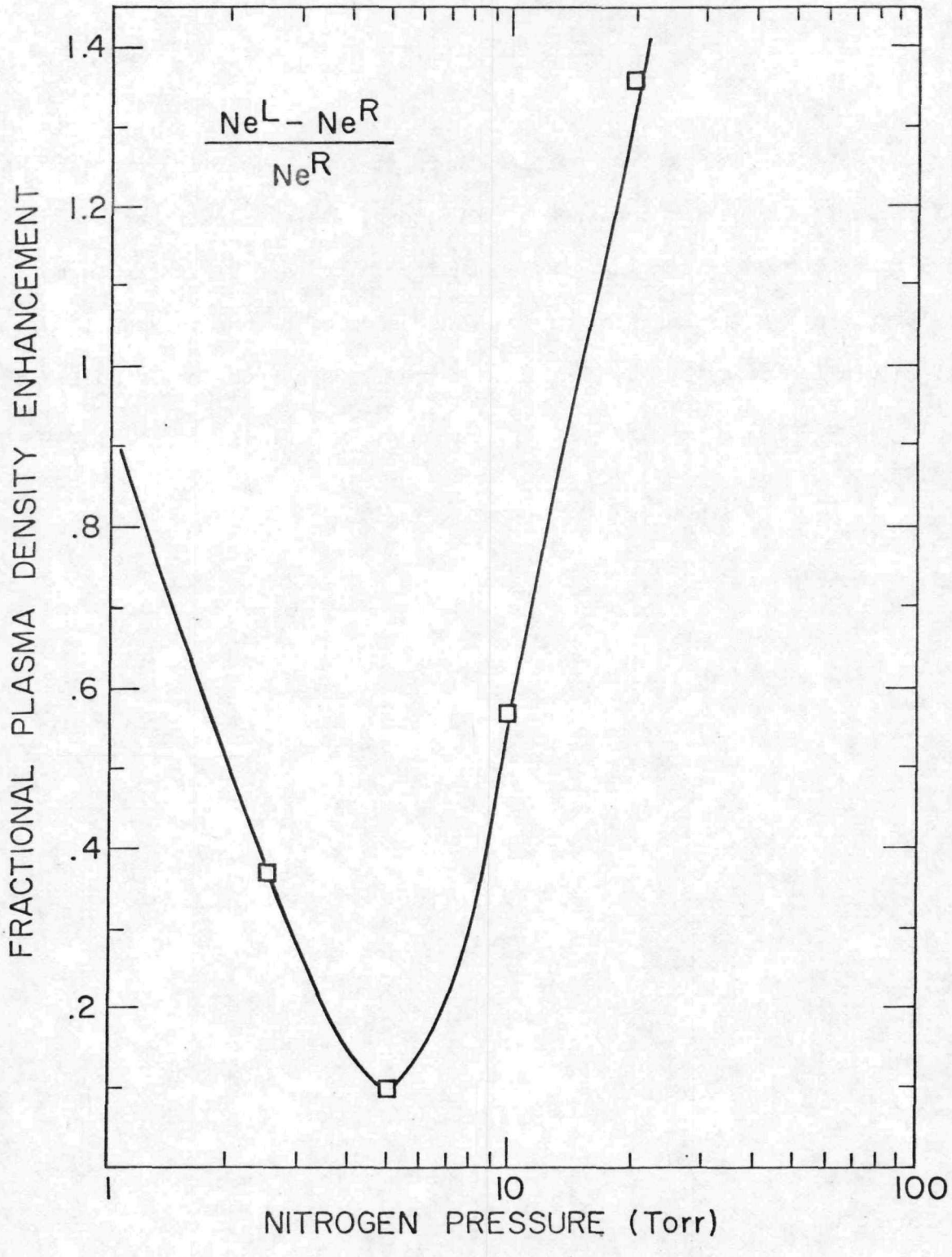

Fig. 28. Fractional enhancement in plasma density as a function of nitrogen partial pressure.

6.. Cs - N_2 MIXTURE: THE PULSE DISCHARGE

a. Theory

The relaxation time for the excited molecular nitrogen is known to be quite long either for vibrational excitations or several important electronic excitations, i. e. the N_2 (A) state. An interesting possibility for excitation and eventual stepwise collisional ionization of cesium might be the application of high voltage pulses to a N_2-Cs system. This would lead to the creation of a strong non-equilibrium distribution of N_2 which decay slowly and in the process transfer energy to cesium atoms by collisions. Thus, in the afterglow the excited nitrogen would act as an energy storage medium injecting energy to cesium over a considerable period of time. If the applied pulse is short with respect to the decay time the thermionic converter would operate successfully when the applied pulse is off with considerable cesium ionization continuously replenished by energy from the excited nitrogen.

The mechanism of cesium ionization by N_2 (X) is not entirely clear at this time. Controversy exists as whether the ionization of alkali atoms by N_2 (X) is a one-step or multi-step process. Since the excitation cross section depends critically on the energy matching between the Cs electronic excitation energy and the vibrational energy exchange Δv in N_2 (X) (Fig. 29a). Haug[30] performed experimental measurements and showed the ionization is indeed one-step.

Tibilov and Shukhtin[31] used pulsed discharges of a mixture of sodium with helium and hydrogen and studied the mechanism in such a system. They found that the radiation oscillation power depends linearly on the partial pressure of hydrogen until saturation is reached. Morgulis and Klapchenko[32] discussed the effect of molecular hydrogen on the cesium DC discharge and found that as the partial pressure ratio of hydrogen to cesium reduces less

than 1, the effect is mainly quenching of the cesium radiations, but they did not perform any work in the higher partial pressure ratio cases.

Treanor, Rich, and Rehm[33] have shown that the population distribution over vibrational levels of a diatomic gas in the quasiequilibrium regime has the analytic form:

$$N(\nu) = N(o)\exp\left\{\left[\left[(-hc) / K\right] E(\nu) / \theta(\nu)\right\}\right. \tag{12}$$

where $E(\nu)$ is the vibrational energy of level ν measured from $\nu=0$ and

$$\theta(\nu) = T_\nu / \left\{\left[\nu E(I) / E(\nu)\right]\left[I-(T_\nu / T)\right] + (T_\nu / T)\right\} \tag{13}$$

where θ is the vibration temperature, T and T_ν are the nitrogen kinetic temperature and the effective temperature of the $\nu=1$ level respectively. This distribution is the solution of the master-rate equation in which V-T terms and radiative terms are neglected, and where the principle of detailed balancing and restriction to single quantum transitions have been imposed. For $T_\nu > T$, this distribution predicts a population inversion at

$$\nu_m \simeq \frac{1}{2}\left\{1 + (T / T_\nu)\left[E(1) / w_e x_e\right]\right\} \tag{14}$$

beyond this minimum $N(\nu)$ increases monotonically with ν.

A numerical solution of the master-rate equation in wich V-T and radiative terms are retained has been performed by Caledonia and Center[34]. However, their work does not show this population inversion except under very restricted conditions because V-T terms are as important as V-V terms for high vibrational levels and tend to depopulate these levels. Their analysis indicates that in the region between ν_m and the value of ν for which V-T reactions can force the upper vibrational levels into equilibrium with the rotational-translational mode, the population distribution is

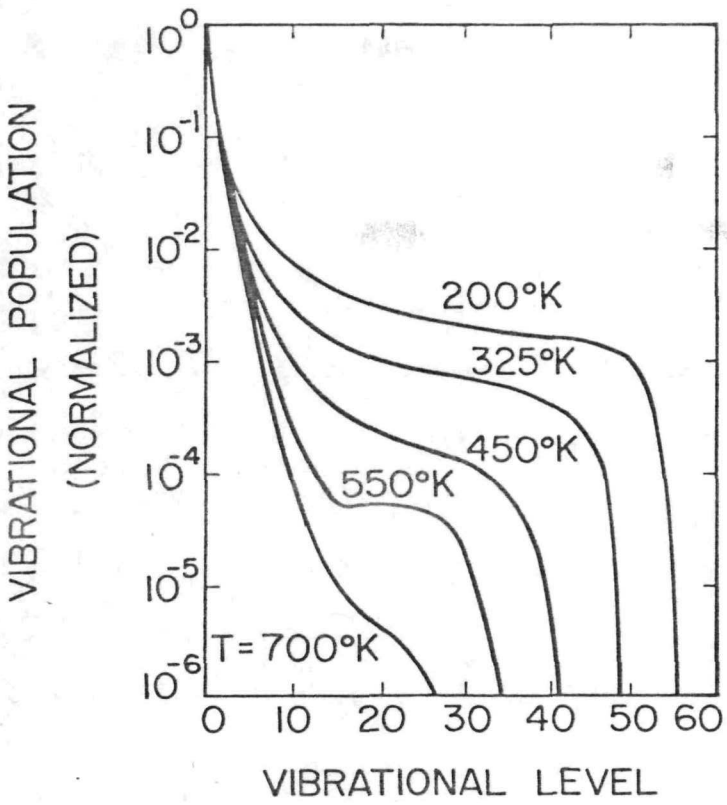

(b) Vibrational population distribution.

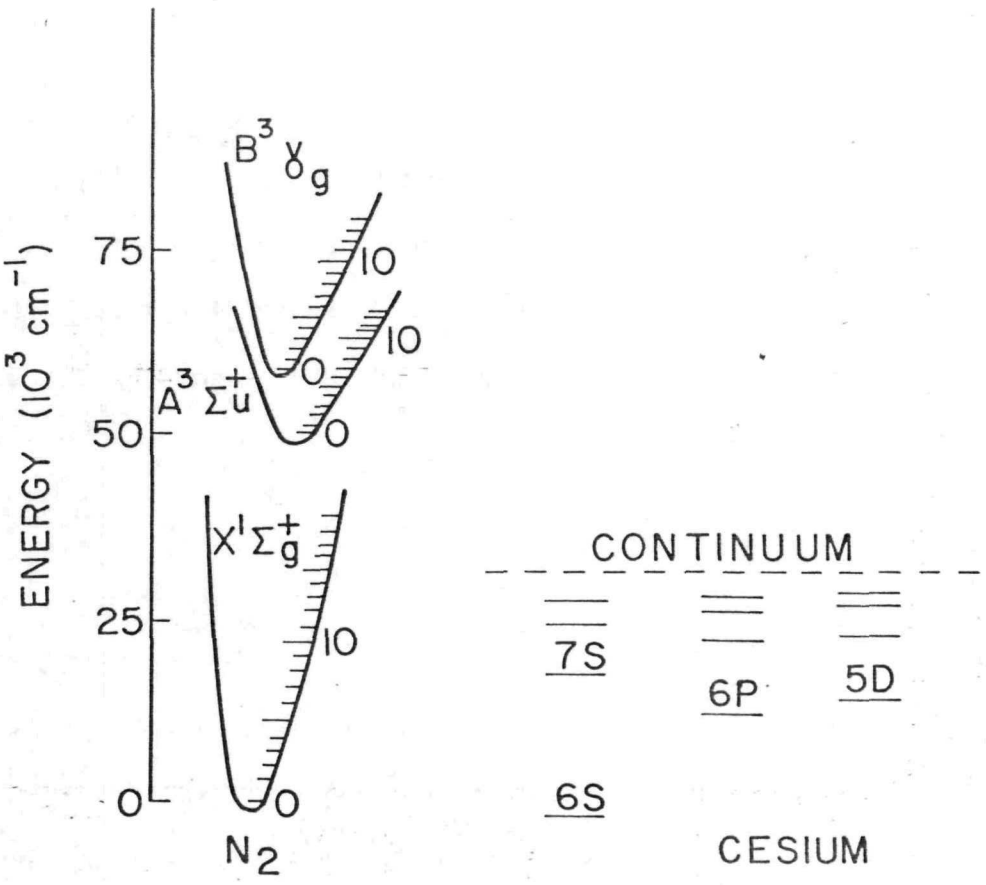

(a) Energy levels of nitrogen and cesium.

Fig. 29.

well approximated by

$$N(\nu) = N(\nu_m)\ \nu_m / \nu \qquad (15)$$

The results of Caledonia and Center are reproduced in Fig. 29b which shows that the population distribution is a very sensitive function of the gas kinetic temperature. This implies that in order to produce a high concentration for N_2 (X) at highly excited states (high ν) the collector temperature must be maintained as low as possible, possibly by a combination of cooling and large interelectrode spacing. Furthermore, the cesium ions are produced predominantly near the collector and migrate toward the emitter.

The Recombination Coefficient

The radiative recombination in Cs has been extensively studied. D. W. Macross and P. M. Stone[35] give the recombination rate equation as

$$\frac{dn_p}{dt} = a_p\ n_i\ n_e, \qquad (16)$$

where n_i = ion concentration, n_e = electron concentration, a_p = recombination coefficient, and n_p = number of Cs atoms in a quantum state "p".

Since $n_i = n_e$ in arc mode of operation and because the number of atoms gained in "p" state means a loss of equal number of electrons in the plasma, equation (16) can, therefore, be written

$$\frac{dn_e}{dt} = - a_p\ n_e^2 \qquad (17)$$

Equation (17) describes the loss of electrons due to a radiative recombination into p states. As the total loss of electrons is the combined effect of all the recombination processes to any arbitrary state, therefore, the total loss of electrons is simply the sum of all possible contributions of the form of

equation (17). In other words, the total rate equation of the electron concentration is

$$\frac{dn_e}{dt} = - \alpha n_e^2 , \tag{18}$$

where

$$\alpha = \sum_p \alpha_p .$$

Many efforts have been put into finding α[36]. Practically, the most useful information for the recombination coefficient α is given by R. H. Curry[37]. In their work, they have established the empirical recombination coefficient as a function of the electron concentrations n_e and temperature T_e,

$$\alpha = \alpha_o \, e^{\frac{E_a}{(K T_e)^{1/2}}} \tag{19}$$

where values of α_o, E_a are listed in the above cited article. Substituting (19) into (18)

$$\frac{dn_e}{dt} = - \left(\alpha_o \, e^{\frac{E_a}{(K T_e)^{1/2}}} \right) \cdot n_e^2$$

$$= - \left(\alpha_o \, n_e \, e^{\frac{E_a}{(K T_e)^{1/2}}} \right) \cdot n_e \tag{20}$$

$$\equiv - \frac{1}{\tau} n_e$$

$$\tau \equiv \left(\alpha_o \, n_e \, e^{\frac{E_a}{(K T_e)^{1/2}}} \right)^{-1} \tag{21}$$

is the decay time for the plasma.

Making use of τ, one can, in principle, evaluate the theoretical value of the decay time. However, as can be seen from Ref. (37), although α_o, and

$E_a / \sqrt{K}$ are relatively slow-varying functions of n_e, the ratio

$$E_a / \sqrt{K} = 107.6 \times E_a \simeq 300 - 480,$$

is a large number. Consequently, a change of $\sqrt{T_e}$ in the exponent $\exp\left[\left(E_a / \sqrt{K} \right) / \sqrt{T_e} \right]$ introduces a significant change of τ. Physically, this is not surprising, as equation (19) merely states that the recombination coefficient is affected by the thermal energy spreading through $\sqrt{K T_e}$. A change of $1 / \sqrt{T_e}$ with a large coefficient naturally implies that the spreading of the energy spectrum strongly affects the overall behavior of the system.

Since the experiment is performed utilizing a method employing two spectroscopic lines, the information of the electron temperature is thus lost. As a result, no precise evaluation of the decay time τ is possible in this work. However, a rough estimation, using (19), (21) and the experimentally obtained n_e and putting T_e to be roughly between $1500^{\circ}K$ to $2500^{\circ}K$, indicate that the experimental decay time falls in the range of the theoretical value. In other words, in the absence of N_2, the results are consistent with the theory as well as the previous works.

b. The Probe Measurements

In a time varying plasma mixture of Cs - N_2 often needed to know the recombination coefficient and the decay time after the end of the pulse. Knowledge of the electron density is a requirement for these calculations. The probe method is preferable because of it's performance in low density plasmas ($N_e < 10^{14}$). The use of double probes, in transient plasma is not new. But using double pulsed floating probes in a rapid discharge plasma is quite new and only a little information exists in the literature. In addition, since it is desired to retain the option of spectroscopic measurements (for the low density plasma method) and because of probe mounting problems, the discharge vessel is chosen to be a pyrex tube with covar transition (Varian pyrex to covar adapter on non-rotatable conflat flange part number 952-5018). The probes are mounted either parallel to each other or colinear, in which case the interelectrode capacitance is greatly minimized.

Since the plasma is transient (discharge pulse from 250 μs to 10 μs) the author has to pulse the probes in order to be able to measure the I-V curves. In addition bacause of the variation of the plasma potential with probe current (which falsifies the electron measurements) use is made of double floating probes which are pulsed in either the plasma excitation or in the afterglow. To accomplish this, a special instrument, the pulse probe reader (PPR),is built. The function of the PPR is to take two values (pulses), namely the voltage across the two probes, and current through the probes and passes the value of current through appropriate almost noise free amplifiers. Then both of the values of V, I will be applied to sample and hold (S/H) gates (synchronized by a master clock). After this point the pulses are converted to DC. Next the voltage is applied to the X axis of an X-Y recorder, and the current is

applied to the Y axis through a log amplifier. Thus the plot of V / lnI is obtained which is helpful in the evaluation of the parameters of the plasma, such as electron temperature (Te) and electron density (Ne).

In Fig. 30 a block diagram is shown of the pulse probe reader and in Appendix B full documentation is given. In Fig. 31 an overall picture of the electronic instrumentation is given where the main pulse amplifier, the PPR, and the associated electronic instruments are shown. These components are synchronized by a master clock, so that probe measurements, during and after the pulse, can be taken with a resolution of 500 μsec (pulse position) and pulse width up to 1 μsec, thus minimizing pulse deletion[38].

The special construction of the probes and decontamination electronic circuits will minimize problems with the thermal edge effects[39],[40] and the contamination of probes[41], [42], [43]. Chemical cleaning of the probe has been performed before enclosure in the vacuum chamber which is desirable although awkward and ineffective. After the enclosure in the vacuum chamber electron bombartment is used because it only requires a possitive potential of a few volts with respect to the plasma potential and because one can observe the probe glowing brightly during cleaning; but a combination of electron and ion cleaning is best. For this study, the probes are heated to approximately 1500°C (as observed with an optical pyrometer) and held at this temperature for 45 sec. Longer periods and/or higher temperatures do not alter the probe traces. It is necessary to allow approximately 15 sec for the probe to cool before a trace is taken. To prevent contamination during this cooling period, the probe is continuously bombarded by attracting ions through a potential of 200-300 V. This sputtering removes all the dark deposit left by electron cleaning and provides a shiny surface. Next the measurement is

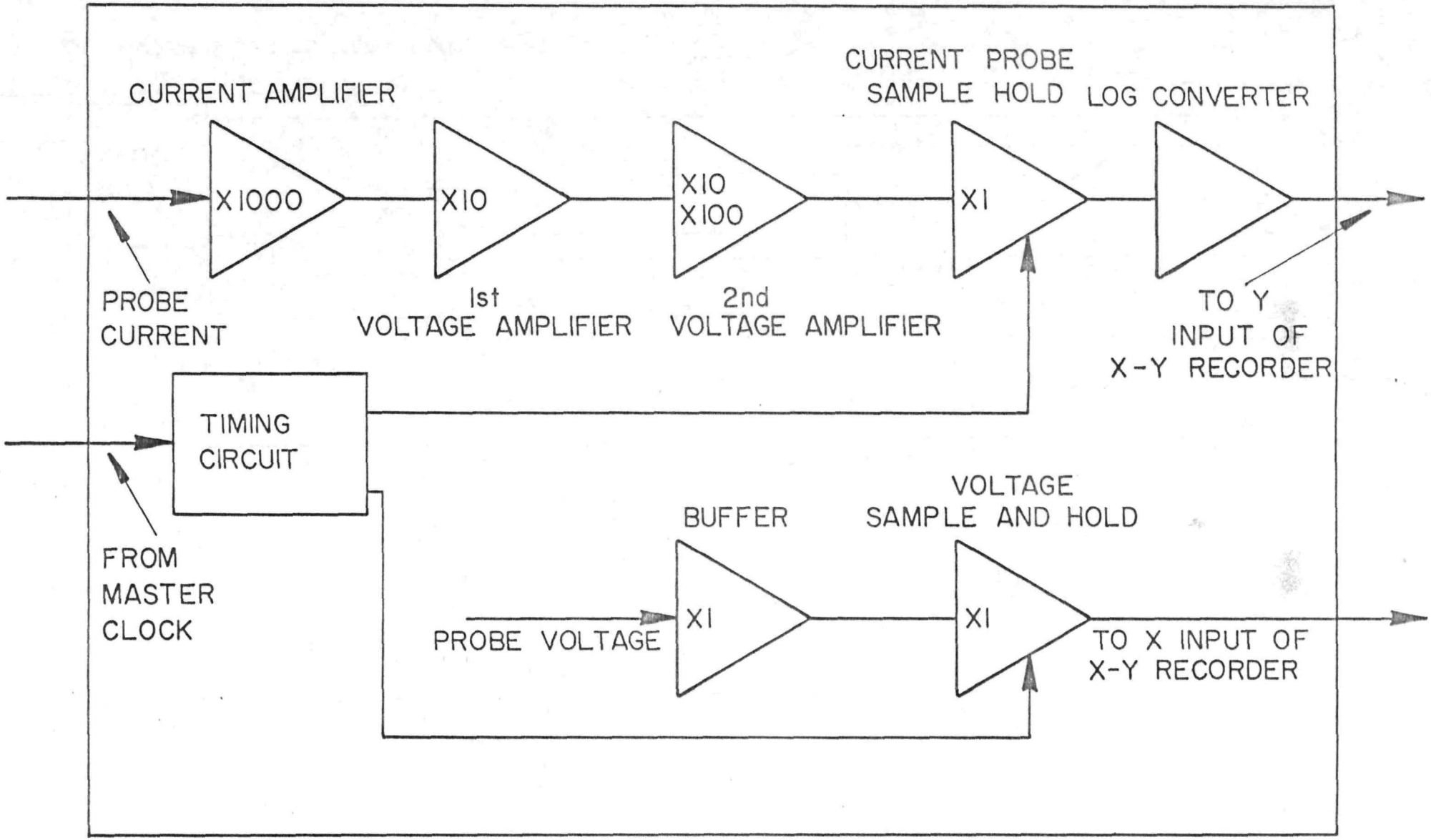

Fig. 30. BLOCK DIAGRAM OF PULSED PROBE READER

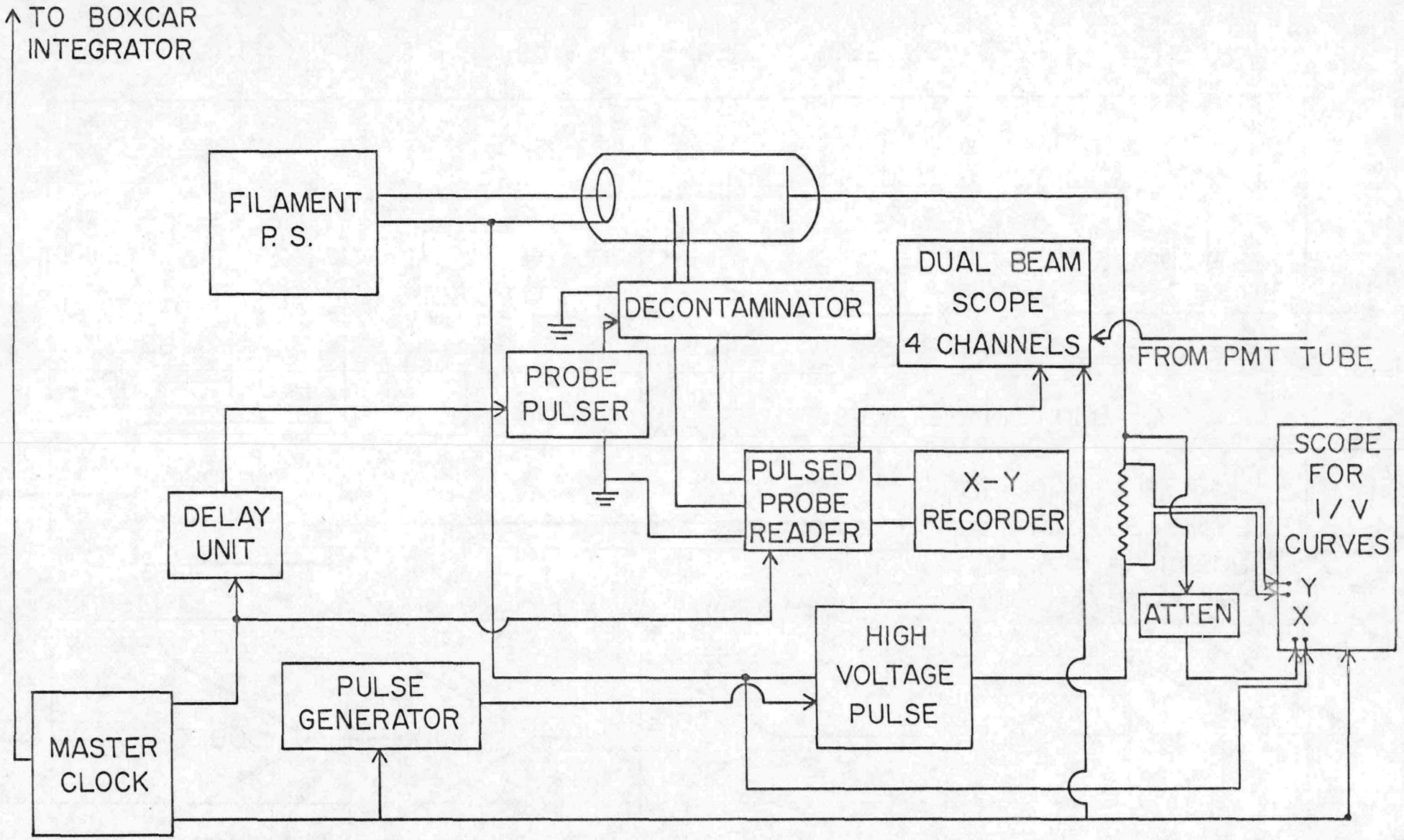

Fig. 31. Electrical discharge circuit and associated electronic instruments for the pulse case.

taken after the immediate removal of the negative potential. The same procedure is followed before each measurement. Appropriate switching relays insure that the electronic I-V tracing circuit will not be disturbed by the cleaning process. Such a circuit is constructed, (the design is shown in Fig. 32) and found to function well under all operating conditions.

A physical description of the contamination process and it's effect is not essential to the purpose of this work, but it is advisable to show (in Fig. 33) the I-V characteristics of the probes (connected as a single probe, after cleaning in Fig. 33a and before in Fig. 33b).

Using the probes a large number of problems are encounted but the bigest, in using floating double pulsed in rapid discharge plasma experiments, arises from the necessity of isolating the probe circuit from the measuring circuit. Further, the "pulling up" of the probe circuit during the discharge towards the high positive - or negative - plasma potential should not disturb the measured probe current due to the inevitable stray capacitances, and thus affect the result of measurement.

Specifically the probes behave like an antenna collecting an unwanted current much higher than the one which is to be measured. The result is the saturation of most amplifiers in PPR. Similar observations are published by Schneider[44]. More work is needed towards the complete isolation of the probe circuit, possibly through optocouplers. More details can be found in Appendix B.

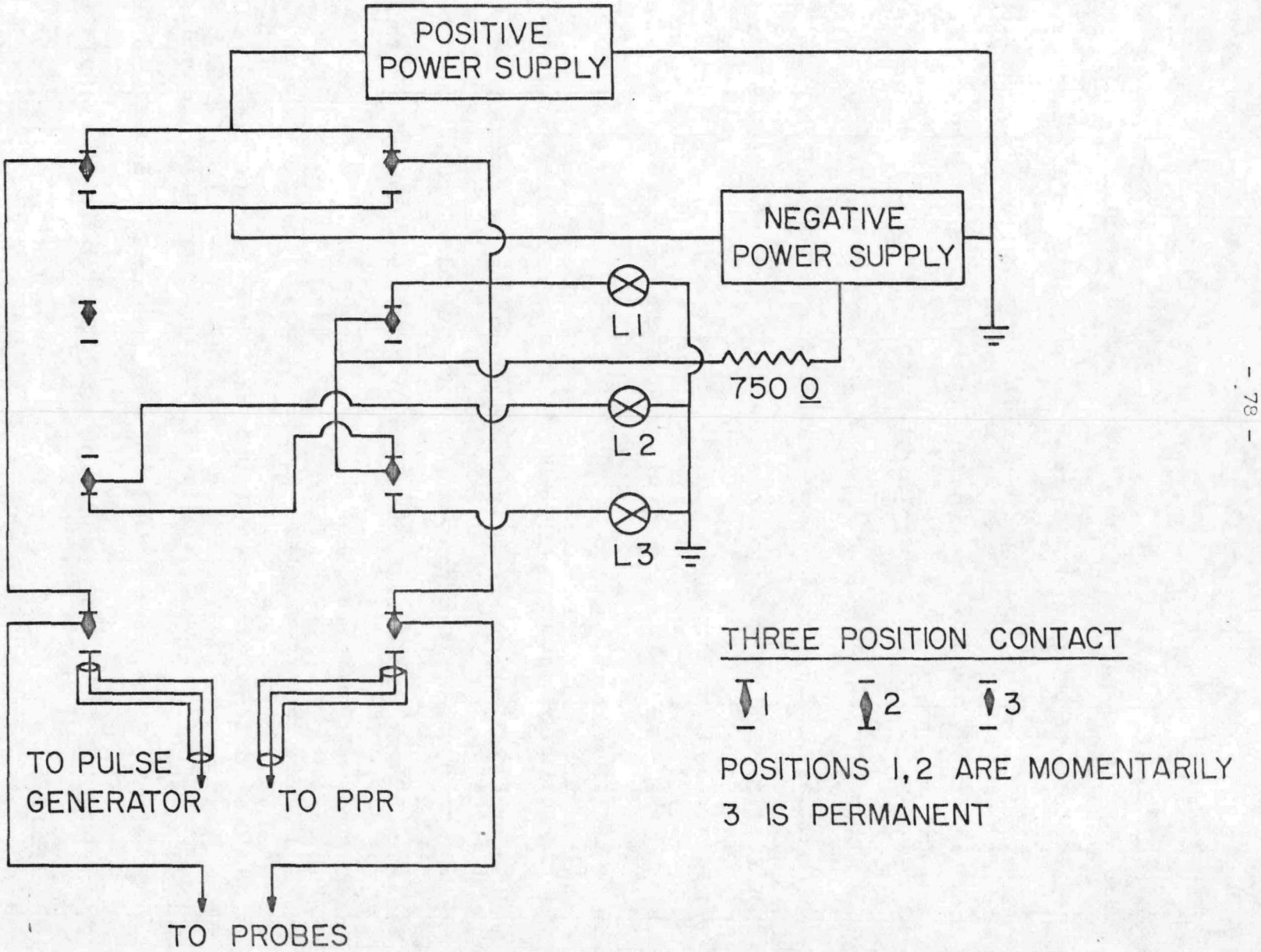

Fig. 32. Decontamination circuit.

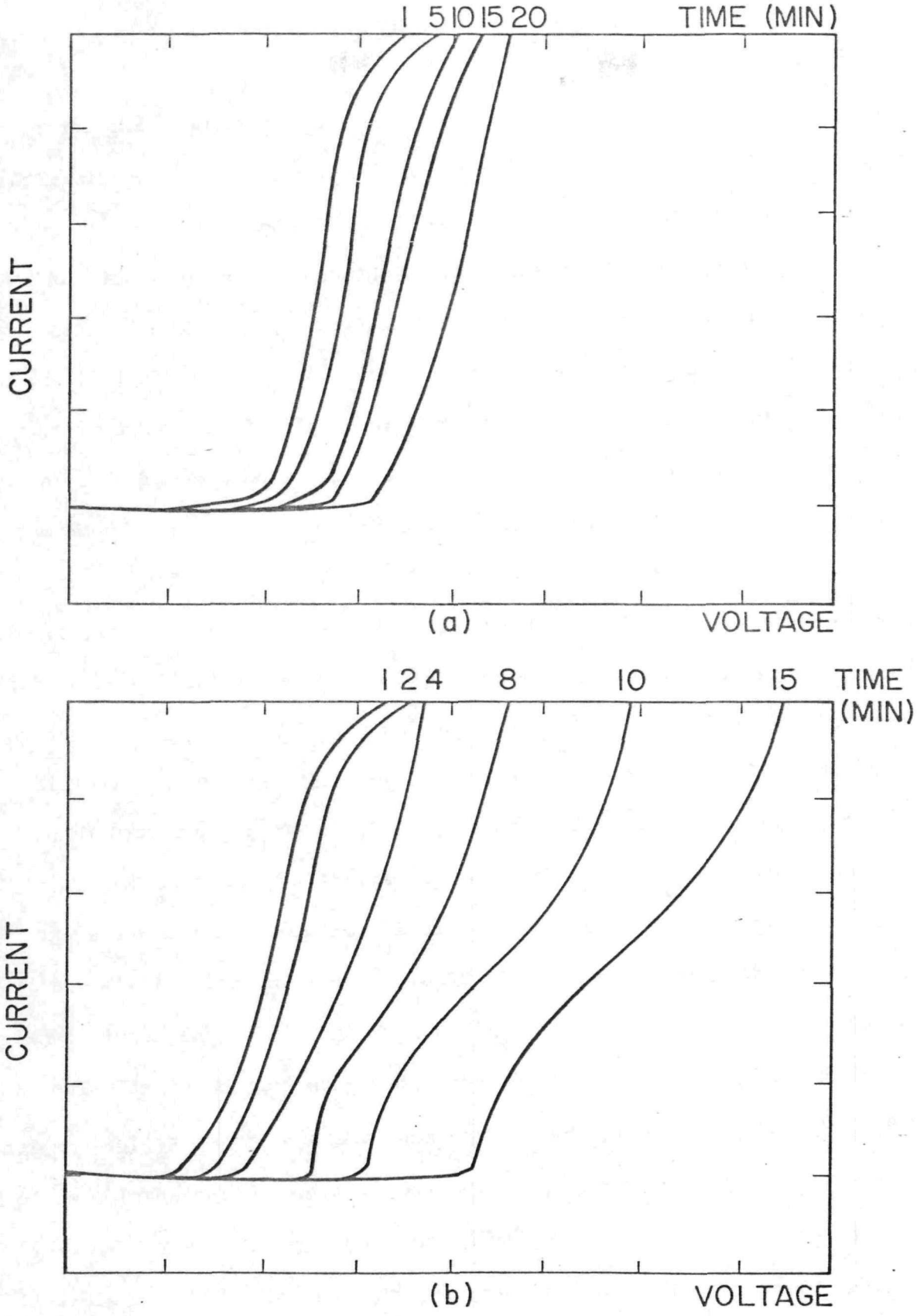

Fig. 33. Probe I-V characteristics with (a) and without (b) electronic cleaning.

c. Experimental Results

The block diagram for the electrical discharge and measurement instrumentation, as well as, the probe associated electronics are shown in Fig. 31. The filament is heated with an NJE model TC - 80 - 20 power supply. For the plasma discharge a Velonex model 340 high power pulse generator is used, modulated by an Intercontinental Instrument model PG-2 pulse generator. In order to avoid reflection of the power and missmatching effects (ringing reverse breakdown etc.), the appropriate Velonex plug in output unit is choosen in each particular case so as to match the impedance of the plasma. The discharge circuit and the probe associated electronics are synchronized by a master clock and a delay unit both (Global Specialties Corp. model 4001). The measurement of the I-V characteristics is done through a Tectronix oscilloscope model 475. The timing signals are simultaneously monitored through a Tectronix model 551 dual bean scope (8 channels total). A typical sequence of the timing signals is shown in Fig. 34. The light output from the plasma tube is collected with an appropriate optical system and analyzed through the monochromator, and finally detected and amplified with the PMT. The resulting electrical signal is applied to a Princeton Applied Research Preamplifier model 114 and Box-car Integrator model 160 which is basically a time-averanging device which opens it's gate and allows the input signal to enter the processor at specified time after each trigger signal. The output of the Box-car Integrator is the time average value of the past few sampled signals memorized by the electronic circuits. The instrument enables as to measure a very short signal by expanding the time scale, it also improves the signal to noise ratio which is very important in the fast transient measurements.

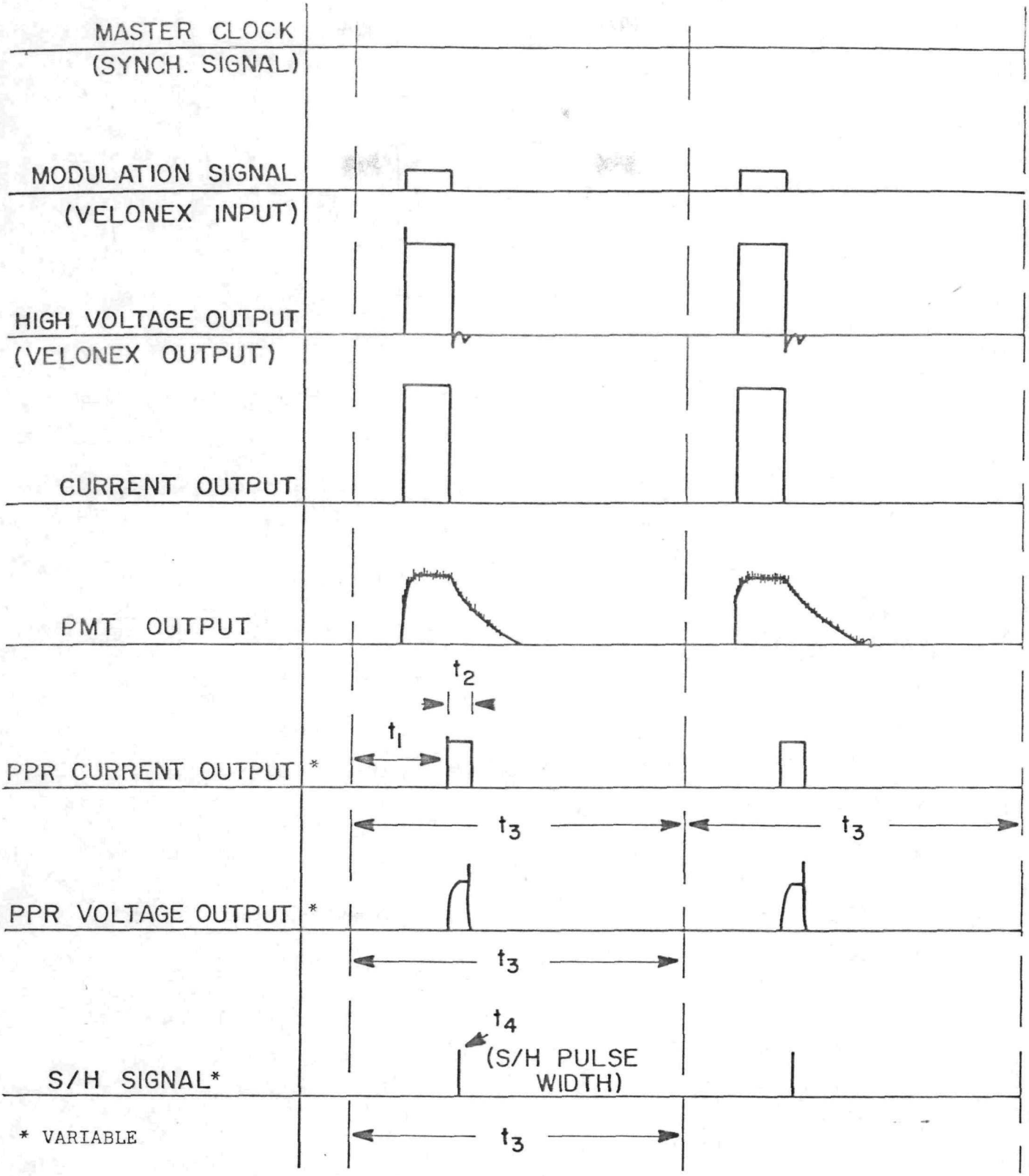

Fig. 34. Relationship among various time functions (discharge, PMT, probe).

The boxcar Integrator has two modes of operation, the delay mode and the scan mode. In the delay mode, the delay time is fixed at the initial delay switch setting t_i with variable aperture. In the scan mode the delay time increases from the setting of the initial delay time t_i to the final delay time setting t_F at a constant rate. The output of the boxcar integrator is plotted on a chart recorder. Fig. 35 shows various typical signals at several points of processing, from the initial PMT output to the chart recorder graphs. As it can be seen by this arrangement one is able to investigate the properties of transient plasma by using steady state diagnostic techniques.

A very large amount of data has been collected from measurements in the afterglow of strongly pulsed N_2 - Cs mixtures. Of particular interest are the lineshapes of several Cs atomic excitation lines. A family of curves for such lines are shown in Fig's 36 and 37. It shows the decay in the afterglow of the 4555 Å line of Cs for different values of the partial pressure of nitrogen in the mixture. The cesium vapor pressure in the mixture is fixed at 0.005 torr.in Fig. 36 and .05 in Fig. 37 respectively. It is interesting to note the unusual characteristic peak in emitted light intensity which occurs some time after the end of the applied excitation pulse in several of these decay curves. Details have been described elsewhere[45].

Some representative portion of the data has been summarized and tabulated in table 4. Two series of mixtures are shown, one with cesium pressure 0.005 torr and the other for 0.05 torr. The values of the decay time for the various combinations are tabulated. The values for pure cesium are also included. It is seen that the presence of nitrogen in the mixture results in considerably slower decay times which for the most part increase as the nitrogen pressure

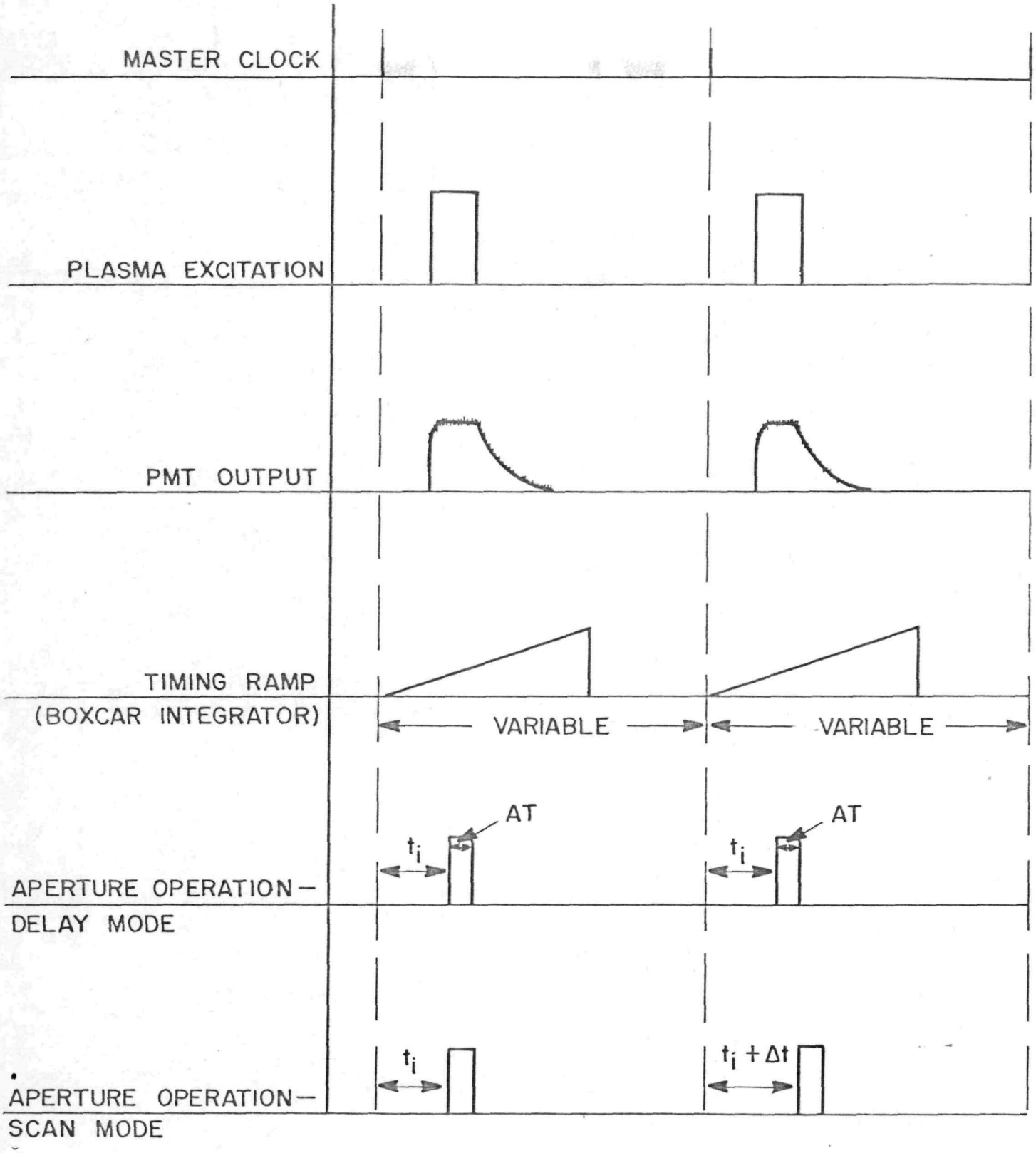

Fig. 35. Relationship among various time functions during the transient measurement using boxcar integrator.

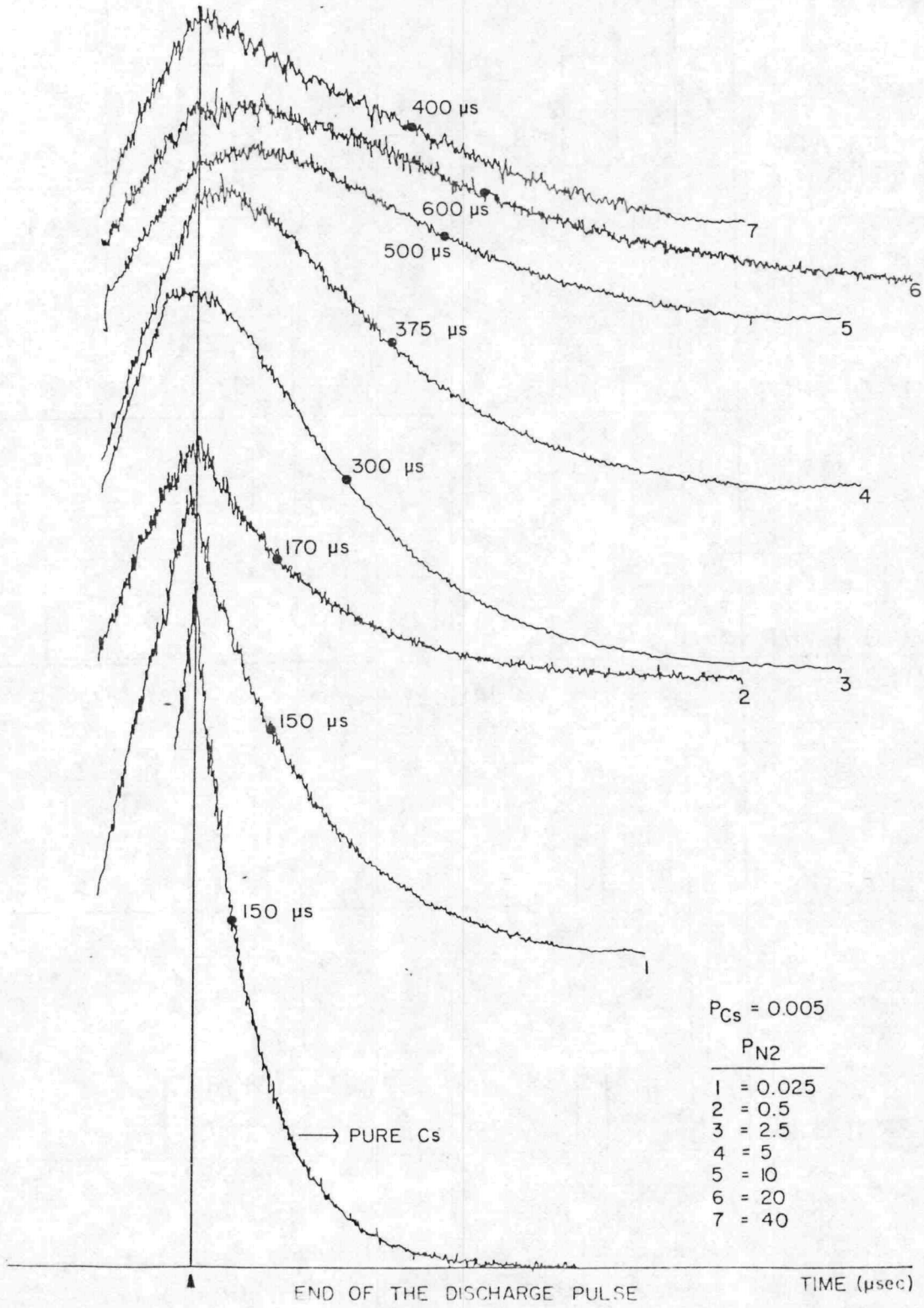

Fig. 36. Family of decay curves, in the afterglow mixture of a molecular gas with an alkali seed.

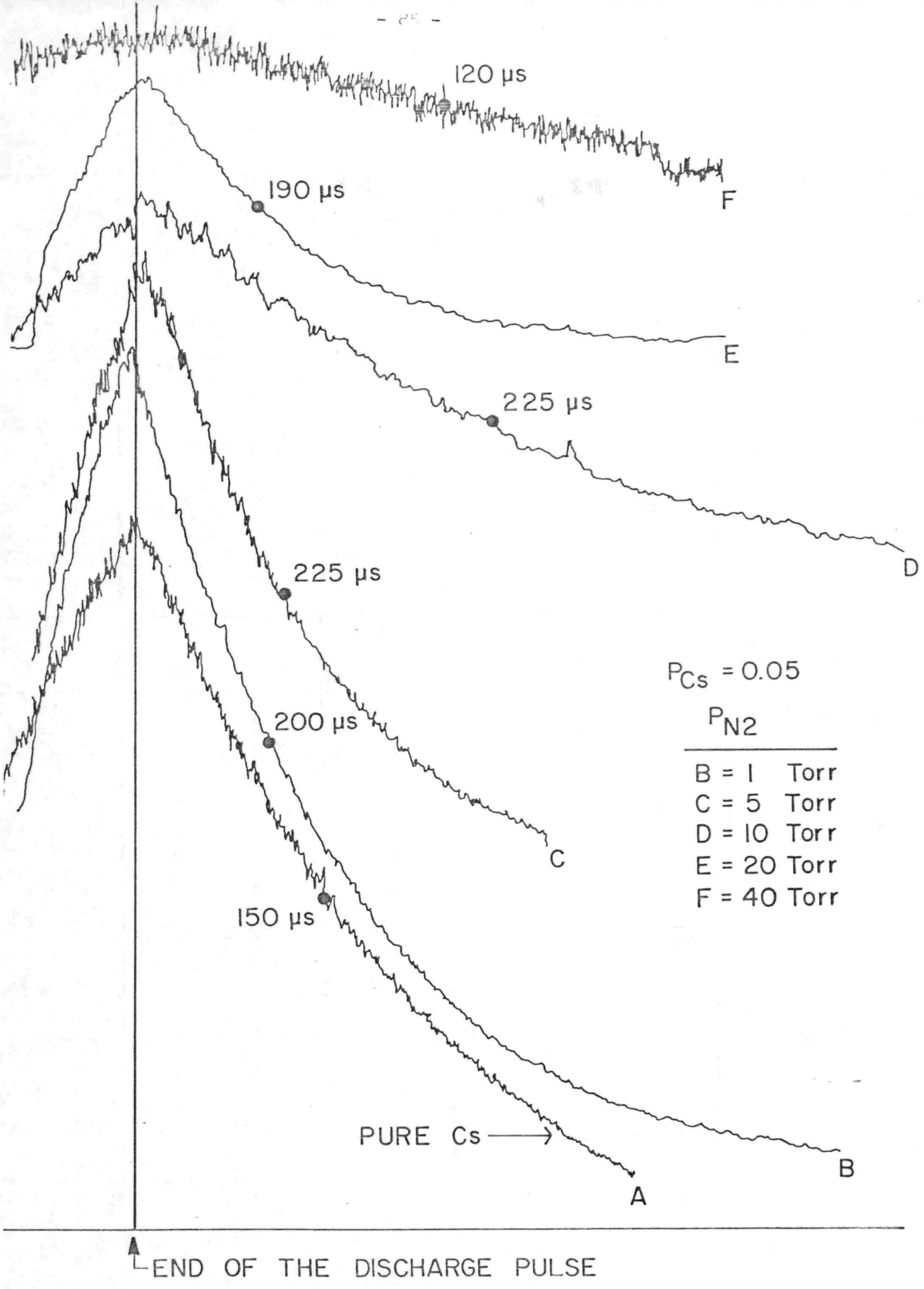

Fig. 37. Family of the decay curves, in the afterglow mixture of a molecular gas with alkali seed.

TABLE # 4. N_2 - Cs PULSE MIXTURE DATA

PURE CESIUM	PURE CESIUM DECAY TIME (μsec)	0.025	0.5	2.5	5	10	20	40	P_{N_2} (Torr)
		5	100	500	1000	2000	4000	8000	RATIOS
P_{Cs} = 0.005	150	150	170	300	375	500	600	400	DECAY TIME OF A 250 μs PULSE 10% DUTY FACTOR (μsec)
	185	175	180	360	390	510	600	375	DECAY TIME OF A 500 μs PULSE 30% DUTY FACTOR (μsec)
				1	5	10	20	40	P_{N_2} (Torr)
				20	100	200	400	800	RATIOS
P_{Cs} = 0.05	150			200	225	225	190	120	DECAY TIME OF A 250 μs PULSE 10% DUTY FACTOR (μsec)
	170			185	220	250	225	165	DECAY TIME OF A 250 μs PULSE 30% DUTY FACTOR (μsec)

increases.

The decay time versus nitrogen partial pressure in the mixture has been plotted for the two cesium pressures of 0.005 and 0.05 torr in Fig. 38 and 39. A definite peak exists which is at about 20 torr in the former and 10 torr in the latter. All the decay time values are considerably larger than that of pure cesium. It is interesting to note that the plot for the higher cesium pressure has a much shallower and broader peak which may be related to increased collisions in the afterglow.

The afterglow of a mixture of a molecular gas with an alkali seed, as the N_2 - Cs mixture, contains a large number of very complicated processes very difficult to unravel. Yet some points as well as some conjectures can be made in this work based on the experimental measurements as well as other results in the published literature.

The DC properties of several of these mixtures have been studied in detail in the earlier parts of this work. In particular the case of 0.05 torr cesium and 5 torr nitrogen has been investigated. The extreme values in plasma density are found to be 1.2×10^{13} and $1.3 \times 10^{13} cm^{-3}$. The measured decay time in the pulsed mixture is found to be 225μs. In the case of 0.05 torr cesium and 10 torr nitrogen the DC values of plasma density have been measured and found to be between 5.2×10^{12} and $8.2 \times 10^{12} cm^{-3}$. The decay time in the pulse afterglow is found to be 225μs. The DC values of plasma density should be very close to the values existing at the end of the pulse because when the measurements have been made for larger and larger pulse widths up to 1 msec for which DC like equilibrium should be obtained, no significance change in the results is seen. It is seen that although the plasma density from one mixture to the other changes

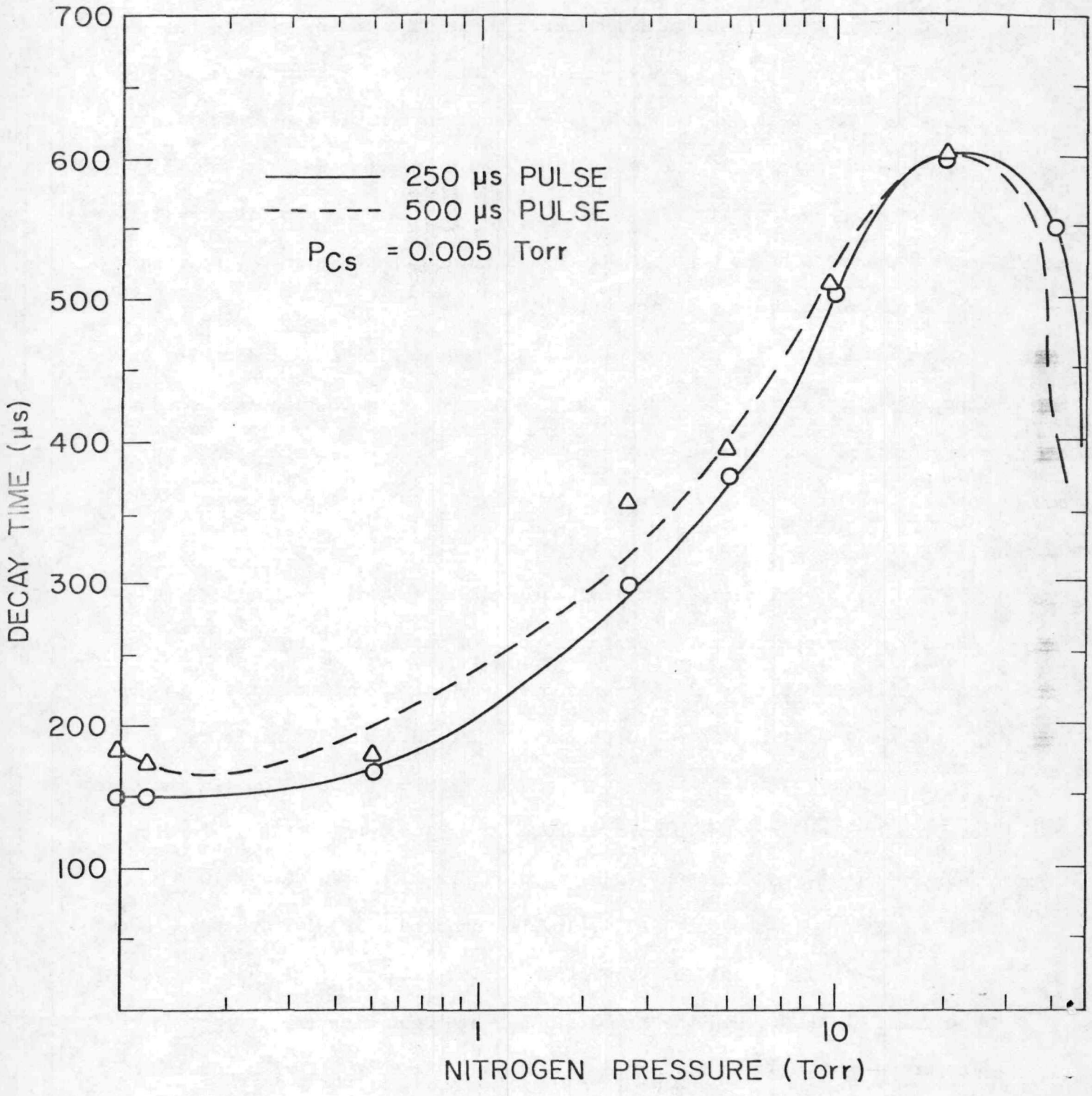

Fig. 38. Decay time versus nitrogen pressure.

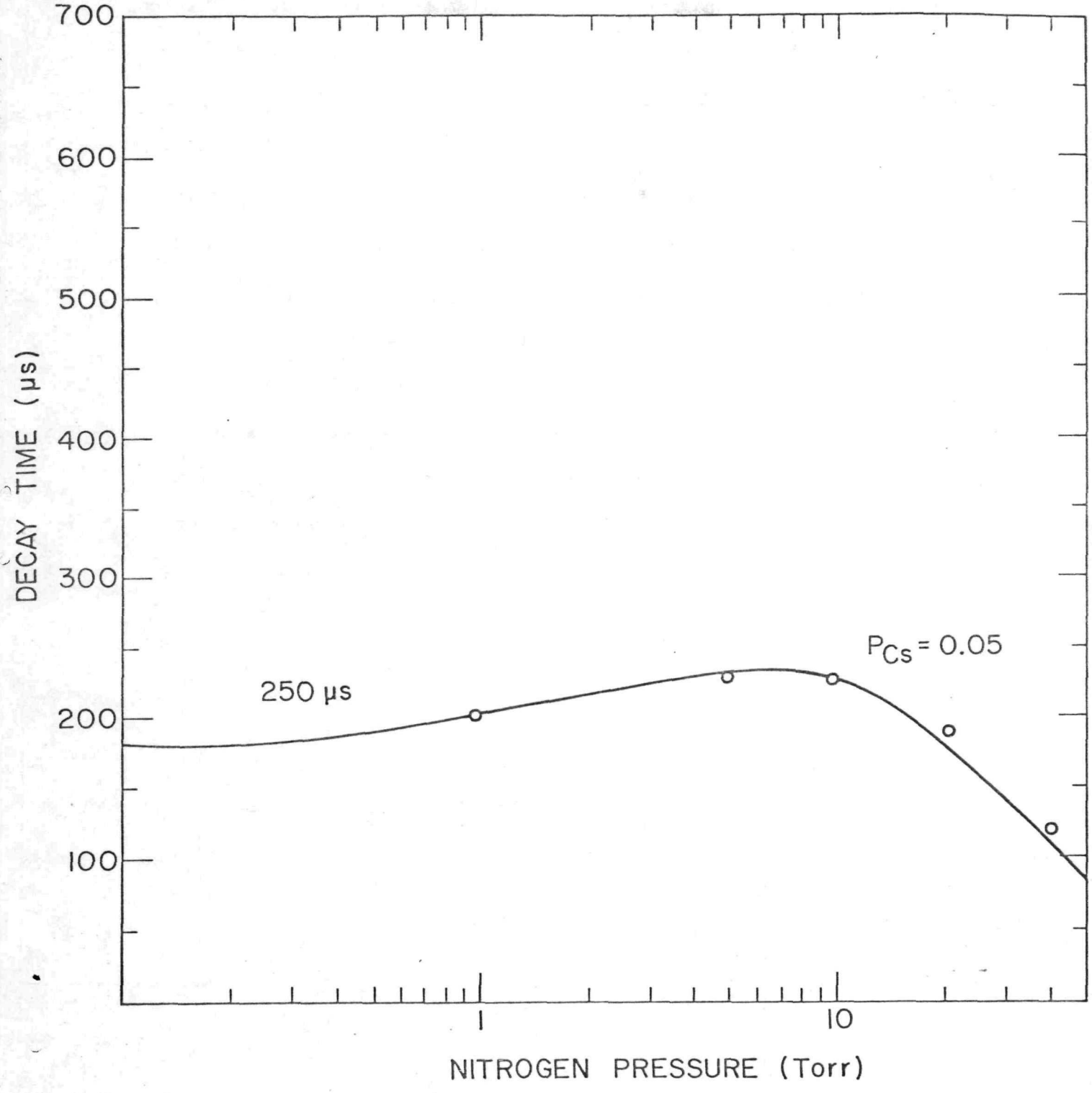

Fig. 39. Decay time of a 250 μs pulse versus nitrogen pressure.

more than a factor of two on average no change in the decay time is measured. This strongly suggests that the larger observed decay times may not be due to some collisional recombination effect cascading down through the excited states, since such a process should exhibit a very strong dependence on plasma density.

Evidence also exists from the work of D. Y. Dudko et al[46] that this effect is not caused by some reabsorption processes in the afterglow either. The reason given in this dissertation is the lack of any large number of states beneath the 7P state of the monitored transition; in fact only the 6P state exists between the 7P state and the ground state.

One remaining interesting possibility is that of a pumping process in the afterglow where some long lived excited vibrational or electronic states of nitrogen keep on suppluing energy to the cesium atoms lifting them to high excited states for a long time after the pulse has ended.

References

1. S. H. Lam. Preliminary report on plasma arc-drop in thermionic converters, AT (11-1)-2533, March 1976.

2. The advan. thermionic conver. with microwave power as an auxiliary ionization source. C. N. Manicopoulos, M. Hatziprokopiou, H. S. Chiu and D. T. Shaw.

3. The advan. thermionic conver. with external ionization mechanisms. M. Hatziprokopiou, C. H. Lee, Nisar Shah and D. T. Shaw. The 1978 IEEE Intern. Conference on plasma science.

4. J. B. Taylor and I. Langmuir, Phys. Rev., 51 753 (1937).

5. H. Shelton, R. F. Wuerker and J. M. Sellen, ARS Meeting, San Diego, Pape no 882-59.

6. L. L. Marino, A. C. H. Smith and E. Caplinger, Phys. Rev., 128, 2243 (1962).

7. J. Taillet, Am. J. of Phys., Vol. 37, pp. 423-441, (April 1969).

8. Auxiliary Ionization in Advance Thermionic Converters, M. Hatziprokopiou, R. Chandra, D. T. Shaw, 1980 IEEE International Conference on Plasma Science.

9. W. L. Nigham, Appl. Phys. Lett., Vol 20, No 2, 96 (1972).

10. G. Black, H. Wise, S. Schechter and R. L. Sharpless, J. Chem. Phys., Vol. 60, No. 9, 3526 (1974).

11. C. N. Manicopoulos, Tao Chang, D. T. Shaw, Proceedings of Thermionic Power Generation Conference, Eindhoven, The Netherlands, 1975.

12. A. C. Mitchell and N. W. Zemansky. "Resonance radiation and excited states" p. 189 (Cambridge U Press, London, 1961).

13. D. A. Magills and L. Krause, P. R. 153 44 (1967).

14. D. R. Jenkins, Prod. Roy. Soc. (London) A303 453 (1968).

15. R. Haug, G. Rappenecker and C. Schmidt, Chem. Phys., 5, 255 (1974).

16. H. F. Krause, J. Frick and W. L. Fite, Chem. Phys., 56, 4563 (1972).

17. J. D. Anderson Jr. J. A. P. 43 534 (1972).

18. R. C. Benson, J. Chem. Phys. 61 1652 (1974).

19. R. G. Gann, F. Kaufman, and M. A. Biondi, Chem. Phys. Lett. 16 380 (1972).

20. C. H. Dugan, and C. M. Sadowski. Chem. Phys. Lett. 14 190 (1972).

21. D. M. Hunten. J. Atm. Terr. Phys. 27 538 (1965).

22. G. J. Schulz, P. R. 125 229 (1962).

23. H. F. Krause, J. Fricke, and W. L. Fite, J. Chem. Phys., 56, 4593 (1972).

24. H. R. Griem, Plasma Spectroscopy (McGraww-Hill, New York, 1964).

25. H. R. Griem, Phys. Rev. 128, 515 (1962).

26. B. Sayer, M. Sassi, and J. C. Jeannet, Compt. Rend. 271, 839 (1970).

27. M. Fubry and J. R. Cussenot, J. Appl. Phys., Vol. 43, No. 2, Feb.1972.

28. H. W. Drawin, Rapport C. E. A. -Conf. 1628, 1970 (unpublished).

29. C. Lee, Ph. D. Dissertation, S. U. N. Y. / Buffalo, Feb. 1978.

30. Haug, R., et al (1974) Chemical Physics, 5, 255.

31. A. S. Ticilov and A. M. Shukhtin, Opt., 25, 3 (1968).

32. N. D. Morgulis and V. I. Klapchenco, Sov. Phys. Tech. Phys. 19 911 (1975).

33. C. E. Treanor, J. W. Rich, and G. R. Rehm, J. Chem. Phys., 48, 1998 (1968).

34. G. E. Caledonia and E. R. Center, Chem. Phys., 55, 552 (1971).

35. Radiative Recombination in Cs, J. Quart. Spectrosc. Radiat. Transfer 6, 277 - 290, 1966.

36. See, for example, "Thermionic Converters and Low - Temperature Plasmas", by F. G. Baksht, G. A. Dynzher, A. M. Martsinovshiy, B. Ya. Moyzhec, G.

Ye. Pikus, E. B. Soniu, V. G. Yur'yev, and Ed. L. H. Hausen, English Edition, Technical Information Center / DOE, 1978; R. H. Curry, D. W. Norcross, and P. M. Stone, Naval Research Report, NR 099 - 385.

37. R. H. Curry, D. W. Norcross, P. M. Stone and K. J. Nygaard, Naval Research Report SRRC - CR - 68 - 4, 1967.

38. J. F. Waymouth, J. Appl. Physics, 37, 4492 (1966).

39. J. F. Morris, NASA, T. M. X - 1294.

40. R. H. Bullis and W. J. Weigand, 23rd Ann. Conference on Physio-Electronics, MIT 1963.

41. Medicus and Wehner, J. Appl. Physics, 23, 1035 (1952).

42. K. Hirad and K. Oyama, J. G. M., 22, 393 (1970).

43. J. C. Holmes and E. P. Szuszczewicz, R. Sci. I, 46, 592 (1975).

44. H. Schneider and J. Szubert, Rev. Sci. Instrum., Vol. 48, No. 4, April 1977.

45. M. Hatziprokopiou, F. Radpour, C. N. Manicopoulos, and D. T. Shaw, 31st Annual Gaseous Elect. Conf., October 1978.

46. D. Y. Dudko et al. Opt. Spectrosc., 17, Vol. 34, No 1, JANUARY 1973.

Appendix A.

CLEANING OF VACUUM COMPONENTS

It is generally recognized that the greatest problem facing the designer and builder of vacuum tubes and vessels is that of removing or reducing contamination from component parts. Submicroscopic particles, gases, and vapors from the environment can and do have harmful effects on the processing and operation of vacuum systems, and on their performance. At the outset, therefore, it should be stressed that a kind of cleanliness beyond that of mere apparent surface purity and sterilization are to be sought after as far as possible.

The chemical cleaning procedures (given below) are not sufficient by themselves to ensure complete freedom from contamination. Ultrasonic methods are used, but only in conjunction with other procedures.

All parts (including glass and containers for transport or storage) are ultrasonically agitated in a 0.05 percent solution of a surface-active (wetting) agent in deionized water, made by passing tap, or preferably distilled, water through a mixed-bed deionizing column. After this treatment nothing is touched by hand. Analytically I observe these methods of cleaning vacuum parts:

A. Assemplies which have not been in a Cesium enviroment are cleaned as follows:

Stainless steel and nickel, vapor degrease, detergent wash, tap water rinse, methanol rinse, deionized water, rinse and dry at room temperature.

Assemblies which include OFHC copper should receive the following cleaning: Vapor degrease, detergent wash, water rinse, methanol rinse, acetone rinse, and warm air-dry (110^{o}-120^{o}F). All rinses should be at room temperature to minimize discoloration of the copper caused by oxide formation. The brushing

of assemblies during rinsing will help remove loose weld oxides.

B. Assemplies which have been in a Cesium environment as follows;

STAINLESS STEEL CLEANING PROCEDURE

1. Trichloroethylene vapor degrease.

Degreasing in liquid solvents is likely to be ineffective because in industrial atmospheres, or places where there are oil burners, internal-combustion engine exhausts, gas burners, etc., an open container or bottle will pick up, even in a very short time, oil - or grease - bearing dust particles. Also, if fingers are dipped into the solvent, it is obvious, as evidenced by the severe drying action on the skin, that the oily dermal secretions have gone into the solvent and will subsequently leave an oily residue on anything put into the solvent.

2. Detergent wash in boiling tap water and then repeat in ultrasonic cleaner.

3. Agitate for 30 seconds in the following solution:

   Tap water...750 ml

   HCI (concentrated)...250 ml

   HNO_3 (concentrated)...200 ml

4. Rinse thoroughly in running tap water and then immerse in HNO_3 (concentrated).

5. Repeat steps 2 and 3 if necessary for a uniform surface.
6. Rinse in running hot tap water for 10 minutes.
7. Rinse in two changes of deionized water. If there are deep recesses or holes, boil in deionized water.
8. Rinse in methanol, reagent-grade.
9. Dry in air oven at 80-100°C.

CLEANING OF SILVER - COPPER BRAZING ALLOYS

1. Vapor degrease.
2. Ultrasonic detergent wash (warm).
3. Matawan #48W (Hanson-VanWinkle-Munning Co.) 8 oz/gal (water).
4. Use at 180-210°F for 5 minutes or more.
5. Rinse in cold water.
6. Rinse in hot distilled or deionized water.
7. Rinse in methanol, reagent quality.
8. Dry in cold air stream.

CLEANING OF OFHC

1. Vapor degrease.
2. Boil in detergent and wash.
3. Ultrasonic agitation in acid bath (50% HCl at room temperature for 1-3 minutes).
4. Tap water rinse.

5. Methanol - Aceton - Methanol rinse.
6. Triple deionized water rinse.
7. Methanol rinse (reagent grade).

Note: All rinsing should be at room temperature to avoid oxide formation.

CLEANING OF MOLYBDENUM (AND TUNGSTEN); REMOVAL OF OXIDES

1. Vapor degrease.
2. Cover parts to be treated in 15% NaOCl (Clorox or equivalent) and heat to about 70°C. Remove parts by inspection when clean; do not overclean. A further oxide may form on molybdenum which will be removed later.
3. Rinse thoroughly in cold or warm tap water. If there are recesses, rinse for one-half hour, or vacuum-boil, with several changes of water, to remove all NaOCl. Discard NaOCl solution when it is no longer effective.
4. Prepare the following solution:

   NH_4OH, 28%...1 part

   H_2O_2, 30%...1 part

   Deionized water...2 parts

   (chemicals are to be reagent grade)

   Place the solution in or near sink; keep tongs handy. D o n o t h e a t. Immerse a few parts which have had treatment, as in step 1 above, into this solution until clean. If not clean after about 30 seconds, remove from solution and rinse to remove loosely adhering oxide. Repeat if necessary. K e e p t h e w o r k l o a d s m a l l t o m i n i m i z e h e a t i n g o f t h e s o l u t i o n. If quite a large quantity of

work is to be done, the solution (step 3 above) should be cooled with an outer jacket of cold running water. Flush mixture down drain immediately after using, or if heating takes place; otherwise, a violent reaction may occur.

5. Rinse work in running tap water for one-half hour, or repeat vacuum-boiling as in step 2 above. The last vacuum rinse should be in deionized water, or if vacuum is not used, in several changes of deionized water.
6. Rinse in reagent-grade methanol.
7. Dry in air at room temperature or in oven at no more than 80°C.

Finally the cleanliness of the parts is tested at appropriate stages by the water-break test. With this method the parts are dipped into a beaker of overflowing deionized water and withdrawn. Then if a uniform, unbroken film of water is left on the part, hydrophobic contaminants are not present.

PUMPING OF THE VACUUM SYSTEM

After the vacuum components are assembled a helium leak test is performed with a Veeco model MS-90 leak detector. Subsequently the system is installed in the oven and the pumping procedure is started as follows;

1. Initially with an Edwards mechanical pump model EDM-12 until a 10 micron vacuum is achieved (oil trap was used in series with the vacuum line).
2. Then two absorption pumps are used in series (models 941-6001 and 941-6002). Two pumps are used because the absorption pumping action is selective. That is, when a mixture of gases is to be pumped, only those gases whose liquefaction temperatures are above or near the surface temperature will be absorbed with any significant capacity. Although certain gases are not pumped well, e.g., neon and helium, it is possible to trap them in the pump, thus removing them from the chamber being evacuated. This is accomplished by allowing the inrushing air to carry all gas constituents, including neon and helium into the pump, then closing off the valve before these non-condensable gases can migrate back out of the pump into the chamber. The second absorption pump is then used to continue the pumpdown to a crossover point where a high vacuum pump takes over. At the same time the system's temperature has been raised to 380^{o}C and pumping was continuous for 48 hours.
3. Finally the temperature is reduced to 150^{o}C and a VARIAN low pump model 911-5030 is connected to a system through a high vacuum valve. Then the temperature is raised again to 380^{o}C and the system is baked for a period of two weeks.

Using the above procedure vacuum of 10^{-8} or lower is universally achieved.